Université de Sherbrooke

Evaluation of the radioprotective ability of cystamine as a function of radiation quality using Monte Carlo simulations of the radiolysis of the Fricke dosimeter

Par

Esteban SEPULVEDA

Département de médecine nucléaire et radiobiologie

Mémoire présenté à la Faculté de médecine et des sciences de la santé en vue de l'obtention du grade de maître ès sciences (M. Sc.) en sciences des radiations et imagerie biomédicale

Sherbrooke, Québec, Canada

Novembre 2018

Jury

Pr Armand Soldera	Examinateur, Département de chimie, Faculté des sciences
Pr Benoit Paquette	Examinateur, Département de médecine nucléaire et radiobiologie, Faculté de médecine et des sciences de la santé
Pr Jean-Paul Jay-Gerin	Directeur de recherche, Département de médecine nucléaire et radiobiologie, Faculté de médecine et des sciences de la santé

RÉSUMÉ

ÉVALUATION DE LA CAPACITÉ RADIOPROTECTRICE DE LA CYSTAMINE EN FONCTION DE LA QUALITÉ DU RAYONNEMENT À L'AIDE DE SIMULATIONS MONTE CARLO DE LA RADIOLYSE DU DOSIMÈTRE AU SULFATE FERREUX DE FRICKE

Par

Esteban SEPULVEDA

Département de médecine nucléaire et radiobiologie

Mémoire présenté à la Faculté de médecine et des sciences de la santé en vue de l'obtention du diplôme de maître ès sciences (M.Sc.) en sciences des radiations et imagerie biomédicale, Faculté de médecine et des sciences de la santé, Université de Sherbrooke, Sherbrooke, Québec, Canada, J1H 5N4

La protection radiologique joue, aujourd'hui, un rôle clé dans de nombreuses applications, y-compris l'ingénierie aérospatiale, les accidents nucléaires, le terrorisme nucléaire/radiologique, la radiobiologie militaire et la radio-oncologie clinique. La cystamine, forme disulfure de la cystéamine – un aminothiol de la même famille, est un composé connu pour son potentiel radioprotecteur en clinique pendant des procédures de radiothérapie. Une manière pratique pour évaluer son efficacité radioprotectrice est basée sur l'utilisation du dosimètre au sulfate ferreux de Fricke en combinaison avec des simulations Monte Carlo. La radiolyse du dosimètre de Fricke, basée sur l'oxydation des ions ferreux en ions ferriques par les espèces oxydantes $^{\bullet}OH$, $HO_2^{\bullet}$ et H_2O_2 produit par la décomposition radiolytique de l'eau en solution acide aérée, forme la base de notre étude. La présence de cystamine dans les solutions pendant l'irradiation empêche la radio-oxydation du Fe^{2+} et entraîne une diminution des rendements (ou valeurs G) en Fe^{3+}. Les résultats indiquent clairement que l'effet protecteur de la cystamine provient de sa capacité à capturer les radicaux libres, ce qui permet à ce composé d'agir en compétition avec les ions Fe^{2+} pour les divers radicaux formés lors de l'irradiation de l'eau environnante. Nos simulations Monte Carlo ont permis de réaliser l'évaluation de l'efficacité protectrice de la cystamine pour diverses qualités de rayonnement, en utilisant des protons, des ions He^{2+} et C^{6+} de différentes énergies allant de 500 MeV à 150 keV par nucléon. La diminution de l'énergie incidente des particules ou, de manière équivalente, l'augmentation du transfert d'énergie linéaire (TEL) du rayonnement produit une diminution notable de $G(Fe^{3+})$, comme prévu par la théorie des structures de trajectoires. Cependant, lorsque la cystamine en concentration 1 M est ajoutée aux solutions, on observe une diminution spectaculaire de $G(Fe^{3+})$, ce qui reflète clairement l'efficacité radioprotectrice de ce composé. Cette diminution dépend cependant beaucoup de l'énergie des ions incidents : plus le TEL du rayonnement est élevé, plus l'efficacité radioprotectrice de la cystamine est faible.

Mots clés: Radiolyse de l'eau, dosimètre de Fricke, protons, ions hélium et carbone, transfert d'énergie linéaire (TEL), schéma réactionnel, cinétique de compétition, radioprotecteur, cystamine, rendement radiolytique (valeur G), simulations Monte Carlo, structure et chimie des trajectoires, hadronthérapie.

SUMMARY

EVALUATION OF THE RADIOPROTECTIVE ABILITY OF CYSTAMINE AS A FUNCTION OF RADIATION QUALITY USING MONTE CARLO SIMULATIONS OF THE RADIOLYSIS OF THE FRICKE DOSIMETER

By

Esteban SEPULVEDA

Département de médecine nucléaire et radiobiologie

Thesis presented at the Faculty of Medicine and Health Sciences in order to obtain the Master degree of Sciences (M.Sc.) in Radiation Sciences and Biomedical Imaging, Faculty of Medicine and Health Sciences, Université de Sherbrooke, Sherbrooke, Québec, Canada, J1H 5N4

Currently, radiation protection plays a fundamental role in many applications, including aerospace engineering, nuclear accidents or possible nuclear/radiological terrorism, military radiobiology, and clinical radiation oncology. Cystamine, the disulfide form of cysteamine – an aminothiol of the same family, is a compound most known for its radioprotective potential in the clinic during procedures of radiotherapy or in case of risk of overexposure in patients. A convenient manner to evaluate its radioprotective efficiency consists in using the ferrous sulfate (Fricke) dosimeter in combination with Monte Carlo simulations. The well-known radiolysis of the Fricke dosimeter, based on the oxidation of ferrous ions to ferric ions by the oxidizing species $^{\bullet}OH$, $HO_2^{\bullet}$, and H_2O_2 produced by the radiolytic decomposition of acid water in aerated solutions, forms the basis of our method. The presence of cystamine in Fricke dosimeter solutions during irradiation prevents the radiolytic oxidation of Fe^{2+} and leads to decreased ferric ion yields (or *G*-values). Results clearly indicate that the protective effect of cystamine originates from its radical-capturing ability, which allows this compound to act by competing with the Fe^{2+} ions for the various free radicals formed during irradiation of the surrounding water. An impressive agreement is found between calculated $G(Fe^{3+})$ values and experiment. Using our simulation modeling, the evaluation of the radioprotective efficiency of cystamine has been performed for various radiation qualities, using irradiating protons, helium and carbon ions of different energies ranging from 500 MeV to 150 keV per nucleon. Decreasing the incident energy of the ion or equivalently, increasing the linear energy transfer (LET) of the radiation, produces a noticeable decrease in $G(Fe^{3+})$, as expected from the track structure theory. However, when 1 *M* cystamine is added to the solutions, we observe a dramatic decrease in $G(Fe^{3+})$, which clearly reflects the radioprotective efficiency of this compound. This decrease very much depends upon the energy of the ion used; the higher the LET of the radiation, the lower the radioprotective efficiency of cystamine.

Keywords: Water radiolysis, aerated ferrous sulfate (Fricke) dosimeter, high-energy irradiating protons, helium and carbon ions, linear energy transfer (LET), reaction scheme, competition kinetics, antioxidant, radioprotector, cystamine, radiolytic yield (*G* value), Monte Carlo track chemistry simulations, hadrontherapy.

TABLE OF CONTENTS

LIST OF FIGURES

LIST OF TABLES

LIST OF ABBREVIATIONS

DNA	Deoxyribonucleic acid
e^-_{aq}	Hydrated electron
eV	Electron-volt
G_X or $g(X)$	Primary yield of the radiolytic species X
$G(X)$	Experimental yield of the final product X
Gy	Gray
IRT	Independent reaction times
k	Reaction rate constant
LET	Linear energy transfer
keV	Kilo-electron-volts
MeV	Mega-electron-volts
μm	Micrometer
μs	Microsecond
ns	Nanosecond
ps	Picosecond
pH	$-\log_{10}[H^+]$, where the square brackets denote concentration
RBE	Relative biological effectiveness
OER	Oxygen enhancement ratio

1. INTRODUCTION

For decades, medical physicists and doctors have been fighting cancer; in 2018, radiotherapy is the most effective technic to treat this disease (BASKAR et al., 2012; MILLER et al., 1981). On average, 50% of cancer patients will receive radiation, either for curative or palliative purposes. Currently in Canada, one out of two persons will develop cancer at some time during their life. Moreover, 50% of these diagnosed patients will develop at least one metastasis in the brain. Therefore, the treatment for those patients should be precise and highly accurate. Nowadays, researchers in radiotherapy and chemotherapy are enhancing and refining conventional technics. These new improvements in radiation therapy come along with new technics that allow better irradiation procedures and optimum treatments (NAIR et al., 2001).

The conventional methods used in clinical radiotherapy show significant weaknesses for the health of the patient; some of those disadvantages and how other new alternative methods can solve those problems are briefly summarized below (JEMAL et al., 2011; LIU et al., 2001; MARRETT et al,. 2008; TORRE et al., 2015).

In general, nowadays there are five different radiotherapy techniques used to treat tumors in human beings: photon (γ- and X-rays)-based therapy, neutron therapy, proton therapy and heavy ion therapy (note that, when the irradiating beams are made of charged particles – protons and other ions, such as carbon – radiation therapy is called "hadrontherapy"). These techniques all deposit energy in a different way, which represents either an advantage or a disadvantage for the treatment. Figure 1.1 shows the depth-dose profiles for all the different types of radiation mentioned before (DURANTE & LOEFFLER, 2010; KRÄMER et al., 2000; HALL & GIACCIA, 2006). As can be seen, the Bragg peak for proton and heavy ion therapies is immensely localised, which means that the energy is deposited within the wished volume. This is a great benefit in cancer treatment because it provides a more precise treatment and more importantly, the irradiation in healthy tissue is very low. In other words, one the biggest problems in conventional radiotherapies is the fact that irradiation in surrounded tissues can lead to secondary cancers or damage in vital organs; using any of the advanced medical

technologies of hadrontherapy mentioned above, the irradiation in healthy organs is lower than using standard treatments (MEDICAL EXCELLENCE JAPAN, 2018).

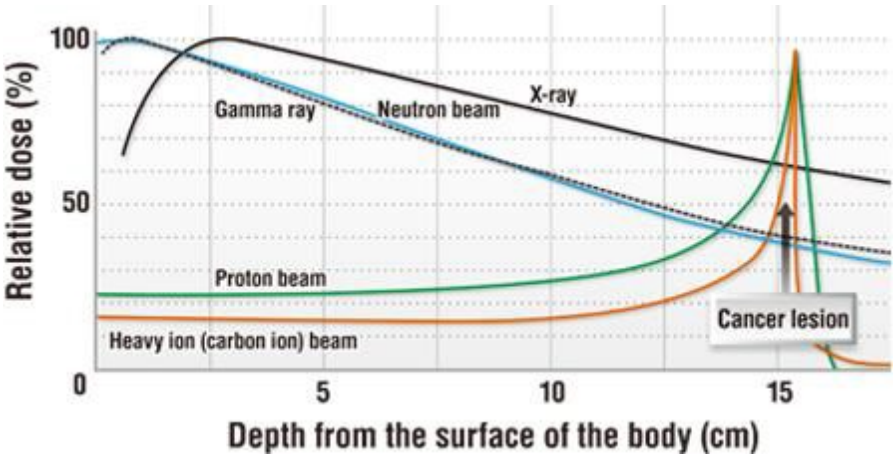

Figure 1.1 – Relative dose in percentage as a function of the depth from the surface of the body of the patient in cm (MEDICAL EXCELLENCE JAPAN, 2018).

As an example, the comparison between two different techniques: conventional radiotherapy (X-rays) and modern radiotherapy (heavy ions) is useful to understand the significant difference between both technologies. The dose deposition using X-rays is mostly on the surface of the body decreasing relatively slowly with depth, whilst the deposition of energy using carbon ions is acutely localized at the tumor site, falling to zero after the Bragg peak and with a low irradiation on the surface. Additionally, for conventional radiotherapy, the energy deposition is not only on the pathway before reaching a tumor, but also, it is likely to measure some dose in the tissue located after the lesion. In contrast, using carbon ion therapy guaranties a low irradiation in organs before and after a tumor in comparison with standard treatments (NODA et al., 2006, 2007).

Although both methods show remarkable results, there are a few discrepancies in the mode they perform and the applicability of these techniques. To discuss these variations it is important to clarify two relevant concepts in medical physics and radiobiology: “relative biological effectiveness” (RBE) and “oxygen enhancement ratio” (OER).

The relative biological effectiveness, on the one hand, refers to the possibility of certain types of radiation to induce a biological damage in the irradiated cells. Although the dose is vital, in radiobiology it is more important to observe the real damage of a given dose in the tissue. The relation between the numerical physical dose and the cell damage is called the relative biological effectiveness. More precisely, the RBE is defined as the ratio of the doses of high-energy photons (e.g., ^{60}Co γ-rays) and charged particles required for equal biological effect (ELSÄSSER et al., 2010; PAGANETTI et al., 2002; STORER et al., 1957; SUZUKI et al., 2000).

On the other hand, the availability of oxygen (O_2) is of vital importance to the radiosensitivity of a cell; well-oxygenated cells respond better to radiotherapy than tumors with extensive hypoxia (GRAY et al., 1953). This relative boosting effect of oxygen on cell-kill is quantified by the oxygen enhancement ratio, which is defined as the ratio of the dose required to produce a given effect in the absence of oxygen to that dose required to achieve the same effect under fully oxygenated conditions. In other words, the use of a radiation type with a low oxygen enhancement ratio will definitely increase the probability of full remission of a patient after treatment. Figure 1.2 shows various types of radiation used in cancer treatments and their respective RBE and OER values (PALCIC & SKARSGARD, 1984; WENZL & WILKENS, 2011). As can be seen, the OER decreases with increasing LET clearly suggesting a potential clinical advantage of high-LET radiotherapy with heavy ion beams compared to low-LET photon or proton irradiation. In fact, for instance, it has been proved today that carbon-ion radiotherapy is significantly more effective in the treatment of radioresistant cancers (e.g., malignant melanoma or colorectal cancers) than conventional photon radiotherapy or even proton therapy. In spite of the high cost of the installations necessary for the production of these ions, carbon-ion radiotherapy looks increasingly appealing as a cancer treatment modality (EBNER & KAMADA, 2016).

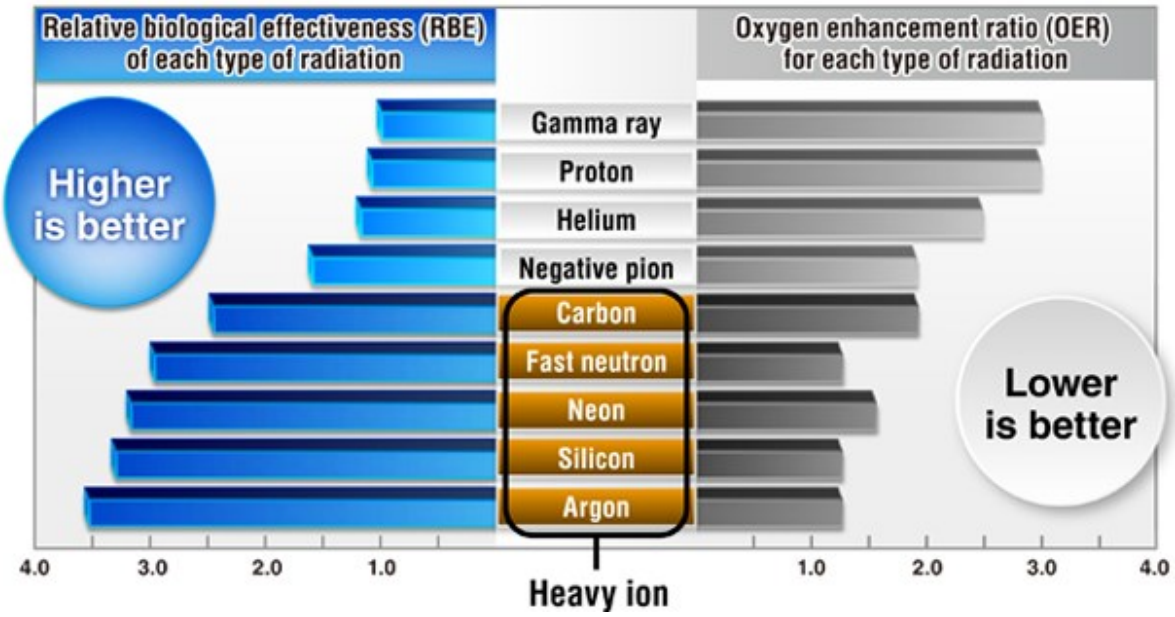

Figure 1.2 – Relative biological effectiveness and oxygen enhancement ratio for γ-rays, protons, negative pions, fast neutrons, helium, carbon, neon, silicon and argon ions (MEDICAL EXCELLENCE JAPAN, 2018).

Figure 1.3 shows all the diverse forms of treatments in which heavy-ion therapy can be used. As it is seen, despite its wide range of applications in solid tumors, this practice is not appropriate for cancers with extensive metastases or blood cancers (BRAHME et al., 1989; ENGHARDT et al., 1999; HAMADA et al., 2010; JÄKEL et al., 2003; KRÄMER et al., 2000; NIKOGHOSYAN et al., 2004; SCHARDT et al., 2010).

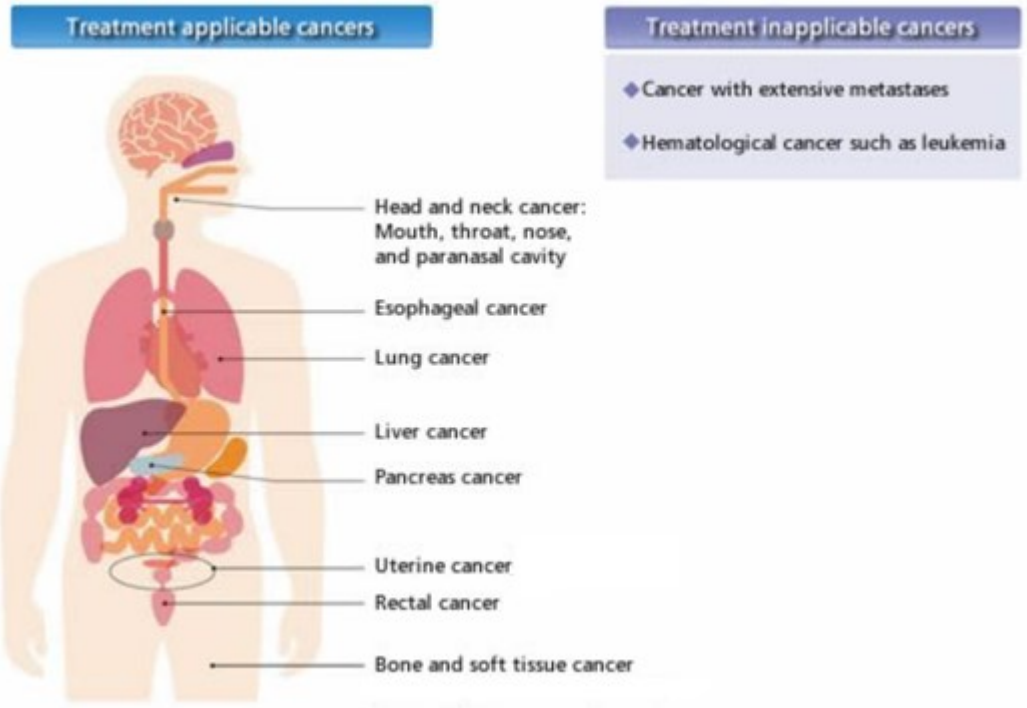

Figure 1.3 – Applicable and inapplicable cancer treatments using heavy-ion therapy (MEDICAL EXCELLENCE JAPAN, 2018).

During a treatment with carbon ion therapy, the depth of the deposition of energy is controlled by the energy of the carbon ion, which can reach up to 70% of the light speed (Fig. 1.5). This energy is delivered precisely to the tumor, taking advantage of the Bragg peak effect, providing less damage to surrounding healthy tissue than with other conventional techniques. Carbon therapy increases the biological efficiency of the dose by a factor between 1.5 and 3 in comparison with conventional photon-based methods (ANDO & KASE, 2009; BLAKELY & KRONENBERG, 1998; KOMATSU et al., 2011; PARODI et al., 2012; SCHOLZ et al., 1997; SCHULZ-ERTNER & TSUJII, 2007).

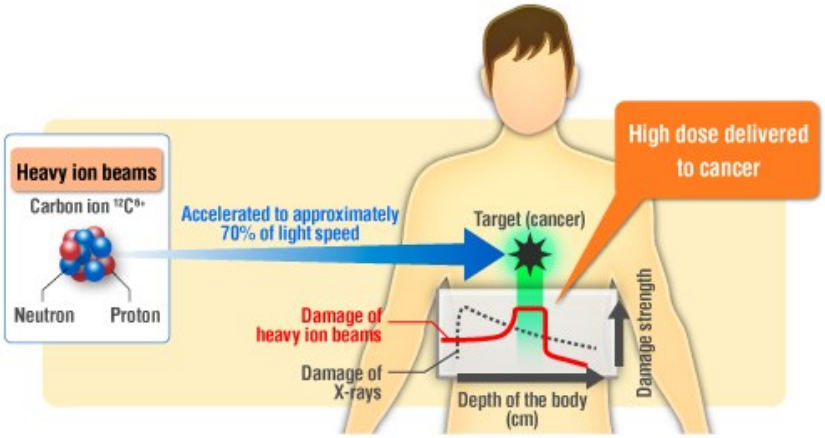

Figure 1.4 – Process of heavy-ion therapy using carbon ions (MEDICAL EXCELLENCE JAPAN, 2018).

Heavy-ion therapy shows magnificent results in cancer treatment, such as low pain, suitable for elderly patients, curative in an early stage of development of the disease, effective on X-rays resistant tumors and feasibility of short-course therapy. Presently, there is a number of cancer centres with these facilities. Figure 1.5 and Table 1.1 show the location and year of first treatment of proton and heavy ion accelerators around the world (GLIMELIUS et al., 2005; KAMADA et al., 2015; OLSEN et al., 2007; SUIT, 2003).

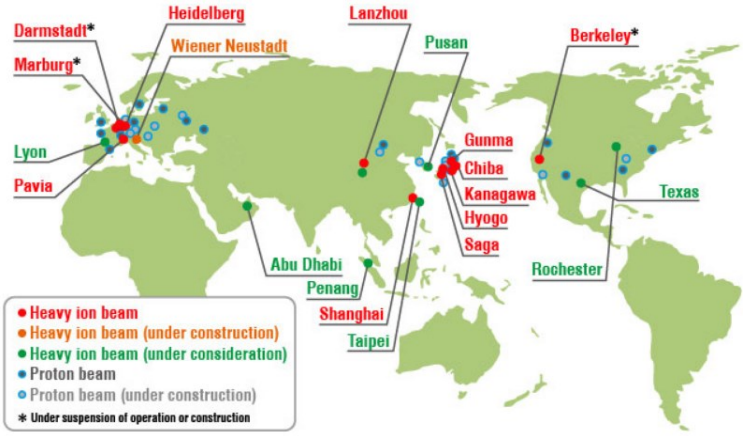

Figure 1.5 – Location of various cancer centres with proton and heavy-ion therapy around the world. With a total amount of five accelerators, nowadays Japan is the country with the highest number of heavy-ion therapy centers (MEDICAL EXCELLENCE JAPAN, 2018).

Table 1.1 – Cancer centres around the world with proton or heavy-ion therapy facilities in a chronological order from 2018 to 1984 (PARTICLE THERAPY CO-OPERATIVE GROUP, 2018).

Institution	Location	Start of treatment
Emory Proton Therapy Center	Atlanta, GA, USA	2018
Centre de protonthérapie CYCLHAD	Caen, Normandie, France	2018
UMC Groningen Protonen Therapie Centrum	Groningen, Netherlands	2018
Miami Cancer Institute	Miami, FL, USA	2017
Beaumont Proton Therapy Center	Royal Oak, MI, USA	2017
Holland Particle Therapy Centre	Delft, Netherlands	2017
Clinical Proton Therapy Center Dr. Berezin Medical Institute	Saint-Petersburg, Russia	2017
Mayo Clinic Cancer Center	Phoenix, AZ, USA	2016
The Marjorie and Leonard Williams Center for Proton Therapy	Orlando, FL, USA	2016
Cancer and Blood Diseases Institute	Liberty Township, OH, USA	2016
Maryland Proton Treatment Center	Baltimore, MD, USA	2016
A. Tsyb Medical Radiological Research Centre	Obninsk, Russia	2016
Ackerman Cancer Center	Jacksonville, FL, USA	2015
The Laurie Proton Therapy Center	New Brunswick, NJ, USA	2015
Texas Center for Proton Therapy	Dallas Fort Worth, TX, USA	2015
Mayo Clinic Jacobson Building	Rochester, MN, USA	2015
St. Jude Red Frog Events Proton Therapy Center	Memphis, TN, USA	2015
Centrum Cyklotronowe Bronowice	Kraków, Poland	2015
SMC Proton Therapy Center	Seoul, Korea	2015
Proton and Radiation Therapy Center, Linkou Chang Gung Memorial Hospital	Taipei, Taiwan	2015
Skandionkliniken	Uppsala, Sweden	2015
Provision Proton Therapy Center	Knoxville, TN, USA	2014
California Proton Cancer Therapy Center	San Diego, CA, USA	2014

Institution	Location	Start of treatment
Centro per la protonterapia	Trento, Italy	2014
PTC Uniklinikum	Dresden, Germany	2014
Shanghai Proton and Heavy Ion Center	Shanghai, China	2014
SCCA Proton Therapy Center	Seattle, WA, USA	2013
Siteman Cancer Center	St. Louis, MO, USA	2013
Westdeutsches Protonentherapiezentrum	Essen, Germany	2013
ProCure Proton Therapy Center	Somerset, NJ, USA	2012
Roberts Proton Therapy Center	Philadelphia, PA, USA	2010
Hampton UniversityProton Therapy Institute	Hampton, VA, USA	2010
ProCure Proton Therapy Center of Oklahoma	Oklahoma City, OK, USA	2009
Heidelberg Ion-Beam Therapy Center	Heidelberg, Germany	2009
Rinecker Proton Therapy Center	Munich, Germany	2009
Proton Therapy Center, Korea National Cancer Center	Seoul, Korea	2007
University of Florida Health Proton Therapy Institute-Jacksonville	Jacksonville, FL, USA	2006
University of Texas MD Anderson Cancer Center	Houston, TX, USA	2006
Wanjie Proton Therapy Center	Zibo, China	2004
Centro di adroterapia oculare	Catania, Italy	2002
Francis H. Burr Proton Center	Boston, MA, USA	2001
Proton Medical Research Center University of Tsukuba	Tsukuba, Japan	2001
Helmholtz-Zentrum Berlin	Berlin, Germany	1998
TRIUMF	Vancouver, Canada	1995
Crocker Nuclear Laboratory	Davis, CA, USA	1994
Research Center for Charged Particle Therapy	Chiba, Japan	1994
Centre de protonthérapie de l'Institut Curie	Orsay, France	1991
Centre Antoine Lacassagne	Nice, France	1991
Loma Linda University Medical Center	Loma Linda, CA, USA	1990
Clatterbridge Cancer Centre NHS Foundation Trust	Liverpool, United Kingdom	1989
Paul Scherrer Institute	Villigen, Switzerland	1984

2. RESEARCH OBJECTIVES

Although the main objective of the radiation therapy of cancer is to induce tumor cell death, there are still healthy cells irradiated around the main target and, as well, along the pathway of the radiation to reach the target. Clearly, in order to obtain better tumor control with a higher dose, the normal tissues should be protected. Consequently, during the last decades, much work has been done on creating and probing different radiation protectors and sensitizers to minimize this problem. A radioprotector, as its name says, protects the surrounded normal tissues from the radiation whilst radiosensitizers increase the radiosensibility of a tumor. In general, radiation modifiers play a critical role in radiotherapy and cancer treatment (MEESAT et al., 2009; NAIR et al., 2001; WARDMAN, 2007).

As human cells contain roughly 80% water, there is a significant irradiation of water molecules generating free radicals such as the hydrated electron (e^-_{aq}), the hydroxyl radical ($^{\bullet}OH$), the hydrogen atom ($H^{\bullet}$), and so on. These free radicals can lead to damages to DNA, RNA, proteins and cell membranes that can cause the death of the cell. Free radicals may attack healthy tissue as well as a tumor; therefore, scientists search to find the possibility to protect healthy tissues from those free radicals with, of course, a preferential protection of normal tissues vs. tumors (BUMP & MALAKER, 1998; LEVIN et al., 2005; LOMAX et al., 2001; MIN et al., 2006; MUNZENRIDER & LIEBSCH, 1999; PAGANETTI, 2012; PEDRONI et al., 1995; SLATER et al., 2004).

By definition, free radicals contain at least one unpaired electron, which makes them highly reactive and thereby able to damage all macromolecules, including lipids, proteins and nucleic acids. The present work aims to examine, from a radiation chemistry point of view, the mechanistic basis for the protection exerted by some compounds, generally called antioxidants or radioprotectors, used to protect cellular components from free radical induced damage (BITZER et al., 2018; HALLIWELL, 1994; HALLIWELL & GUTTERIDGE, 2015; PREMARATNE et al, 2018; REINA & MARTÍNEZ, 2017; VALKO et al., 2007).

Currently, there is a wide range of radioprotectors studied by researchers in a number of laboratories, but, certainly, cystamine is among the most interesting ones due to its well-known high radioprotective effects in radiobiology (see Appendix, where we present a list of important radioprotector agents and their mechanisms of action, along with a brief history of their development). This compound comes from a chemical family, called thiols (which are analogous to alcohols but in which sulfur replaces the oxygen of the hydroxyl group), and its chemical structure can be represented as (JAYSON et al., 1967)

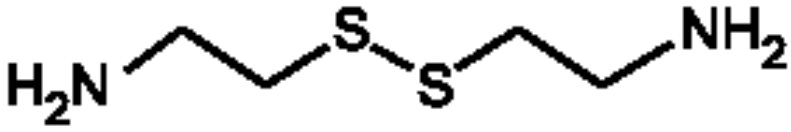

Figure 2.1 – Chemical structure of cystamine.

or, in abbreviated form, RSSR with R = NH_2-CH_2-CH_2. Interestingly, it is the disulfide form of cysteamine (or 2-aminoethanethiol, RSH), an organic aminothiol well known also for its radioprotective properties.

The chemistry of radiation modifiers is not fully understood nowadays. The present study defines, from a radiation chemistry perspective, the basis of how chemical (i.e., non-biologic) radioprotectors – such as cystamine – actually work at the molecular level. In cellular systems, these compounds are usually thought to exert their protective effects by a combination of different individual mechanisms that include free-radical scavenging and $H^{\bullet}$ atom donation (BUMP & MALAKER, 1998; VON SONNTAG, 2006; HALL & GIACCIA, 2006). If the radiolysis water-produced reactive intermediates are scavenged by the protector agent before they can interact with vital cellular components (especially DNA), the damaging effect of radiation is reduced. Cytoprotection by radioprotective compounds containing sulfhydryl –SH groups (i.e., with labile hydrogen atoms) is also formulated in terms of $H^{\bullet}$-atom donation to chemically repair DNA damage (and restore it to its initial state), which would otherwise be fixed by oxygen (VON SONNTAG, 2006; WARDMAN, 2009). In this latter case, sulfhydryl compounds exert their protective activity by efficiently competing with

oxygen in reactions with key DNA free radicals (WARD, 1983), thereby reducing DNA damage and increasing cell survival.

More specifically, we study in this report the chemical action and the radical scavenging properties of cystamine using a model system developed previously combining the well-known aerated ferrous sulfate (Fricke) dosimeter with Monte Carlo track chemistry simulations (FRICKE & HART, 1966; JAYSON & WILBRAHAM, 1968; LALITHA & MITTAL, 1971; MEESAT et al., 2009, 2012). Benefiting from the fact that cystamine is reasonably well characterized in terms of radiation chemistry, this computer model proposes reaction mechanisms and incorporates specific reactions describing the radiolysis of cystamine in aerated Fricke solutions that lead to the observable quantitative chemical yields. As we know relatively little about protection against densely ionizing radiation, our specific aim here is to assess quantitatively the radioprotective ability of this compound as a function of the quality of the radiation (i.e., the radiation type and energy), using irradiating protons, and helium and carbon ions of different energies ranging from 500 MeV to 150 keV per nucleon.

3. RADIOLYSIS OF WATER

Water radiolysis is the dissociation of water molecules by ionizing radiation. The complex events that accompany the absorption of energetic radiations by water can usually be divided into three, more or less clearly demarcated, consecutive, temporal stages: physical, physicochemical, and chemical (PLATZMAN, 1958; KUPPERMANN, 1959; TIPPAYAMONTRI et al., 2009; MEESUNGNOEN & JAY-GERIN, 2011). During the first or "physical" stage, the energy deposition results in both ionizations and excitations leading to extremely unstable species that undergo fast reorganisation in the second or "physicochemical" stage. These processes produce free radical and molecular products of radiolysis that are distributed in a highly nonhomogeneous track structure, which depends on the type and energy of the radiation used. Secondary electrons slow down to sub-excitation energies and following thermalization, they become trapped (e^-_{tr}) and hydrated (e^-_{aq}) (~10^{-12} s). The third or "chemical" stage consists of diffusion and reactions of the reactive species (e^-_{aq}, $H^\bullet$, H_2, $^\bullet OH$, H_2O_2, H^+, OH^-, $O_2^{\bullet-}$ (or its protonated form $HO_2^\bullet$ depending on the pH; pK_a = 4.8 in water at 25 °C, etc.) present at the end of the physicochemical stage. We usually divide this stage into two parts. The first part corresponds to the stage of "nonhomogeneous chemistry" during which tracks develop in time (PLANTE et al., 2005; MUROYA et al., 2006). A number of radicals will combine to form the molecular products H_2 and H_2O_2 and to re-form water, while the remainder will diffuse out into the bulk solution. At room temperature, all intra-track reactions are essentially complete by ~10^{-7}-10^{-6} s (BUXTON, 1987; SANGUANMITH et al., 2012). At this time, the species that have escaped from track reactions become homogeneously distributed throughout the bulk of the solution (i.e., the system at large). This is the second part of the chemical stage, the so-called stage of "homogeneous chemistry" that takes place beyond a few microseconds. The radical and molecular products that emerge from the tracks are then available for reaction with dissolved solutes (if any) present (in low or moderate concentrations) at the time of irradiation.

Figure 3.1 illustrates the time scale of the different stages of pure deaerated water radiolysis.

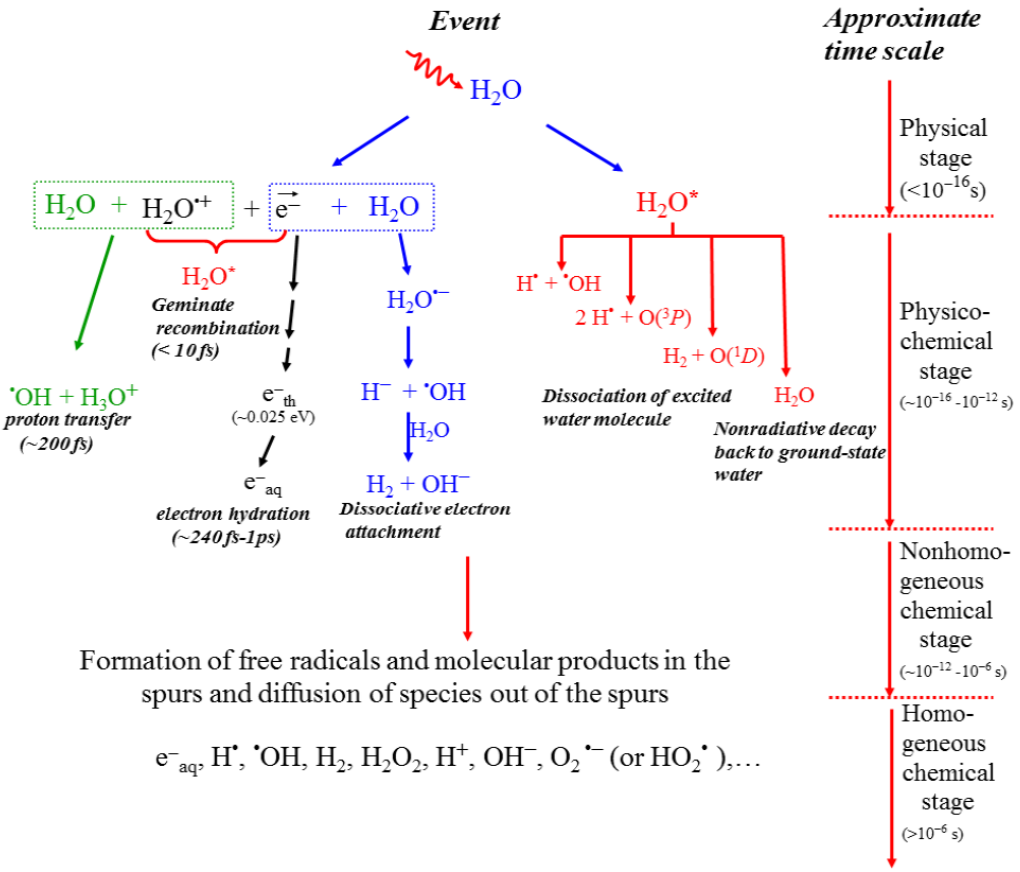

Figure 3.1 – Time scale of events that occur in the radiolysis of pure, deaerated water (MEESUNGNOEN & JAY-GERIN, 2011). As a guide to the eyes, we use different colors in the figure in order to contrast the individual processes occurring during the radiolysis of water.

In air-saturated solutions (where the concentration of dissolved oxygen in the water is ~0.25 m*M* at 25 °C), e^-_{aq} and $H^\bullet$ atoms are rapidly converted (on a time scale of a few tenths of a microsecond) to superoxide radical anion ($O_2^{\bullet-}$)/hydroperoxyl ($HO_2^\bullet$) radicals, according to:

$$e^-_{aq} + O_2 \rightarrow O_2^{\bullet-} \qquad k_1 = 2.3 \times 10^{10}\ M^{-1}\ s^{-1} \qquad [1]$$

$$H^\bullet + O_2 \rightarrow HO_2^\bullet \qquad k_2 = 1.3 \times 10^{10}\ M^{-1}\ s^{-1} \qquad [2]$$

where k_1 and k_2 are the rate constants for the two individual reactions (ELLIOT & BARTELS, 2009). Accordingly, in an aerobic environment at pH 7, the major reactive

species at homogeneity include $O_2^{\bullet -}$, $^{\bullet}OH$, and H_2O_2. The other molecular product, H_2, is relatively inert and normally plays only a limited role in the radiolysis of aqueous solutions, most of it escaping from solution (SPINKS & WOODS, 1990).

Finally, in a physiologic system, there follows a "biological" stage in which the cells respond to the damage resulting from the products formed in the preceding stages (for a review on the subject, see: AZZAM et al., 2012).

3.1 The "physical" stage

The physical stage consists of the phenomena by which energy is transferred from the incident high-energy radiation to the water. Its duration is less than $\sim 10^{-16}$ s. The result of this energy absorption is the production, along the path of the radiation, of a large number of ionized and electronically excited water molecules, denoted $H_2O^{\bullet +}$ and H_2O^*, respectively:

$$H_2O \rightsquigarrow H_2O^{\bullet +} + e^- \quad \text{(ionization)} \qquad [3]$$

$$H_2O \rightsquigarrow H_2O^* \quad \text{(excitation)} \qquad [4]$$

During this deposition of energy, ionization is the dominant scattering process. Note also that H_2O^* represents here many excited states, including the so-called "superexcited" states (PLATZMAN, 1962*a*) and the excitations of collective electronic oscillations of the "plasmon" type (HELLER et al., 1974; KAPLAN & MITEREV, 1987; LAVERNE & MOZUMDER, 1993; WILSON et al., 2001).

Generally, the electron ejected in the ionization event has sufficient energy either to ionize or excite one or more other water molecules in the vicinity; this leads to the formation of track entities that contain the products of the events (see below).

The so-called "track structure" is determined by the distribution of the physical energy deposition events and their geometrical dispositions, or, in other words, by the radiation type and energy, a measure of which is given by the "linear energy transfer" or LET (ICRU REPORT 16, 1970). Two different radiation track structures are generally considered as a function of LET:

i) Low-LET radiation tracks

Ionizing radiations such as fast electrons generated from γ- or X-ray beams have high energy and low LET. For example, the average LET of a 1-MeV Compton recoil electron produced by a ^{60}Co γ-ray source in liquid water at room temperature is ~0.3 keV/μm. The track-averaged mean energy loss per collision event by such an electron, as obtained from Monte Carlo simulations, is in the range ~47-56.8 eV (LAVERNE & PIMBLOTT, 1995; COBUT et al., 1998; MIRSALEH KOHAN et al., 2013). This means that the energy-loss events are, on the average, separated by distances of ~200 nm. This nonhomogeneous distribution of energy deposition events in space gives rise to the "spur" theory for low-LET track structure (ALLEN, 1948; MAGEE, 1953; MOZUMDER & MAGEE, 1966*a*,*b*), according to which the entire track is to be viewed as a random succession of (more or less spherical) spurs. The few tens of electron-volts deposited in a spur may cause one (or more) secondary electron to be ejected from a molecule. As the ejected electron moves away, it undergoes collisions with surrounding water molecules, loses its excess energy, and becomes thermalized (~0.025 eV at 25 °C) within ~8-12 nm of its geminate positive ion (GOULET et al., 1990, 1996; PIMBLOTT & MOZUMDER, 2004; MEESUNGNOEN et al., 2002*a*; UEHARA & NIKJOO, 2006). This average "electron thermalization distance" or "penetration range" can be viewed as an estimate of the spur's initial radius, prior to spur expansion. Thus, under ordinary irradiation conditions, the individual spurs produced by a low-LET radiation are so far apart along the track that they are not initially overlapping.

In their pioneering work to model the radiation-chemical consequences of different energy-loss processes, MOZUMDER & MAGEE (1966*a*,*b*) considered, somewhat arbitrarily, a low-LET track as composed of a random sequence of three types of essentially non-overlapping entities: "spurs, blobs, and short tracks" (Fig. 3.2). The spur category contains all track entities created by the energy losses between the lowest excitation energy of water and 100 eV. Blobs are defined as track entities with energy transfers between 100-500 eV, and short tracks as those with energy transfers between 500 eV and 5 keV. Secondary electrons produced in energy transfers above 5 keV were

considered as "branch tracks". Short and branch tracks are described collectively as δ-rays. This old concept of track entities proved to be very helpful in greatly facilitating the visualization of track processes and in modeling radiation-chemical kinetics. It is still a useful approach for the classification of track structures, since it takes into account the spatial arrangements of initial species, which affect their subsequent reactions.

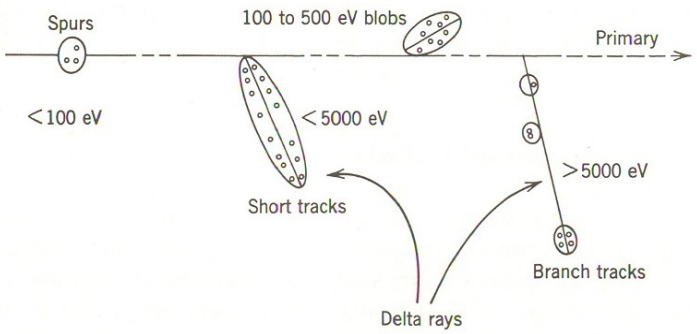

Figure 3.2 – Classification of energy deposition events in water by track structure entities so-called spurs (spherical entities, up to 100 eV), blobs (spherical or ellipsoidal, 100-500 eV), and short tracks (cylindrical, 500 eV-5 keV) for a primary high-energy electron (not to scale). Short and branch tracks are described as δ-rays. From BURTON (1969), with permission.

Figure 3.3 shows typical two-dimensional representations of the track segments for 300-MeV and 150-keV irradiating protons (LET ~ 0.3 and 70 keV/μm, respectively) in liquid water at 25 °C, calculated using Monte Carlo simulations (KANIKE et al., 2015). It illustrates the nonhomogeneity of the energy deposition on a sub-microscopic scale. At the lowest LET (Fig. 3.3*a*), tracks are formed initially by well-separated "spurs" (more or less spherical in shape) that develop independently in time (without interference from the neighbouring spurs). As LET increases, the mean separation distance between the spurs decreases and the isolated spur structure changes to a situation in which the spurs overlap and form a dense continuous column (cylindrical shape) (Fig. 3.3*b*).

ii) High-LET radiation tracks

The column of species defined initially by the overlapping spurs along the path of a high-LET particle makes up what is referred to as the track "core". It is surrounded by

a coaxial region traversed by large numbers of emergent, comparatively low-LET secondary electrons (δ-rays), called the "penumbra" (for example, see: PUCHEAULT, 1961; MOZUMDER et al., 1968; CHATTERJEE & SCHAEFER, 1976; FERRADINI, 1979; MAGEE and CHATTERJEE, 1980, 1987; PARETZKE, 1987; MOZUMDER, 1999; LAVERNE, 2000, 2004). Such a "high-LET" radiation track structure can actually be seen in heavy-ion irradiations (PLANTE et al., 2005; MUROYA et al., 2006). It is illustrated schematically in Figs. 3.4 and 3.5.

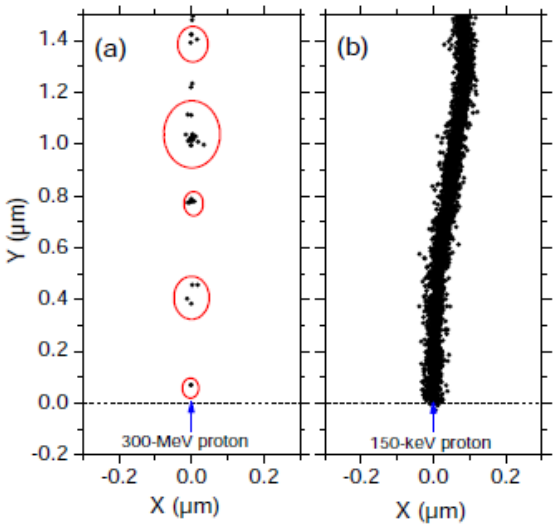

Figure 3.3 – Projections into the *XY*-plane of figure of track segments of 300 (*a*) and 0.15 (*b*) MeV protons (LET ~ 0.3 and 70 keV/μm, respectively) incident on liquid water at 25 °C (KANIKE et al., 2015). The two irradiating protons are generated at the origin and start moving along the *Y* axis. Dots represent the energy deposited at points where an interaction occurred.

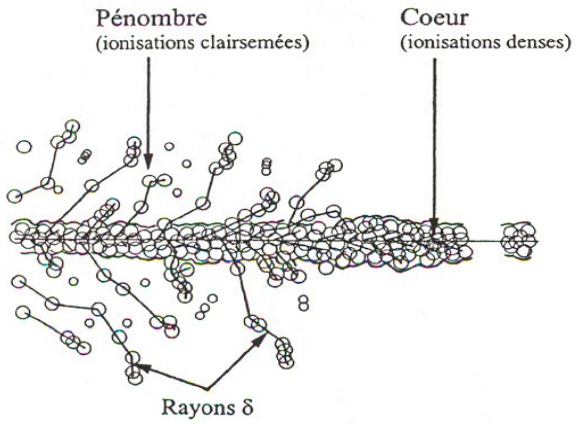

Figure 3.4 – Primary energy-loss events in high-LET radiation tracks (FERRADINI, 1979).

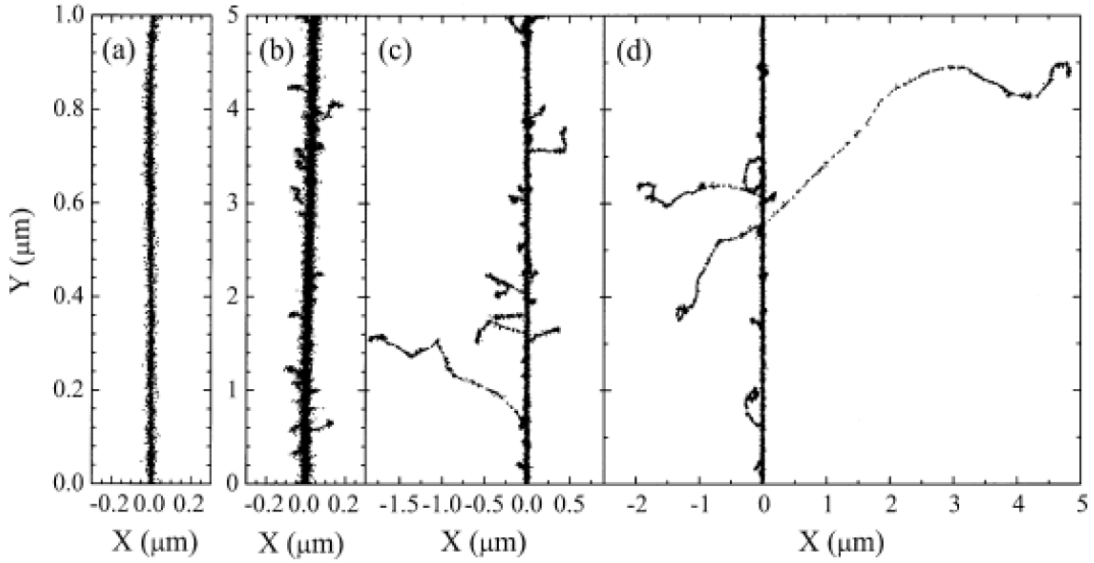

Figure 3.5 – Projections over the *XY*-plane of track segments calculated (at ~10^{-13} s) using Monte Carlo simulations for (a) H^{+} (0.15 MeV), (b) $^{4}He^{2+}$ (1.75 MeV/nucleon), (c) $^{12}C^{6+}$ (25.5 MeV/nucleon), and (d) $^{20}Ne^{10+}$ (97.5 MeV/nucleon) impacting ions. Ions are generated at the origin and along the *Y* axis in liquid water under *identical* LET conditions (~70 keV/μm). Dots represent the energy deposited at points where an interaction occurred. From MUROYA et al. (2006), with permission.

Figure 3.5 illustrates typical two-dimensional representations of short (1-5 μm) track segments of H^{+}, $^{4}He^{2+}$, $^{12}C^{6+}$, and $^{20}Ne^{10+}$ ions, calculated with Monte Carlo simulations under the same LET conditions (namely, ~70 keV/μm) (MUROYA et al., 2006). As one can see, these tracks can be considered as straight lines with the ejected high-energy secondary electrons travelling to a greater average distance away from the track core as the velocity of the incident ion increases, from protons to neon ions. In other words, even though all those particles are depositing the same amount of energy per unit path length, that energy is lost in a volume that increases in the order $H^{+} < {}^{4}He^{2+} < {}^{12}C^{6+} < {}^{20}Ne^{10+}$. This indicates that the higher-*Z* particles (where *Z* is the ion charge number) have the lower mean density of reactive species (MUROYA et al., 2006; MEESUNGNOEN & JAY-GERIN, 2011). The fact that tracks of different ions with the

same LET have different radial distributions of energy deposited by δ-rays therefore indicates that the LET is not a unique descriptor of the radiation chemical effects within heavy-charged particle tracks (SCHULER & ALLEN, 1957; SAUER et al., 1977; LAVERNE & SCHULER, 1987; KAPLAN & MITEREV, 1987; FERRADINI, 1990; FERRADINI & JAY-GERIN, 1999; LAVERNE, 2000, 2004) (see the Discussion Chapter 7, Sect. 7.1). Attempts have been made to introduce other comparative characteristics of radiation track effects to replace the LET. Let us mention, for example, the $(Z^*/\beta)^2$ factor (where Z^* is an energy-dependent effective charge of the ion and β is the ratio of its velocity to that of light) (KATZ, 1970; WALIGÓRSKI et al., 1986; YAMASHITA et al., 2008) or yet the parameter MZ^2/E (where M is the ion mass and $E = ½MV^2$ its kinetic energy) (LAVERNE, 2004). Several sets of radiation chemical data appear to be better unified using these phenomenological parameters instead of the LET, others do not. Following PIMBLOTT & LAVERNE (2002), it should be recognized, however, that no deterministic parameterization can realistically represent a phenomenon that is stochastic in nature. Nevertheless, despite its limitations, the LET still remains the most useful single parameter in the radiation chemistry of heavy ions.

3.2 The "physicochemical" stage

The ions and excited-state water molecules formed during the physical stage are extremely unstable and undergo fast reorganization in this second or physicochemical stage, which lasts not more than ~10^{-12} s after the initial energy deposition. These processes produce radical and molecular products of the radiolysis that are distributed in a highly nonhomogeneous track structure.

In the time scale of ~40-200 fs (MARSALEK et al., 2011; LI et al., 2013), the positive ion (also called cationic "hole") $H_2O^{\bullet+}$ decomposes to form an $^{\bullet}OH$ radical by transferring a proton to a neighboring water molecule:

$$H_2O^{\bullet+} + H_2O \rightarrow H_3O^+ + {}^{\bullet}OH, \qquad [5]$$

where H_3O^+ represents the hydrated proton. However, before reaction [5] occurs, $H_2O^{\bullet+}$ may undergo a random walk via a sequence of resonant electron transfers (about 21, on

the average) from neighboring water molecules to the $H_2O^{\bullet+}$ hole (or electron-loss center) (OGURA & HAMILL, 1973; MOZUMDER & MAGEE, 1975). The ranges of a migrating hole are a few molecular diameters (COBUT et al., 1998).

The secondary ("dry") electron ejected from an ionized water molecule undergoes scattering as it moves away from its parent cation. It can cause further ionization and excitation to occur if it has sufficient kinetic energy. Eventually, its energy falls below the first electronic excitation threshold of water (~7.3 eV), forming the so-called "subexcitation electron" (e^-_{sub}) (PLATZMAN, 1955). The latter loses the rest of its energy relatively slowly by exciting vibrational and rotational modes of water molecules. Once it is thermalized (e^-_{th}) (after ~10-40 fs at 25 °C; see: GOULET et al., 1990, 1996; MEESUNGNOEN et al., 2002*b*), it can readily become localized or "trapped" in a pre-existing potential energy well of appropriate depth in the liquid. It then forms the so-called "wet" electron whose exact physicochemical nature is still the subject of investigation, before reaching a fully relaxed, hydrated state (e^-_{aq}) as the dipoles of the surrounding molecules orient in response to the negative charge of the electron. In liquid water at room temperature, *thermalization*, *trapping*, and *hydration* can then follow in quick succession on the time scale of ~240 fs-1 ps, as revealed from time-resolved femtosecond laser spectroscopic studies (MOZUMDER, 1999; MEESUNGNOEN & JAY-GERIN, 2011):

$$e^- \rightarrow e^-_{sub} \rightarrow e^-_{th} \rightarrow e^-_{tr} \rightarrow e^-_{aq} . \qquad [6]$$

In the course of its thermalization, the slowing-down electron can be recaptured by its parent cation (prior to the occurrence of reaction [5]) due to the Coulomb attraction of the latter which tends to draw them back together to undergo electron-cation geminate recombination:

$$e^-_{aq} + H_2O^{\bullet+} \rightarrow H_2O^* . \qquad [7]$$

As the electron is recaptured, the parent ion is transformed into an excited neutral molecule.

In the course of its thermalization, the ejected electron can also be temporarily captured *resonantly* by a water molecule to form a transient molecular anion:

$$e^- + H_2O \rightarrow H_2O^{\bullet -} . \qquad [8]$$

This anion then undergoes dissociation mainly into H^- and $^\bullet OH$ according to

$$H_2O^{\bullet -} \rightarrow H^- + {}^\bullet OH , \qquad [9]$$

followed by the reaction of the hydride anion (H^-) with another water molecule through a fast proton transfer reaction:

$$H^- + H_2O \rightarrow H_2 + OH^- . \qquad [10]$$

Reactions [8]-[10] correspond to the so-called "dissociative electron attachment" or DEA process, which has been observed in amorphous solid water at ~20 K for electron energies between about 5 and 12 eV (ROWNTREE et al., 1991). DEA was suggested to be responsible, at least in part, for the yield of "nonscavengeable" molecular hydrogen observed experimentally in the radiolysis of liquid water at early times (PLATZMAN, 1962*b*; FARAGGI & DÉSALOS, 1969; GOULET & JAY-GERIN, 1989; KIMMEL et al., 1994; COBUT et al., 1996; MEESUNGNOEN et al., 2015). Experiments by PASTINA et al. (1999) have sustained this proposed mechanism for the production of H_2, by showing that the previously accepted nonscavengeable yield of H_2 is due to the precursors to e^-_{aq} (i.e., electrons prior to their hydration) and it can be lowered with suitable pre-hydrated electron scavengers in sufficiently high concentrations. Most recently, however, this mechanism has been challenged by STERNICZUK & BARTELS (2016) whose experiments have allowed them to suggest that the formation of H_2 in the subpicosecond physicochemical stage of track evolution is dominated by electron-hole charge recombination events of nearly thermalized, not yet trapped electrons (e^-_{th}) (see reactions [7] and [11*b*]) rather than by DEA. In view of the fact that this subject has been controversial for so many years, further experiments are needed to confirm this conclusion.

Excited water molecules can be produced either directly in an initial act (reaction [4]) or by electron-cation geminate recombination (reaction [7]). Very little is known about the decay channels for an electronically/vibrationally excited water molecule in the liquid phase and the branching ratios associated with each of them. Fortunately, the contribution of the water excited states to the primary radical and molecular products in

water radiolysis is of relatively minor importance in comparison with that of the ionization processes, so that the lack of information about their decomposition has only limited consequences. Hence, the competing de-excitation mechanisms of H_2O^* are generally assumed to be essentially the same as those reported for an *isolated* water molecule, namely (for example, see: SWIATLA-WOJCIK & BUXTON, 1995; COBUT *et al.*, 1998; MEESUNGNOEN & JAY-GERIN, 2005; SANGUANMITH et al., 2011):

$$H_2O^* \rightarrow H^\bullet + {}^\bullet OH \qquad [11a]$$

$$H_2O^* \rightarrow H_2 + O(^1D) \qquad [11b]$$

$$H_2O^* \rightarrow 2H^\bullet + {}^\bullet O^\bullet(^3P) \qquad [11c]$$

$$H_2O^* \rightarrow H_2O + \text{release of thermal energy} , \qquad [11d]$$

where $O(^1D)$ and ${}^\bullet O^\bullet(^3P)$ represent the oxygen atom in its singlet ^1D first excited state and triplet ^3P ground state, respectively (see Fig. 3.1). Specific to the liquid phase, the following dissociation reaction:

$$H_2O^* \rightarrow e^-_{aq} + H_2O^{\bullet+} \qquad [11e]$$

also needs to be considered in the menu of possibilities that can lead to the decay of H_2O^*. Its threshold is at ~6.5 eV (NIKOGOSYAN et al., 1983; MIGUS et al., 1987; BERNAS et al., 1997).

It is believed that reaction [11*a*] is the main source of the "initial" (i.e., at $\sim 10^{-12}$ s, prior to spur/track expansion) yield of hydrogen atoms. Note also that the $O(^1D)$ atoms produced in reaction [11*b*] react very efficiently with water to form H_2O_2 (or probably also $2{}^\bullet OH$) (TAUBE, 1957; BIEDENKAPP et al., 1970). By contrast, the ground-state ${}^\bullet O^\bullet(^3P)$ atoms in aqueous solution are rather inert to water but react with most additives (AMICHAI & TREININ, 1969). As for the values of the branching ratios (or decay probabilities) used for the different decay channels [11*a-e*], they are chosen in such a way that the calculated yields consistently match the observed picosecond *G*-values of the various spur species (MUROYA *et al.*, 2002; MEESUNGNOEN & JAY-GERIN, 2005).

By ~1 ps following the passage of the radiation, the various initial radiolysis products are: e^-_{aq}, $H^\bullet$, H_2, ${}^\bullet OH$, H_2O_2, H^+ (or H_3O^+), OH^-, $O_2^{\bullet-}$ (or $HO_2^\bullet$, depending on the pH), ${}^\bullet O^\bullet(^3P)$, etc. At this time, these species begin to diffuse away from the position

where they were originally produced. The result is that a fraction of them react together within the spurs/tracks as they develop in time while the remainder escape into the bulk solution in the chemical stage.

3.3 The "chemical" stage

The third or chemical stage consists of diffusion and reactions of the reactive species present at the end of the physicochemical stage of spur/track evolution and leading to the reestablishment of chemical equilibrium. As stated above, the various "initial" decomposition products present at ~1 ps are distributed nonhomogeneously with high concentrations in the center of spurs or along the axis of tracks. These species then proceed to diffuse away from the site where they were originally produced according to macroscopic diffusion laws and to react with themselves or with dissolved solutes (if any) present at the time of irradiation. This stage is usually divided into two parts. The first part corresponds to the stage of "nonhomogeneous chemistry", which consists of the period during which spurs or tracks develop in time. A number of radicals will combine to form the molecular products H_2 and H_2O_2 and to re-form H_2O, while the remainder will diffuse out into the bulk of the solution. Table 3.1 gives the set of reactions that are likely to occur while the spurs/tracks expand. At 25 °C, this expansion is essentially complete by ~10^{-7}-10^{-6} s (for example, see: BUXTON et al., 1987; SANGUANMITH et al., 2012). By this time, the species that have escaped from spur or track reactions become homogeneously distributed throughout the bulk solution (i.e., the system at large) and the track of the radiation no longer exists (PLANTE et al., 2005; MUROYA et al., 2006; BOSCOLO et al., 2018). Beyond a few microseconds, the reactions that occur in the bulk solution can usually be described with conventional homogeneous chemistry methods (PASTINA & LAVERNE, 2001). This is the second part of the chemical stage, the so-called stage of "homogeneous chemistry". The radical and molecular products which emerge from the spurs/tracks are then available to react with solutes (treated as spatially homogeneous) present in low or moderate concentrations.

At homogeneity, the radiolysis of liquid water can thus be described by the following *global* reaction, traditionally given for low-LET radiation (e.g., ^{60}Co γ-rays,

Table 3.1 – Main reaction scheme and rate constants (k) in the radiolysis of liquid water at 25 °C (MEESUNGNOEN & JAY-GERIN, 2011; ELLIOT & BARTELS, 2009)

Reaction	k (M^{-1} s^{-1})	Reaction	k (M^{-1} s^{-1})
$H^{\bullet} + H^{\bullet} \rightarrow H_2$	5.2×10^{9}	$e^{-}_{aq} + e^{-}_{aq} \rightarrow H_2 + 2\ OH^{-}$	7.3×10^{9}
$H^{\bullet} + {}^{\bullet}OH \rightarrow H_2O$	1.6×10^{10}	$e^{-}_{aq} + H^{+} \rightarrow H^{\bullet}$	2.1×10^{10}
$H^{\bullet} + H_2O_2 \rightarrow H_2O + {}^{\bullet}OH$	3.6×10^{7}	$e^{-}_{aq} + O_2^{\bullet-} \rightarrow H_2O_2 + 2\ OH^{-}$	1.3×10^{10}
$H^{\bullet} + e^{-}_{aq} \rightarrow H_2 + OH^{-}$	2.8×10^{10}	$e^{-}_{aq} + HO_2^{-} \rightarrow O^{\bullet-} + OH^{-}$	3.51×10^{9}
$H^{\bullet} + OH^{-} \rightarrow H_2O + e^{-}_{aq}$	2.4×10^{7}	$e^{-}_{aq} + O^{\bullet-} \rightarrow 2\ OH^{-}$	2.31×10^{10}
$H^{\bullet} + O_2 \rightarrow HO_2^{\bullet}$	1.3×10^{10}	$e^{-}_{aq} + H_2O \rightarrow H^{\bullet} + OH^{-}$	15.8
$H^{\bullet} + HO_2^{\bullet} \rightarrow H_2O_2$	1.1×10^{10}	$e^{-}_{aq} + O_2 \rightarrow O_2^{\bullet-}$	2.3×10^{10}
$H^{\bullet} + O_2^{\bullet-} \rightarrow HO_2^{-}$	1.1×10^{10}	$e^{-}_{aq} + HO_2^{\bullet} \rightarrow HO_2^{-}$	1.3×10^{10}
$H^{\bullet} + HO_2^{-} \rightarrow {}^{\bullet}OH + OH^{-}$	1.5×10^{9}	$e^{-}_{aq} + O(^3P) \rightarrow O^{\bullet-}$	2.0×10^{10}
$H^{\bullet} + O(^3P) \rightarrow {}^{\bullet}OH$	2.0×10^{10}	$e^{-}_{aq} + O_3 \rightarrow O_3^{\bullet-}$	3.6×10^{10}
$H^{\bullet} + O^{\bullet-} \rightarrow OH^{-}$	2.0×10^{10}	$H^{+} + O^{\bullet-} \rightarrow {}^{\bullet}OH$	5.0×10^{10}
$H^{\bullet} + O_3 \rightarrow O_2 + {}^{\bullet}OH$	3.7×10^{10}	$H^{+} + O_2^{\bullet-} \rightarrow HO_2^{\bullet}$	5.0×10^{10}
$H^{\bullet} + O_3^{\bullet-} \rightarrow OH^{-} + O_2$	1.0×10^{10}	$H^{+} + OH^{-} \rightarrow H_2O$	1.2×10^{11}
${}^{\bullet}OH + {}^{\bullet}OH \rightarrow H_2O_2$	6.3×10^{9}	$H^{+} + O_3^{\bullet-} \rightarrow {}^{\bullet}OH + O_2$	9.0×10^{10}
${}^{\bullet}OH + H_2O_2 \rightarrow HO_2^{\bullet} + H_2O$	2.9×10^{7}	$H^{+} + HO_2^{-} \rightarrow H_2O_2$	5.0×10^{10}
${}^{\bullet}OH + H_2 \rightarrow H^{\bullet} + H_2O$	4.0×10^{7}	$OH^{-} + O(^3P) \rightarrow HO_2^{-}$	4.2×10^{8}
${}^{\bullet}OH + e^{-}_{aq} \rightarrow OH^{-}$	3.6×10^{10}	$OH^{-} + HO_2^{\bullet} \rightarrow O_2^{\bullet-} + H_2O$	1.3×10^{10}
${}^{\bullet}OH + OH^{-} \rightarrow O^{\bullet-} + H_2O$	1.3×10^{10}	$O_2 + O^{\bullet-} \rightarrow O_3^{\bullet-}$	3.7×10^{9}
${}^{\bullet}OH + HO_2^{\bullet} \rightarrow O_2 + H_2O$	9.0×10^{9}	$O_2 + O(^3P) \rightarrow O_3$	4.0×10^{9}
${}^{\bullet}OH + O_2^{\bullet-} \rightarrow O_2 + OH^{-}$	1.1×10^{10}	$HO_2^{\bullet} + O_2^{\bullet-} \rightarrow HO_2^{-} + O_2$	9.7×10^{7}
${}^{\bullet}OH + HO_2^{-} \rightarrow HO_2^{\bullet} + OH^{-}$	8.3×10^{9}	$HO_2^{\bullet} + HO_2^{\bullet} \rightarrow H_2O_2 + O_2$	1.94×10^{8}
${}^{\bullet}OH + O(^3P) \rightarrow HO_2^{\bullet}$	2.02×10^{10}	$HO_2^{\bullet} + O(^3P) \rightarrow O_2 + {}^{\bullet}OH$	2.02×10^{10}
${}^{\bullet}OH + O^{\bullet-} \rightarrow HO_2^{-}$	1.0×10^{9}	$HO_2^{\bullet} + H_2O \rightarrow H^{+} + O_2^{\bullet-}$	1.4×10^{4}
${}^{\bullet}OH + O_3^{\bullet-} \rightarrow O_2^{\bullet-} + HO_2^{\bullet}$	8.5×10^{9}	$O_2^{\bullet-} + O^{\bullet-} \rightarrow O_2 + 2\ OH^{-}$	6.0×10^{8}
${}^{\bullet}OH + O_3 \rightarrow O_2 + HO_2^{\bullet}$	1.11×10^{8}	$O_2^{\bullet-} + H_2O \rightarrow HO_2^{\bullet} + OH^{-}$	0.155
$H_2O_2 + e^{-}_{aq} \rightarrow OH^{-} + {}^{\bullet}OH$	1.1×10^{10}	$O_2^{\bullet-} + O_3 \rightarrow O_3^{\bullet-} + O_2$	1.5×10^{9}
$H_2O_2 + OH^{-} \rightarrow HO_2^{-} + H_2O$	1.33×10^{10}	$HO_2^{-} + H_2O \rightarrow H_2O_2 + OH^{-}$	1.27×10^{6}
$H_2O_2 + O(^3P) \rightarrow HO_2^{\bullet} + {}^{\bullet}OH$	1.6×10^{9}	$HO_2^{-} + O^{\bullet-} \rightarrow O_2^{\bullet-} + OH^{-}$	8.02×10^{8}
$H_2O_2 + O^{\bullet-} \rightarrow HO_2^{\bullet} + OH^{-}$	5.55×10^{8}	$HO_2^{-} + O(^3P) \rightarrow O_2^{\bullet-} + {}^{\bullet}OH$	5.3×10^{9}
$H_2 + O(^3P) \rightarrow H^{\bullet} + {}^{\bullet}OH$	4.77×10^{3}	$O^{\bullet-} + O^{\bullet-} \rightarrow H_2O_2 + 2\ OH^{-}$	1.0×10^{8}
$H_2 + O^{\bullet-} \rightarrow H^{\bullet} + OH^{-}$	1.3×10^{8}	$O^{\bullet-} + O_3^{\bullet-} \rightarrow 2\ O_2^{\bullet-}$	7.0×10^{8}
$O(^3P) + O(^3P) \rightarrow O_2$	2.2×10^{10}	$O^{\bullet-} + H_2O \rightarrow {}^{\bullet}OH + OH^{-}$	1.3×10^{6}
$O(^3P) + H_2O \rightarrow 2\ {}^{\bullet}OH$	1.9×10^{3}	$O_3^{\bullet-} + H_2O \rightarrow O^{\bullet-} + O_2$	46.5

fast electrons or high-energy protons) and for an absorbed energy of 100 eV (FERRADINI & JAY-GERIN, 1999):

$$g(\text{-}H_2O)\, H_2O \rightsquigarrow g(e^-_{aq})\, e^-_{aq} + g(H^\bullet)\, H^\bullet + g(^\bullet OH)\, ^\bullet OH + g(H^+)\, H^+ + g(OH^-)\, OH^- + g(H_2)\, H_2 + g(H_2O_2)\, H_2O_2 + \ldots, \qquad [12]$$

where the coefficients $g(X)$ are the so-called "primary" (or "escape") radical and molecular yields, representing the numbers of the various radiolytic species that remain throughout the bulk of the solution at the end of the nonhomogeneous chemical stage (i.e., after spur expansion). At this stage, $g(\text{-}H_2O)$ denotes the corresponding number of water molecules dissociated per 100 eV energy absorbed. We should note here that the term *g*-value is reserved for the primary yields of the species indicated after they have escaped the spurs. Other symbols have been used in the past for the primary yields, the most common one being G_X (symbol G with the formula of the species as subscript) (SPINKS & WOODS, 1990). The term *G*-value always refers to the measured yield of an experiment, given in the form G(product).

Throughout this thesis, radiation chemical yields are given in the traditional units of molecules per 100 eV. For conversion into SI units (mol/J), 1 molecule/100 eV ≈ 0.10364 μmol/J (FERRADINI & JAY-GERIN, 1999, 2000).

4. THE FERROUS SULFATE (OR FRICKE) DOSIMETER

Shortly after the discovery of X-rays (RÖNTGEN, 1895), radioactivity (BECQUEREL, 1986), polonium (CURIE & CURIE, 1898*a*) and radium (CURIE et al., 1898*b*), a number of applications came out to "solve and enhance" lifestyle. Radioactive toothpaste, rejuvenating creams and soaps are just a few examples of the usage of radiation at the beginning. However, the deleterious effects of ionizing radiation were soon recognized. In particular, to guard against the injurious effects of radiation in medical application, dose-measuring methods were considered necessary.

The interest in the chemical effects of ionizing radiation in the 1920's stemmed from the extensive radiobiological research that was conducted owing to the expanded application of higher-energy X-ray machines in medicine and in industry. Although several dosimetry systems were already in use (CHORZEMPA, 1971), the one that proved most reliable was the ferrous sulfate system, first studied by FRICKE & MORSE (1927, 1929). The chemical reaction that serves as the basis for this dosimeter is the oxidation of ferrous (Fe^{2+}) to ferric (Fe^{3+}) ions, in aerated, dilute sulfuric acid (see below). The concentration of ferric ions is generally determined by absorption spectroscopy as irradiation causes an increase in the optical density (OD) of the solution. The relationship between the absorbed dose to the Fricke solution and the ferric-ion yield, $G(Fe^{3+})$, is given by (for example, see: KLASSEN et al., 1999):

$$D = \frac{\Delta(\mathrm{OD})}{\varepsilon\, G(\mathrm{Fe}^{3+})\, \rho\, d}, \qquad [13]$$

where Δ(OD) is the increase in the optical density of the Fricke solution due to irradiation, ρ is the density of the Fricke solution (1.0227 g/cm^3), ε is the molar absorptivity of Fe^{3+} at the wavelength of 304 nm (2174 M^{-1} cm^{-1}), and d is the length of the light path.

Nowadays, the "Fricke dosimeter" is certainly the best understood, and the most commonly used, liquid chemical dosimeter (FRICKE & HART, 1966; DAS, 1971; MATTHEWS, 1982; SPINKS & WOODS, 1990; TIPPAYAMONTRI et al., 2009). It is widely accepted as a standard in radiation chemistry and in many practical applications of

ionizing radiations because of the accuracy, reproducibility, and linearity of its response as a function of dose. With care, one may measure dose in absolute units to an accuracy of the order of 0.1% (KLASSEN et al., 1999; ICRU REPORT 34). The normal dose range of the dosimeter is 20 to 400 Gy with usual γ- or electron irradiations.

The standard Fricke solution consists of 1 m*M* $FeSO_4$ in 0.4 *M* H_2SO_4 (pH 0.46) and is saturated with air (the O_2 concentration is ~0.25 m*M*). The mechanism for the radiolytic oxidation of Fe^{2+} ions to Fe^{3+} is well-understood and the rate constants at 25 °C of the individual reactions taking place are known (ALLEN, 1961; FRICKE & HART, 1966; SPINKS & WOODS, 1990; BĚGUSOVÁ & PIMBLOTT, 2002; AUTSAVAPROMPORN et al., 2007; TIPPAYAMONTRI et al., 2009; MEESAT et al., 2012). The major reactions for ferric ion production in a Fricke solution are:

$$e^-_{aq} + H^+ \rightarrow H^\bullet \qquad k_{14} = 2.1 \times 10^{10}\ M^{-1}\ s^{-1} \qquad [14]$$

$$H^\bullet + O_2 \rightarrow HO_2^\bullet \qquad k_2 = 2.1 \times 10^{10}\ M^{-1}\ s^{-1} \qquad [2]$$

$$^\bullet OH + Fe^{2+} \rightarrow Fe^{3+} + OH^- \qquad k_{15} = 3.4 \times 10^{8}\ M^{-1}\ s^{-1} \qquad [15]$$

$$HO_2^\bullet + Fe^{2+} \rightarrow Fe^{3+} + HO_2^- \qquad k_{16} = 7.9 \times 10^{5}\ M^{-1}\ s^{-1} \qquad [16]$$

$$HO_2^- + H^+ \rightarrow H_2O_2 \qquad k_{17} = 5.0 \times 10^{10}\ M^{-1}\ s^{-1} \qquad [17]$$

$$H_2O_2 + Fe^{2+} \rightarrow Fe^{3+} + {}^\bullet OH + OH^- \qquad k_{18} = 52\ M^{-1}\ s^{-1} \qquad [18]$$

$$H^\bullet + Fe^{2+} \xrightarrow{H^+} Fe^{3+} + H_2 \qquad k_{19} = 1.3 \times 10^{7}\ M^{-1}\ s^{-1}. \qquad [19]$$

At the acid concentration of 0.4 *M* H_2SO_4, the H^+ ions very rapidly scavenge most, if not all, of the e^-_{aq} radicals in spurs to form $H^\bullet$ atoms (FERRADINI & JAY-GERIN, 2000). In the presence of oxygen, each $H^\bullet$ atom reacts with O_2 to give a hydroperoxyl radical $HO_2^\bullet$, and each of these radicals oxidizes three Fe^{2+} ions. Each $^\bullet OH$ radical oxidizes one Fe^{2+} ion, and each molecule of H_2O_2 oxidizes two Fe^{2+} ions. Summing all sources of Fe^{3+} ions, the yield of ferric ions in *aerated* solution can be expressed in terms of the "escape" yields of the free radicals and molecular species of the radiolysis of the solution by the following stoichiometric equation (ALLEN, 1961; FRICKE & HART, 1966; SPINKS & WOODS, 1990):

$$G(Fe^{3+})_{aerated} = 3\,g(e^-_{aq} + H^\bullet) + g(^\bullet OH) + 2\,g(H_2O_2) + 3\,g(HO_2^\bullet), \qquad [20]$$

where $g(e^-_{aq} + H^\bullet)$ represents the sum of the primary yields of the reducing radicals e^-_{aq} and $H^\bullet$. Note that some $H^\bullet$ atoms may also directly react with Fe^{2+} (reaction [19]). However, at 25 °C and a ferrous ion concentration of 1 m*M*, the contribution of this reaction to the formation of Fe^{3+} can be neglected. Note also that, for solutions of 0.4 *M* in H_2SO_4, there is a small amount of $^\bullet OH$ radicals that react with HSO_4^- to form the sulfate radical $SO_4^{\bullet -}$ according to (JIANG et al., 1992; MEESUNGNOEN et al., 2001)

$$^\bullet OH + HSO_4^- \rightarrow H_2O + SO_4^{\bullet -} \quad k_{21} = 1.5 \times 10^5\ M^{-1}\ s^{-1}. \qquad [21]$$

However, the overall ferric ion yield remains the same as given by equation [20] since the sulfate radical reacts with Fe^{2+} in the same way as $^\bullet OH$ (NETA et al., 1988):

$$SO_4^{\bullet -} + Fe^{2+} \rightarrow Fe^{3+} + SO_4^{2-} \qquad [22]$$

with $k_{22} = 9.9 \times 10^8\ M^{-1}\ s^{-1}$ (in the limit of infinite dilution). For ^{60}Co γ-irradiated 0.4 *M* H_2SO_4 aqueous solutions, the escape yields of free radicals and molecular products are well determined. Most representative values at a reference temperature of 25 °C are (FERRADINI & JAY-GERIN, 2000):

$$\left.\begin{array}{lll} g(e^-_{aq} + H^\bullet) = 3.70 & g(H_2) = 0.40 & g(HO_2^\bullet) = 0.02 \\ g(^\bullet OH) = 2.90 & g(H_2O_2) = 0.80\ . & \end{array}\right\} \qquad [23]$$

Using these primary radiolytic yield values in equation [20] leads to a value for the yield of Fe^{3+}, which is well within the range of 1-2% of the recommended yield of 15.5 ± 0.2 ions/100 eV reported in the literature for ^{60}Co γ-radiation (ICRU REPORT 34, 1982). Interestingly, note that more accurate ^{60}Co γ-ray Fricke *G*-value measurements have been reported recently. Let us mention in particular those of $G(Fe^{3+})$ = 15.56 (±0.3%) (KLASSEN et al., 1999) and 15.53 (±0.5%) (McEWEN et al., 2014) obtained by the Ionizing Radiation Standards group at the National Research Council of Canada.

5. MONTE CARLO TRACK CHEMISTRY SIMULATIONS

The "Monte Carlo method" is a general term (named after the famous European gambling center in Monaco) used to describe any computational algorithm that employs repeated random sampling to obtain means of probabilistic features of models that we cannot compute analytically. If the probability law for the elementary processes of the relevant phenomenon is known, these processes are generated on the computer as if they actually occur and the behavior of the whole system is investigated. Thus, Monte Carlo simulation is able to reproduce faithfully the phenomenon without any approximation. The concept was first popularized right after World War II, to study nuclear fission. Today there are multiple types of Monte Carlo simulations, used in fields from particle physics to engineering, finance and more (for example, see: TURNER et al., 2012; NIKJOO et al., 2012; HAGHIGHAT, 2015).

Because of the stochastic nature of radiation, the complex sequence of events that follow absorption in liquid water of ionizing radiation can be modeled successfully by the use of Monte Carlo methods. Such a procedure allows one to reconstruct the intricate action of the radiation and to study the relationship between the initial track structure and the ensuing chemical processes that occur in the radiolysis of both pure water and water-containing solutes (for a comprehensive list and reviews, see, for example: BALLARINI et al., 2000; UEHARA & NIKJOO, 2006; KREIPL et al., 2009; MEESUNGNOEN & JAY-GERIN, 2011); KARAMITROS et al., 2011; BOSCOLO et al., 2018). Two main approaches have been widely used: (1) the "step-by-step" (or "random flights" Monte Carlo simulation) method, in which the trajectories of the diffusing species of the system are modeled by time-discretized random flights and in which reaction occurs when reactants undergo pair wise encounters, and (2) the "independent reaction times" (IRT) method (CLIFFORD et al., 1986; PIMBLOTT et al., 1991; PIMBLOTT & GREEN, 1995), which allows the calculation of reaction times without having to follow the trajectories of the diffusing species. Of these two approaches, the most reliable is certainly the full random flights simulation, which is generally considered a measure of reality. However, this method can be exceedingly consuming in computer time when large systems (such as complete radiation tracks or track segments) are studied. The IRT

method, a computer efficient stochastic simulation technique, has been devised to achieve much faster realisation than are possible with the full Monte-Carlo model. In essence, it relies on the approximation that the distances between pairs of reactants evolve independently of each other, and therefore the reaction times of the various potentially reactive pairs are independent of the presence of other reactants in the system.

In a program begun in 1988, our Sherbrooke group developed and progressively refined with very high levels of detail several Fortran-based Monte Carlo computer codes that simulate the radiolysis of liquid water by fast electrons, high energy protons, and accelerated light and heavy ions (COBUT, 1993; COBUT et al., 1998; FRONGILLO et al., 1998; MUROYA et al., 2002, 2006; PLANTE, 2009; TIPPAYAMONTRI et al., 2009; MEESUNGNOEN and JAY-GERIN, 2005, 2011). Since their introduction in 1993, these codes have been continuously upgraded to take advantage of the availability of new experimental or theoretical advances from the literature and extended largely driven by practical applications. In the present work, we have used the most recent version of the Sherbrooke codes, known as IONLYS-IRT. A detailed description of the IONLYS-IRT program (illustrated schematically in Fig. 5.1) and its implementation have already been reported (COBUT et al., 1998; FRONGILLO et al., 1998; MEESUNGNOEN and JAY-GERIN, 2005, 2011; SANGUANMITH et al., 2011) and will not be reproduced here. Only a brief overview of the most essential features of the simulation methodology and reaction scheme, pertinent to the current calculations, is given below.

The IONLYS simulation program covers the early "physical" and "physicochemical" stages of radiation action up to ~1 ps. It models, event by event, all the basic physical interactions (energy deposition) and the subsequent establishment of thermal equilibrium in the system (conversion of the physical products created locally after completion of the physical stage into the various initial radical and molecular products of the radiolysis, which are distributed in a highly nonhomogeneous track structure). The complex spatial distribution of reactants at the end of the physicochemical stage [namely, e^-_{aq}, $H^\bullet$, H_2, $^\bullet OH$, H_2O_2, H^+ (or H_3O^+), OH^-, $O_2^{\bullet-}$ (or $HO_2^\bullet$, depending on pH), $^\bullet O^\bullet(^3P)$, etc.; see above], which is provided as an output of the IONLYS program, is then used directly as the starting point for the subsequent

"nonhomogeneous chemical" stage (from ~1 ps to ~0.1-1 μs at room temperature). This third stage, during which the individual reactive species diffuse randomly at rates determined by their diffusion coefficients and react with one another or, competitively, with any added solutes present at the time of irradiation until all spur processes are complete, is covered by our IRT program. This IRT program can obviously also be used efficiently to describe the "homogeneous" chemical stage that takes place at longer times, as is precisely the case in this study for the simulation of the Fricke dosimeter in which ferric ions are produced at a wide variety of times (BĚGUSOVÁ & PIMBLOTT, 2002; AUTAVAPROMPORN et al., 2007; TIPPAYAMONTRI et al., 2009; MEESAT et al., 2012). This program employs the IRT method whose implementation has been described in detail (FRONGILLO et al., 1998; HERVÉ DU PENHOAT et al., 2000). The ability of this program to give accurate time-dependent chemical yields under different irradiation conditions has been well validated by comparison with full random flights (or "step-by-step") Monte Carlo simulations (GOULET et al., 1998; PLANTE, 2009).

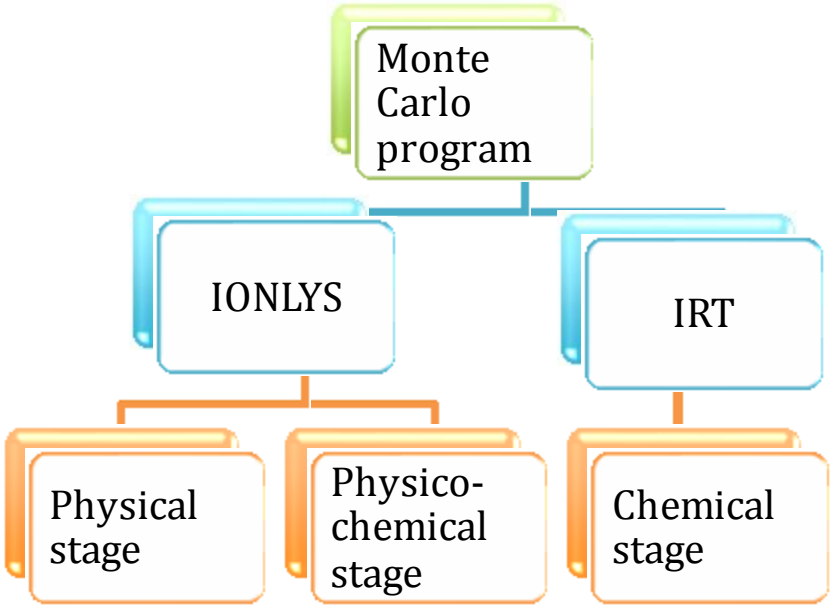

Figure 5.1 – Diagram of the Monte Carlo computer program developed by the group in radiation chemistry of the Université de Sherbrooke and used in the present study.

The model assumptions and procedures employed to carry out the Monte-Carlo simulations of the radiolysis of 0.4 *M* H_2SO_4 aqueous solutions with IONLYS-IRT have already been given (AUTSAVAPROMPORN et al., 2007; TIPPAYAMONTRI et al., 2009). To summarize briefly, the effects of the background concentration of H^+ in solutions were added to the IRT program as pseudo first-order reactions. We also supplemented the reaction scheme for the radiolysis of pure liquid water (see Table 3.1) to include the reactions listed in Table 5.1, which account for the species (HSO_4^-, SO_4^{2-}, $SO_4^{\bullet -}$, and $S_2O_8^{2-}$) present in irradiated sulfuric acid solutions (MEESAT et al., 2012).

Table 5.1 – Reactions added to the pure water reaction scheme to simulate the radiolysis of aqueous H_2SO_4 solutions, at 25 °C (AUTSAVAPROMPORN et al., 2012). The rate constants given here for the reactions between ions are in the limit of zero ionic strength (i.e., at infinite dilution of ions).

Reaction	k (M^{-1} s^{-1})
$H^\bullet + SO_4^{\bullet -} \rightarrow HSO_4^-$	1.0×10^{10}
$H^\bullet + S_2O_8^{2-} \rightarrow SO_4^{\bullet -} + HSO_4^-$	2.5×10^{7}
$^\bullet OH + HSO_4^- \rightarrow H_2O + SO_4^{\bullet -}$	1.5×10^{5}
$e^-_{aq} + S_2O_8^{2-} \rightarrow SO_4^{\bullet -} + SO_4^{2-}$	1.2×10^{10}
$H_2O_2 + SO_4^{\bullet -} \rightarrow HO_2^\bullet + HSO_4^-$	1.2×10^{7}
$OH^- + SO_4^{\bullet -} \rightarrow {}^\bullet OH + SO_4^{2-}$	8.3×10^{7}
$SO_4^{\bullet -} + SO_4^{\bullet -} \rightarrow S_2O_8^{2-}$	4.4×10^{8}

To stochastically model the chemistry of the Fricke dosimeter (see Chapter 4), we added to the IRT program the reactions (3), (4), and (6) of Fe^{2+} ions with the oxidizing species $^\bullet OH$, $HO_2^\bullet$, and H_2O_2 that are formed in the water of the irradiated solutions under *aerated* conditions, respectively. Under normal irradiation conditions, the concentrations of radiolytic products are low compared with the background concentrations of Fe^{2+} ions and O_2 (~0.25 m*M*) in solution, so that their reactions could also be modeled in the IRT program as pseudo first-order. Finally, to simulate the radiolysis of the aerated Fricke dosimeter in the presence of cystamine, we supplemented the ferrous-sulfate Fricke

dosimeter reaction scheme to include the 27 reactions listed in Table 5.2. This set of reactions is proposed here to account for the experimental values of the Fe^{3+} ion yield as a function of the concentration of added cystamine, in the presence of oxygen.

Table 5.2 – Chemical reactions and rate constants used in simulations of the radiolysis of cystamine (RSSR) in the Fricke dosimeter in the presence of oxygen, at 25 °C (MEESAT et al., 2012). The rate constants quoted here for the reactions between ions are in the limit of zero ionic strength.

Symbol	Reactions	$k(M^{-1} s^{-1})$
R1	$RSSR + e^-_{aq} \rightarrow (RSSR)^{\bullet -}$	4.1×10^{10}
R2	$RSSR + H^\bullet \rightarrow RS^\bullet + RSH$	8×10^9
R3	$RSSR + {}^\bullet OH \rightarrow (RSSR)^{\bullet +} + OH^-$	1.7×10^{10}
R4	$RS^\bullet + RSH \rightarrow (RSSR)^{\bullet -} + H^+$	3.5×10^8
R5	$RS^\bullet + RS^\bullet \rightarrow RSSR$	1.5×10^9
R6	$Fe^{2+} + RS^\bullet \rightarrow Fe^{3+} + RS^-$	2.5×10^8
R7	$RS^- + H^+ \rightarrow RSH$	10^{10}
R8	$RS^\bullet + RS^- \rightarrow (RSSR)^{\bullet -}$	8×10^8
R9	$RSH + {}^\bullet OH \rightarrow RS^\bullet + H_2O$	1.7×10^{10}
R10	$RSH + H^\bullet \rightarrow RS^\bullet + H_2$	1.8×10^9
R11	$RSH + H_2O_2 \rightarrow RSOH + H_2O$	1
R12	$RS^\bullet + RSSR \rightarrow RSSSR + R^\bullet$	10^6
R13	$Fe^{3+} + (RSSR)^{\bullet -} \rightarrow Fe^{2+} + RSSR$	10^8
R14	$(RSSR)^{\bullet -} + H^+ \rightarrow RS^\bullet + RSH$	4.2×10^9
R15	$R^\bullet + O_2 \rightarrow ROO^\bullet$	2×10^9
R16	$Fe^{2+} + ROO^\bullet (+ H^+) \rightarrow Fe^{3+} + ROOH$	7.9×10^5
R17	$RS^\bullet + O_2 \rightarrow RSOO^\bullet$	2×10^9
R18	$RSOO^\bullet \rightarrow RS^\bullet + O_2$	$6.2 \times 10^5\ s^{-1}$
R19	$Fe^{2+} + RSOO^\bullet (+ H^+) \rightarrow Fe^{3+} + RSOOH$	10^7
R20	$RSSR^{\bullet -} + O_2 (+ H^+) \rightarrow RSSR + HO_2^\bullet$	5.1×10^8
R21	$RSOO^\bullet + RSH \rightarrow RSO^\bullet + RSOH$	2×10^6
R22	$Fe^{2+} + RSO^\bullet (+ H^+) \rightarrow Fe^{3+} + RSOH$	5×10^5
R23	$R^\bullet + RSH \rightarrow RH + RS^\bullet$	1.1×10^8
R24	$Fe^{2+} + RSSR^{\bullet +} \rightarrow Fe^{3+} + RSSR$	2×10^6
R25	$RSSR^{\bullet +} + RSSR^{\bullet +} \rightarrow RSSR^{2+} + RSSR$	2.5×10^9
R26	$RSSR^{\bullet +} + OH^- \rightarrow$ products	9×10^8
R27	$RSH + HO_2^\bullet \rightarrow RS^\bullet + H_2O_2$	6×10^2

In addition, we have introduced in the IRT program the effects due to the ionic strength of the solutions for all reactions between ions, except for the peculiar bimolecular self-recombination of e^-_{aq} for which there is no evidence of any ionic strength effect (SCHMIDT & BARTELS, 1995). At 25 °C, the correction to the reaction rate constants was made using the following equation (WESTON & SCHWARZ, 1972; ELLIOT et al., 1990):

$$\log\left(\frac{k}{k_0}\right) = 1.02\ Z_a Z_b \left(\frac{I^{1/2}}{1 + I^{1/2}}\right), \qquad [24]$$

where k is the rate constant at ionic strength I, k_0 is the rate constant in the limit of zero ionic strength, Z_a and Z_b are the algebraic numbers of charges on the reactants (positive for cations and negative for anions), and I (in M) is defined as (SOLOMON, 2001)

$$I = \frac{1}{2} \sum_i Z_i^{\,2} C_i\ , \qquad [25]$$

where Z_i is the charge number of the i_{th} ion and C_i is its molar concentration (the sum extends over all ionic species present in the solution). According to equation [24], the rate constants will increase, decrease, or remain the same with increasing ionic strength, depending on whether the ions have the same sign, opposite signs, or whether one species is uncharged. Finally, in our simulations the "direct" action of ionizing radiation on the various solutes (sulfuric acid anions, ferrous ions, oxygen, and cystamine) present in the solution was neglected, which is a reasonably good approximation over the range of H_2SO_4 (0.4 M)/$FeSO_4$ (1 mM)/O_2 (0.25 mM)/RSSR (5×10^{-7}-1 M) concentrations studied.

Most importantly, it should be recalled here the IONLYS-IRT code was originally devised for *protons* as primary particles (COBUT et al., 1998; FRONGILLO et al., 1998). This choice was adopted owing to the fact that protons represent, by far, the most comprehensive database of cross sections for bare ion collisions (for example, see: RUDD, 1990; TOBUREN, 2004) and because they constitute a valuable tool for studying LET effects on radiolytic yields (COBUT et al., 1998). Another great advantage of the IONLYS-IRT code is that, while it was devised for protons, it can also readily be used for heavier ion projectiles by assuming that the interaction cross-sections scale as Z^2, where Z

is the projectile charge number. In this scaling procedure, based on the lowest-order (or first Born) approximation of perturbation theories, the cross-sections for bare ion impact are approximately Z^2 times the cross-sections for proton impact *at the same velocity* (INOKUTI, 1971; ICRU REPORT 55, 1996; MEESUNGNOEN & JAY-GERIN, 2005, 2011). This simple Z^2 scaling rule, which holds at sufficiently high impact energies (>1 MeV per nucleon) where the interactions are not too strong, is useful for providing cross-sections for ionization and excitation by ion projectiles, especially as there are only very limited experimental data available involving ions heavier than proton or helium in collision with water molecules. Moreover, at the irradiating ion energies of interest in this study, interactions involving electron capture and loss by the moving ion (charge-changing collisions) have been neglected (LAVERNE, 2004; ZIEGLER et al., 2015). The effects of multiple ionizations of water under high-LET heavy-ion impact (MEESUNGNOEN & JAY-GERIN, 2005) are also ignored as their occurrence is of relatively little importance in the range of LET considered here.

The influence of the LET on the Fe^{3+} ion yields in irradiated Fricke/cystamine solutions at ambient temperature is investigated in this study by using different types of radiation, including $^{1}H^{+}$, $^{4}He^{2+}$, and $^{12}C^{6+}$ ions in the energy range of 500 MeV-150 keV per nucleon (~0.23-72.2 keV/μm) for H^{+}, 500-1 MeV per nucleon (~1-105 keV/μm) for He^{2+}, and 500-3 MeV per nucleon (~9.4-400 keV/μm) for C^{6+}. The calculations are performed with IONLYS-IRT by simulating short (~1.5-100 μm) proton (ion) track segments, over which the energy and LET of the proton (ion) are well defined and remain nearly constant. Such model calculations thus gave "track segment" yields at a well-defined LET (LAVERNE, 2004). The primary particle is simulated until it has penetrated the chosen length of the track segment into the medium. Note that, due to its large mass, the proton (or the impacting heavy ion) is almost not deflected by collisions with the target electrons. In the present simulations, these deflections are simply neglected. The number of individual proton (ion) "histories" (usually ~2-150, depending on the irradiating particle and energy) was chosen to ensure only small statistical fluctuations in the computed averages of chemical yields, while keeping acceptable computer time limits.

Finally, to reproduce the effects of ^{60}Co γ-radiolysis, we used short (typically, ~150 μm) segments of 300-MeV proton tracks, over which the average LET value obtained in the simulations was equal to ~0.3 keV/μm at 25 °C.

In the simulations reported here, the time evolution of $G(Fe^{3+})$ has been followed until ~200 s.

6. ARTICLE

Evaluation of the radioprotective ability of cystamine for 150 keV-500 MeV proton irradiation: a Monte Carlo track chemistry simulation study.

Authors: *Esteban Sepulveda*, Sunuchakan Sanguanmith, Jintana Meesungnoen and Jean-Paul Jay-Gerin

Status: *Canadian Journal of Chemistry*: Accepted (September 23, 2018)

Foreword: We present a differential study of the radioprotective effect of cystamine for irradiating protons of various energies in the range of 150 keV–500 MeV or equivalently, for LET values between ~72.2 and 0.23 keV/μm. Our goal is to better understand the mechanisms of how this compound actually works at the molecular level under high-LET irradiation conditions. The well-known radiolytic oxidation of Fe^{2+} ions to Fe^{3+} in irradiated Fricke dosimeter solutions with cystamine forms the basis for our method of radioprotective evaluation. A Monte Carlo code is used to simulate the radiation-induced chemistry of the studied Fricke/cystamine solutions while covering a wide range of cystamine concentrations. Results indicate that the protective activity of cystamine is due to its radical-capturing ability, a clear signature of the strong antioxidant profile of this compound. A main result of this study is that the protective efficiency of cystamine decreases with increasing LET, in agreement with previous experimental work.

Résumé : Nous présentons une étude sur l'effet radioprotecteur de la cystamine sous irradiations par protons de diverses énergies comprises entre 150 keV et 500 MeV, soit pour des valeurs de TEL entre 72,2 et 0,23 keV/μm. Notre but est de mieux comprendre les mécanismes par lesquelles ce composé intervient au niveau moléculaire dans des conditions d'irradiations à TEL élevé. L'oxydation radiolytique des ions Fe^{2+} en Fe^{3+} dans des solutions du dosimètre de Fricke constitue notre méthode de mesure de l'effet radioprotecteur. Un code de calcul Monte Carlo est utilisé pour simuler la chimie radio-induite des solutions de Fricke/cystamine pour une large gamme de concentrations de cystamine. Les résultats indiquent que l'activité protectrice de la cystamine est due à sa capacité de capture des radicaux libres, une signature claire du profil fortement antioxydant de ce composé. Un résultat important de l'étude est que l'efficacité protectrice de la cystamine diminue lorsque le TEL augmente, en accord avec les études expérimentales publiées sur le sujet.

Evaluation of the radioprotective ability of cystamine for 150 keV-500 MeV proton irradiation: a Monte Carlo track chemistry simulation study

by

Esteban Sepulveda, Sunuchakan Sanguanmith, Jintana Meesungnoen, and Jean-Paul Jay-Gerin[(1)]

Département de médecine nucléaire et de radiobiologie, Faculté de médecine et des sciences de la santé, Université de Sherbrooke, 3001, 12ème Avenue Nord, Sherbrooke QC J1H 5N4, Canada

Number of pages: **49**
Number of figures: **10**
Running head: **Fricke dosimeter and radioprotection evaluation of cystamine**

Canadian Journal of Chemistry
Manuscript No. cjc-2018-0382.R1
(accepted: September 23, 2018)

[(1)] Corresponding author (Tel. +1-819-821-8000, ext. 74682 or 74773; e-mail: jean-paul.jay-gerin@USherbrooke.ca)

Abstract

Cystamine, an organic diamino-disulfide, is among the best of the known radiation-protective compounds although the underlying molecular mechanisms by which it operates remain poorly understood. This study aims to use the aqueous ferrous sulfate (Fricke) dosimeter to evaluate the protective properties of this compound when present during irradiation by fast incident protons in the energy range of 150 keV-500 MeV, that is, for "linear energy transfer" (LET) values between ~72.3 to 0.23 keV/μm. The presence of cystamine in irradiated Fricke solutions prevents the oxidation of Fe^{2+} ions by the oxidizing species produced in the radiolysis of acidic water, resulting in reduced Fe^{3+} ion yields. A Monte Carlo computer code is used to simulate the radiation-induced chemistry of the studied Fricke/cystamine solutions under aerated conditions while covering a wide range of cystamine concentrations from 5×10^{-7} to 1 *M*. Results indicate that the protective activity of cystamine is due to its radical-capturing ability, a clear signature of the strong antioxidant profile of this compound. In addition, our simulations show that at low and intermediate concentrations of cystamine its protective efficiency decreases with increasing LET, which is consistent with previous work. This finding stems from differences in the geometry of the track structures that change from low-LET isolated spherical "spurs" to high-LET dense continuous cylindrical tracks as LET increases. This study concludes that Monte Carlo simulations represent a powerful method for understanding, at the molecular level, indirect radiation damage to complex molecules, such as cystamine.

Keywords: cystamine, radioprotector, antioxidant, aerated ferrous sulfate (Fricke) dosimeter, water radiolysis, high-energy protons, linear energy transfer (LET), Monte Carlo track chemistry simulation, reaction scheme, competition kinetics, radiation chemical yields (*G*-values), proton therapy, space radiation risk assessment models.

1. INTRODUCTION

The need to elucidate the mode of action of radioprotectors at the molecular level

Ionizing radiation remains one of the most effective tools in the treatment of cancer with about 50% of all cancer patients receiving antitumor radiation therapy during their course of illness. The main goal of radiation therapy is to deprive the cancer cells of their potential for proliferation (cell division) and eventually kill the cancer cells. It is also of great importance to deliver to the tumor the highest dose possible with minimal toxicity to adjacent healthy tissues. In order to obtain better tumor control at a higher dose, normal tissue around the tumor should be protected from radiation damage. Radioprotective agents, therefore, play a very important role in clinical radiotherapy and aim to modulate tissue and tumor responses to radiation and thus to enhance the therapeutic benefit for cancer patients.[1-6]

The potential use of radioprotective agents to protect a large population from large-scale exposure to radiation, such as a nuclear power plant accident, nuclear weapons deployment, possible nuclear/radiological terrorism, or even astronauts and cosmonauts to high doses of radiation in long distance space missions, however, is limited, mainly, because of their adverse side effects. Further research on the currently available radioprotector and radiomitigator compounds and the development of new, more effective and less toxic (or nontoxic) compounds that could be used immediately in case of unwanted/unexpected radiation exposure and accidental radiological emergencies are, therefore, of great interest.[7,8]

In this context, a deeper understanding of how cytoprotective compounds actually act *at the molecular level* is clearly an important objective to better control and optimize their biological effects. This is particularly true when considering that short-lived, radiation-generated free radicals are precursors to radiobiological damage in the complex

pathways that ultimately lead to cell death or pathological tissue changes after irradiation.[6]

Radiolysis of water, generation of chemically reactive species, and influence of the quality of the radiation

For applications in radiobiology, aqueous systems have received considerable attention. In fact, since water is by far the most abundant component in living cells and tissues (~70-85% by weight), the radiolytic products of cellular water can attack target biomacromolecules such as DNA and are largely responsible for chemical damage ("indirect effect" of ionizing radiation).[9] On a quantitative basis, the main species generated by radiolysis of pure deaerated water are the hydrated electron (e^-_{aq}), $H^\bullet$, H_2, $^\bullet OH$, H_2O_2, H^+, OH^-, superoxide/hydroperoxyl ($O_2^{\bullet-}/HO_2^\bullet$) radicals, where the $O_2^{\bullet-}$ radical exists in a pH-dependent equilibrium with its conjugate acid ($pK_a = 4.8$ at 25 °C), etc.[10-14] Of these, the $^\bullet OH$ and e^-_{aq} radicals are produced in the highest concentrations, and $^\bullet OH$ is considered to be the most harmful.[15] Under normal irradiation conditions, the yields (or G values)[(2)] of these different species and their initial, spatially nonhomogeneous geometrical distributions are strongly dependent on the quality of the radiation (i.e., the type and energy of the radiation), a measure of which is given by the "linear energy transfer" (LET) (also called "stopping power" by physicists).[16] For low-LET radiation such as γ-rays from ^{60}Co, hard X-rays, fast electrons or high-energy protons (typical LET values of approximately 0.3 keV/μm), the tracks consist of strings of well-separated Magee-type "spurs" (clusters of reactive species, spherical in shape)[17,18] that develop independently in time (i.e., without interference from the adjacent spurs). In

---

[(2)] Throughout this paper, radiation chemical yields are quoted in units of molecule per 100 eV of absorbed energy. For conversion into SI units (mol/J), 1 molecule/100 eV ≈ 0.10364 μmol/J.[11,12]

this case, the predominant effect of radiolysis is the formation of free radicals. However, as the LET increases, the isolated spur structure changes such that the spurs eventually overlap and form (initially) a dense continuous column (cylindrical in shape) of the species.[13,14,19] This leads to increased intra-track chemistry, favoring radical-radical reactions in the diffusing tracks. Under these conditions, the yield of free radicals decreases with increasing LET, while the yield of molecular products increases.

Depending on the diffusion from their initial positions, the radiolytic products either react within the spurs/tracks as they expand or escape into the bulk solution. After spur expansion is complete (typically, on the μs time scale at 25 °C), the species that have escaped from spur/track reactions are homogeneously distributed and the radiation "track structure" no longer exists.[20,21] The yields of the species that remain after spurs/tracks have dissipated are the so-called "primary" (or "escape") yields.[13] They are denoted by $g(e^-_{aq})$, $g(H^\bullet)$, $g(H_2)$, $g(^\bullet OH)$, $g(H_2O_2)$, etc.[(3)] At homogeneity, these species then become available to react with dissolved solutes present at low or moderate concentrations (if any) at the time of irradiation. In a cellular environment, they can readily react with DNA and membrane lipids and their associated proteins, which are considered the most significant targets in radiation-induced cell death, mutagenicity, and neoplastic cell transformation.[1,9,15,22-25]

Objectives: A study of the mechanistic of cystamine radioprotection using high-energy proton irradiation, Fricke dosimetry, and Monte Carlo track chemistry simulations

The present study deals with *chemical* (i.e., non-biological) radioprotectors from a purely radiation chemistry perspective. At the molecular level, it is believed that chemical radioprotectors exert their effects through one or more likely a combination of

---

[(3)] A lower case *g* is used to represent the primary yields of the species indicated, whereas experimentally measured or final yields are given in the form $G(X)$.[11]

various individual mechanisms that include free-radical scavenging and $H^{\bullet}$ atom (or electron/proton) donation.[3,15] Scavenging of free radicals refers to the ability of the protector compound to remove ("scavenge") the reactive products of water radiolysis *before* they can interact with vital cellular components (in other words, it prevents "indirect" damage) (timescale: ≤ 1 μs). Cytoprotection by radioprotective compounds containing sulfhydryl –SH groups (i.e., with labile hydrogen atoms) can also be achieved by $H^{\bullet}$-atom transfer to chemically repair the "direct" and "indirect" molecular lesions in target macromolecules *after* they occur (but prior to "fixation" of the damage by oxygen addition, given the inherent abundance of O_2 in most living systems) (timescale: ~1 μs-1 ms).[(4)]

Cystamine is an organic diamino-disulfide compound (RSSR, R = NH_2-CH_2-CH_2). It is the disulfide form of cysteamine (or 2-aminoethanethiol, RSH), an aminothiol of the same family, well known for its radioprotective properties. Below pH 8, cystamine predominantly exists in the form of the double protonated molecule $^{+}NH_3$-CH_2-CH_2-S-S-CH_2-CH_2-NH_3^{+} (pK_a ~ 8.7-9 for both of the $-NH_3^{+}$ groups).[27,28] The mutual Coulombic repulsion of the two positive charges at opposite ends of the protonated molecule favors an open conformation that provides high collision-accessibility of the –S-S– center for approaching radicals.[27] This property is an important determinant of the susceptibility of this compound to water-based free-radical attacks, such as $^{\bullet}OH$ and $H^{\bullet}$ (see *infra*).

[(4)] The attack of $^{\bullet}OH$ and other reactive radicals on biomolecules often occurs through $H^{\bullet}$ abstraction. O_2 "fixes" (or makes permanent) the damage by forming other (peroxyl) radicals that cannot regenerate the original compound. Sulfhydryl compounds exert their protective effect by efficiently competing with oxygen in reactions with key DNA free radicals,[26] thereby reducing DNA damage and increasing cell survival.

Previously published studies[29-32] used the well-known radiolytic oxidation of ferrous (Fe^{2+}) ions in the aqueous ferrous sulfate (Fricke) dosimeter[11,33] to quantify the radical scavenging properties of cystamine and thereby evaluate its radioprotective ability. Indeed, the production of ferric (Fe^{3+}) ions is most sensitive to radical species generated by radiolysis of water. When a radioprotective substance, such as cystamine, is present in Fricke solutions during irradiation, it acts by competing with the ferrous ions for the various free radicals resulting from irradiation of the surrounding water, and the yield of Fe^{3+} will be reduced; i.e., Fe^{2+} will be protected. These studies clearly demonstrated that the protective effect of cystamine over the Fricke dosimeter solution is based on its radical-capturing ability. This result was further confirmed using Monte Carlo track chemistry simulations of the radiolysis of cystamine in both aerated and deaerated Fricke solutions.[32]

In this work, we extend our previous Monte Carlo simulations of the radiolysis of Fricke/cystamine solutions[32] to irradiations by *fast protons* in the energy range of 150 keV-500 MeV or, equivalently, for LET values varying between ~72.3 and 0.23 keV/μm (obtained from our simulations; see also ref. 34). The use of high-energy protons is particularly relevant for clinical applications of proton radiation therapy, in which the proton energies can be continuously adjusted upon entry into the patient so that the protons can deliver their dose at a defined depth within the tumor volume,[(5)] while

---

[(5)] A dosimetric characteristic called the "Bragg peak". Note that proton radiation has been studied for cancer treatment since the 1950s. The physical properties of the proton beam, with most of the dose deposition occurring in the Bragg peak with no exit dose, provide important advantages over photon-based radiation in certain scenarios.

sparing tissues distal to the tumor[1,35] High-energy protons[(6)] also play an important role in the development of radiation risk assessment models for astronauts participating in "International Space Station" missions and for exploration missions to Mars and other deep space destinations.[36] Unlike our previous study, which considered only sparsely ionizing low-LET (~0.3 keV/μm) γ-irradiation, our aim here is *to examine the effects of increasing the LET of radiation on the radioprotective ability of cystamine*. Since relatively little is known about the protection against densely ionizing high-LET radiation,[37-40] Monte Carlo simulations offer an interesting opportunity to elucidate the mechanisms underlying the protective effect of a radioprotector under high-LET irradiation conditions. As before, the oxidation of Fe^{2+} ions to Fe^{3+} was used as a measure of the radioprotective ability of cystamine and formed the basis of our method.

2. THE FERROUS SULFATE (FRICKE) DOSIMETER

Of all the aqueous systems studied, the ferrous sulfate dosimeter known as the "Fricke dosimeter" after Hugo Fricke who first published accounts of its properties in 1927-1929,[33] is certainly the best understood, and the most commonly used liquid chemical dosimeter.[11,33,41-43] Due to its accuracy, reproducibility, and linearity of its response as a function of dose, it is widely accepted in radiation-chemical work.[44-46]

The standard Fricke solution consists of 1 m*M* $FeSO_4$ in air-saturated (~0.25 m*M* O_2) aqueous 0.4 *M* H_2SO_4.[33] The mechanism for the radiolytic oxidation of Fe^{2+} ions to Fe^{3+} is well understood,[11,33,41-43,47,48] and the rate constants at 25 °C of the individual reactions taking place are known. In short, the main reactions for ferric ion production in an irradiated Fricke dosimeter solution under aerated conditions are:[32]

[(6)] Protons are a major component of the "galactic cosmic rays", which largely constitute the radiation environment in space.

[1]	$e^-_{aq} + H^+ \rightarrow H^\bullet$	$k_1 = 2.3 \times 10^{10}\ M^{-1}\ s^{-1}$ [7] $pK_a(H^\bullet/e^-_{aq}) = 9.59$
[2]	$H^\bullet + O_2 \rightarrow HO_2^\bullet$	$k_2 = 2.1 \times 10^{10}\ M^{-1}\ s^{-1}$
[3]	$^\bullet OH + Fe^{2+} \rightarrow Fe^{3+} + OH^-$	$k_3 = 3.4 \times 10^{8}\ M^{-1}\ s^{-1}$
[4]	$OH^- + H^+ \rightarrow H_2O$	$k_4 = 5.97 \times 10^{10}\ M^{-1}\ s^{-1}$ $pK_a(H_2O/OH^-) = 13.999$
[5]	$HO_2^\bullet + Fe^{2+} \rightarrow Fe^{3+} + HO_2^-$	$k_5 = 7.9 \times 10^{5}\ M^{-1}\ s^{-1}$
[6]	$HO_2^- + H^+ \rightarrow H_2O_2$	$k_6 = 5 \times 10^{10}\ M^{-1}\ s^{-1}$ [7] $pK_a(H_2O_2/HO_2^-) = 11.62$
[7]	$H_2O_2 + Fe^{2+} \rightarrow Fe^{3+} + {}^\bullet OH + OH^-$	$k_7 = 52\ M^{-1}\ s^{-1}$
[8]	$H^\bullet + Fe^{2+} \xrightarrow{H^+} Fe^{3+} + H_2$	$k_8 = 1.3 \times 10^{7}\ M^{-1}\ s^{-1}$.

At the acid concentration of 0.4 *M* H_2SO_4, all of the e^-_{aq} radicals are rapidly (timescale: ~110 ps) converted into $H^\bullet$ atoms in the expanding spurs.[49] In the presence of oxygen, each $H^\bullet$ atom created directly by radiolysis and by scavenging of e^-_{aq} forms[8] a hydroperoxyl radical, which in turn oxidizes three Fe^{2+} ions, one by reaction [5] and two by the reaction sequences [6], [7], and [3]. Each $^\bullet OH$ radical oxidizes one Fe^{2+} ion, and each molecule of H_2O_2 oxidizes two Fe^{2+} ions. Summing up all sources of Fe^{3+} ions, the Fricke *G*-value valid for low-LET proton beam irradiation (which mimic ^{60}Co γ-rays or fast electrons) can be expressed in terms of the "escape" yields of the free radicals and

---

[7] Rate constant in the limit of infinite dilution, i.e., *not* corrected for the effects due to the ionic strength of the solutions.

[8] Some $H^\bullet$ atoms can also react directly with Fe^{2+} (reaction [8]). This reaction is important when no oxygen is present initially. In aerated solutions at 25 °C and a Fe^{2+} ion concentration of 1 m*M*, however, the contribution of this reaction to the formation of Fe^{3+} is small and may be neglected.

molecular species of the radiolysis of the solution by the following stoichiometric equation:[11,32,33,41,47,48]

[9] $$G(Fe^{3+})_{aerated} = 3g(e^-_{aq} + H^\bullet) + g(^\bullet OH) + 2g(H_2O_2) + 3g(HO_2^\bullet),$$

where $g(e^-_{aq} + H^\bullet)$ represents the sum of the primary yields of the reducing radicals e^-_{aq} and $H^\bullet$.[(9)] For ^{60}Co γ-irradiated 0.4 *M* H_2SO_4 aqueous solutions at room temperature, representative values of the primary free-radical and molecular product yields are:[49]

[12] $$g(e^-_{aq} + H^\bullet) = 3.70 \qquad g(HO_2^\bullet) = 0.02 \qquad g(H_2) = 0.40$$
$$g(^\bullet OH) = 2.90 \qquad g(H_2O_2) = 0.80 \qquad g(-H_2O) = 4.50\ .$$

Using these primary radiolytic yield values in eq. [9] leads to a value for $G(Fe^{3+})$ which agrees well with published data in the literature for ^{60}Co γ-rays.[(10)]

Equation [9] shows that the production of Fe^{3+} ions is highly sensitive to factors that alter the primary free-radical yields. Experimentally, the presence of cystamine in

---

[(9)] Note that, for solutions of 0.4 *M* in H_2SO_4, there is a small proportion of $^\bullet OH$ radicals that react with HSO_4^- ions to form the sulfate radical $SO_4^{\bullet -}$ according to[48,50]

[10] $$^\bullet OH + HSO_4^- \rightarrow H_2O + SO_4^{\bullet -} \qquad k_{10} = 1.5 \times 10^5\ M^{-1}\ s^{-1}.$$

However, the overall ferric ion yield remains the same as given by eq. [9] since the sulfate radical (or its protonated form $HSO_4^\bullet$; $pK_a = 1.9$) reacts with Fe^{2+} in the same way as $^\bullet OH$:[51]

[11] $$SO_4^{\bullet -} + Fe^{2+} \rightarrow Fe^{3+} + SO_4^{2-}$$

with $k_{11} = 9.9 \times 10^8\ M^{-1}\ s^{-1}$ (in the limit of zero ionic strength). Contrary to HSO_4^-, the sulfate ion SO_4^{2-} has been reported to be unreactive toward $^\bullet OH$.

[(10)] In particular, those recently obtained by the "Ionizing Radiation Standards" group at the National Research Council Canada, namely, 15.53 and 15.56 ions/100 eV, with quoted uncertainties of ~0.5 and 0.3%, respectively.[44,45]

the Fricke dosimeter solution during γ-irradiation significantly affects the rate of radiolytic oxidation of Fe^{2+}, producing significantly reduced ferric ion yields.[29,30,32] As shown previously,[32] this marked decrease in $G(Fe^{3+})$ as a function of the concentration of added cystamine is a clear indication of the scavenging of these radicals by cystamine, since the latter reacts rapidly with e^-_{aq}, $H^\bullet$, and $^\bullet OH$ (see *infra*).

3. MONTE CARLO TRACK CHEMISTRY SIMULATIONS

The IONLYS-IRT simulation code

A full Monte Carlo computer code, called IONLYS-IRT,[14] was used to simulate the radiolysis of the studied Fricke/cystamine solutions at ambient temperature by energetic irradiating protons. This code first models, in a 3D geometric environment, the initial, highly nonhomogeneous radiation track structure ("IONLYS" program), followed by the ensuing diffusion and chemical reactions of the various radical and molecular products formed by radiolysis ("IRT" program). More specifically, the code we are using here is an extension of our previously developed code for the simulation of the radiolysis of aqueous 0.4 *M* H_2SO_4 (pH ~ 0.46) solutions[48] and the radiation-induced oxidation of $FeSO_4$ solutions in the Fricke dosimeter at ambient temperature.[41,48] It proposes reaction mechanisms and contains specific reactions that describe the radiolysis of Fricke solutions in the presence of added cystamine , which come from various literature sources and lead to the observed quantitative chemical yields. A detailed description and implementation of our Monte Carlo code has been given previously.[32] Only a brief overview of the most essential features of the simulation methodology and the reaction scheme, pertinent to the current calculations, will be given here.

The IONLYS program is used to model the early physical and physicochemical stages of the radiation action up to ~1 ps in track development. It accurately models,

event by event, all the basic physical interactions (energy deposition) and the subsequent conversion of the locally generated physical products into the different initial radical and molecular products e^-_{aq}, $H^\bullet$, H_2, $^\bullet OH$, H_2O_2, H^+, OH^-, $HO_2^\bullet/O_2^{\bullet-}$, $^\bullet O^\bullet$, H^-, $O^{\bullet-}$, etc., of the radiolysis.[53] The complex spatial distribution of the reactants at the end of the physicochemical stage, provided as an output of the IONLYS program, is then used directly as a starting point for the subsequent, nonhomogeneous chemical stage (typically from ~1 ps to the μs timescale at 25 °C, i.e., until spurs/tracks have dissipated). The third stage, during which the various radiolytic species diffuse randomly at rates determined by their diffusion coefficients, and react with one another or, competitively, with any dissolved solutes present in the system until all spur/track processes are completed, is covered by our IRT program. This program uses the "independent reaction times" (IRT) method, a computationally efficient stochastic simulation technique that can simulate reaction times without having to follow the trajectories of the diffusing species.[54-56] Its implementation was previously described in detail.[57] The ability of this program to give accurate time-dependent chemical yields over a wide range of irradiation conditions has been well validated by comparison with full random flights (or "step-by-step") Monte Carlo simulations, which follow the reactant trajectories in detail.[58,59] Obviously, this IRT program can also be used efficiently to describe the reactions that occur at longer times when the radiolytic products are homogeneously distributed throughout the bulk solution. This is precisely the case here for the simulation of the Fricke dosimeter in which ferric ions are produced at a wide variety of times up to ~200 s.[41,48,6025]

Simulation of the radiolysis of Fricke/cystamine solutions: Chemical reaction scheme, effect of ionic strength, and track segment yields for 150 keV-500 MeV irradiating protons

The model assumptions and procedures for carrying out the Monte Carlo simulations of the radiolysis of 0.4 *M* H_2SO_4 aqueous solutions with IONLYS-IRT have

been reported.[41,48] Briefly, we supplemented the reaction scheme for the radiolysis of pure liquid water[14,41,57,61] to include the reactions listed in Table 1 of ref. 48, which account for the species HSO_4^-, SO_4^{2-}, $SO_4^{\bullet-}$, and $S_2O_8^{2-}$ present in irradiated H_2SO_4 solutions.[41,62] To stochastically model the chemistry of the Fricke dosimeter, we added to the IRT program the reactions [3], [5], [7], and [8] of Fe^{2+} ions with the various oxidizing species formed in the water of the irradiated solutions. Under ordinary irradiation conditions, the concentrations of radiolytic products are low compared to the background concentrations of H^+ (~0.4 *M*), Fe^{2+} ions (1 m*M*) and O_2 (~2.5×10^{-4} *M*) in solution, and therefore their reactions could be treated in the IRT program as pseudo first order.

Finally, to simulate the radiolysis of the Fricke dosimeter in the presence of cystamine, we supplemented the Fricke dosimeter reaction scheme to include the 27 chemical reactions listed in Table 2 of ref. 32 which we have proposed to describe the aqueous radiation chemistry of cystamine. In essence, this set of reactions follows directly from the fact that the disulfide linkage of cystamine is very sensitive to the attack of radicals formed by acid water radiolysis,[11] with the dominating reactions in the timescale studied being

[13] $RSSR + e^-_{aq} \rightarrow RSSR^{\bullet-}$ $\quad k_{13} = 4.1 \times 10^{10}\ M^{-1}\ s^{-1}$ [63-65]

followed, in acid solution, by the protonation of $RSSR^{\bullet-}$ to give the sulfenium radical "intermediate" $RSSRH^{\bullet}$ that immediately dissociates into its thiyl ($RS^{\bullet}$) and thiol (RSH) components,[66]

[14] $RSSR + H^{\bullet} \rightarrow RSSRH^{\bullet} \rightarrow RS^{\bullet} + RSH$ [(11)] $\quad k_{14} = 8 \times 10^{9}\ M^{-1}\ s^{-1}$,

---

[(11)] With $RSSRH^{\bullet}$ – generated either from the protonation of $RSSR^{\bullet-}$ or from the reaction of $H^{\bullet}$ atoms with RSSR – assumed to have a very short mean lifetime, it did not have to be explicitly modeled in the simulations.

and the electron-transfer reaction[32]

[15] $RSSR + {}^{\bullet}OH \rightarrow RSSR^{\bullet+} + OH^{-} \qquad k_{15} = 1.7 \times 10^{10}\ M^{-1}\ s^{-1}.$

For most of the cystamine concentrations studied here (with the exception of elevated concentrations, see *infra*), the subsequent oxidation of ferrous ions involves reactions with the thiyl radicals $RS^{\bullet}$ and the $RSSR^{\bullet+}$ radical ions formed by reactions [13]-[15], namely,

[16] $RS^{\bullet} + Fe^{2+} \rightarrow Fe^{3+} + {}^{\bullet}RS^{-} \qquad k_{16} = 2.5 \times 10^{8}\ M^{-1}\ s^{-1}$

and

[17] $RSSR^{\bullet+} + Fe^{2+} \rightarrow Fe^{3+} + RSSR \qquad k_{17} = 2 \times 10^{6}\ M^{-1}\ s^{-1}.$

The proposed mechanism for the aqueous radiation chemistry of cystamine allowed us successfully explain the experimental yields of Fe^{3+} obtained in the ^{60}Co γ-radiolysis of Fricke solutions with a wide range of cystamine concentrations, in the presence, as well as in the absence, of oxygen.[32]

In addition, we have introduced in the IRT program the effect of the ionic strength of the solutions on all reactions between ions.(12) The correction to the reaction rate constants was made using the following equation:[68,69]

[18] $$\log\left(\frac{k}{k_0}\right) = 1.02\ Z_a Z_b \left(\frac{I^{1/2}}{1 + I^{1/2}}\right),$$

where k is the rate constant at ionic strength I, k_0 is the rate constant in the limit of zero ionic strength (i.e., at infinite dilution of ions), Z_a and Z_b are the algebraic numbers of charges on the reactants (positive for cations and negative for anions), and I (in M) is defined as[70]

---

(12) Except for the peculiar bimolecular self-recombination of e^{-}_{aq} for which there is no evidence of any ionic strength effect.[67]

[19] $$I = \frac{1}{2}\sum_i Z_i^2 C_i \ ,$$

where Z_i is the charge number of the i_{th} ion and C_i is its molar concentration (the sum extends over all ionic species present in the solution). According to eq. [18], the rate constants will increase, decrease, or remain constant with increasing ionic strength, depending on whether the ions have the same sign, opposite signs, or whether one species is uncharged.

The diffusion coefficients used for the different species involved in our IRT simulations of the radiolysis of the Fricke dosimeter were taken from refs. 41, 48, 57, and 61, and we used the same value of 2×10^{-5} cm^2 s^{-1} for cystamine[(13)] and for all its derivatives. Finally, in our simulations the "direct" effect of radiation on the various solutes (i.e., sulfuric acid anions, ferrous ions, oxygen, and cystamine) present in the solution was neglected, which is a reasonably good approximation over the range of H_2SO_4 (0.4 *M*)/$FeSO_4$ (10^{-3} *M*)/O_2 (2.5×10^{-4} *M*)/RSSR (5×10^{-7}-1 *M*) concentrations studied.[(14)]

This paper only deals with results at 25 °C. All calculations were performed by simulating short track segments (typically, ~5-150 μm) of 150 keV-500 MeV incident

---

[(13)] The diffusion coefficient of cystamine (in water) has not been reported in the literature. We assumed here that its value was comparable to that of cysteamine.[71]

[(14)] In 0.4 *M* H_2SO_4, only ~3.6% of the total energy consumed in the solution is initially absorbed by HSO_4^- ions rather than by H_2O (assuming that the energy absorbed by each component is proportional to its electron fraction). Note, however, that for the highest cystamine concentration (1 *M*) considered in this study, the corresponding "direct" radiation effect on cystamine is relatively more significant (~14.7%), but was ignored nevertheless in our simulations.

protons whose LET values obtained in the simulations varied from ~72.2 to 0.23 keV/μm, respectively. These LET values agreed well with the data reported by Watt[34] and the recommendations of ICRU 49 [72] for liquid water (of density 1 g/cm^3). Over these simulated track segments, the energy and LET of the protons were well defined and remained nearly constant. To mimic the effects of ^{60}Co γ-radiolysis, we used ~300-MeV proton tracks over which the average LET value was equal to ~0.3 keV/μm at 25 °C.[34,50,72] Such model calculations thus gave "track segment" yields for a well-defined LET.[13,57] The simulations consist of following the transport and energy loss of an incident proton until it has penetrated the chosen length of the track segment into the solution. Due to its large mass, the impacting proton is virtually unaffected by collisions with target electrons. The number of proton histories (usually ~3-150, depending on the irradiating proton energy) was chosen to ensure only small statistical variations in the calculated chemical yield averages, while meeting acceptable computer time limits. In the simulations reported here, the temporal evolution of $G(Fe^{3+})$ was followed to ~200 s.

4. RESULTS AND DISCUSSION

Kinetics of Fe^{3+} formation for 150-keV and 500-MeV irradiating protons and influence of added cystamine in low and moderate concentrations

Figures 1 and 2 show the kinetics of Fe^{3+} formation as obtained from our simulations of the radiolysis of the Fricke dosimeter under aerated conditions, for 150-keV and 500-MeV irradiating protons, respectively, and in the presence of various concentrations of added cystamine. The results clearly show that $G(Fe^{3+})$ decreases at ~200 s with increasing cystamine concentrations for both high- and low-LET proton irradiations. For high-LET 150-keV incident protons, $G(Fe^{3+})$ decreases from ~8.2 to about 3.65 molecules/100 eV (~4.55 *G*-unit decrease) when comparing the Fricke solution with no added cystamine to a solution containing 0.1 *M* of the disulfide (Fig. 1).

Interestingly, this decrease is much more pronounced for low-LET 500-MeV irradiating protons, with $G(Fe^{3+})$ dropping from ~15.5 to 4.75 molecules/100 eV [(15)] (~10.75 *G*-unit decrease) (Fig. 2). Overall, these reduced Fe^{3+} ion yields, when cystamine is present in Fricke solutions during irradiation, obviously give a clear indication that this molecule can readily remove the various primary products of acid water radiolysis (predominantly, $H^{\bullet}$ atoms and $^{\bullet}OH$ radicals) that contribute to the radiolytic oxidation of ferrous ions. Mechanistically, this *radical-capturing ability* of cystamine characterizes the strong "antioxidant profile" of this compound, which allows it to act by *competing* with the Fe^{2+} ions for the various free radicals that result from the irradiation of the surrounding water.

The influence of the concentration of cystamine on the Fricke yield is further illustrated in Fig. 3, where our calculated $G(Fe^{3+})$ values at ~200 s are reported for both 150-keV and 500-MeV irradiating protons, for cystamine concentrations varying from 5×10^{-7} to 1 *M*. Figures 1-3 clearly demonstrate that *the effectiveness of cystamine is reduced in response to high-LET radiation*, which generally agrees with reports that chemical radioprotectors, including radioprotective aminothiols, are more effective for low-LET radiation.[3,8,39,73-75] For instance, as can be seen in Fig. 3, 25 m*M* cystamine reduces the efficacy of 500-MeV protons (LET of ~0.23 keV/μm) by a factor of about 3 while reducing the efficacy of 150-keV protons (LET of ~72.2 keV/μm) by only ~1.8.

Remarkably, Fig. 3 also shows that our calculated Fe^{3+} yields for low-LET 500-MeV incident protons accurately reproduce (without any adjustable parameter) the experimentally measured yields of Fe^{3+} previously reported in the literature for X- and

---

[(15)] It should be noted here that our calculated value of $G(Fe^{3+})$ in the absence of added cystamine is in excellent agreement with the recommended value of 15.5 ± 0.2 molecules/100 eV for the ferric ion yield in the aerated Fricke dosimeter for ^{60}Co γ-rays, high-energy X-rays, or fast electrons.[33,44,45,47,52]

^{60}Co γ-irradiations.[29,30,32] Such a quantitative agreement between calculated and measured $G(Fe^{3+})$ values at low LET strongly supports the validity and consistency of the overall chemical reaction scheme used in this study to describe the radiation chemistry of cystamine in aerated Fricke solutions.

Figures 1 and 2 show that the Fe^{3+} yield is time dependent, as a direct result of the differences in the time scales of the Fe^{2+} oxidation reactions, which contribute to the formation of Fe^{3+} in the radiolysis of the Fricke/cystamine system in the presence of O_2. As an example, we have chosen the kinetics of Fe^{3+} formation in aerated 1 m*M* cystamine solutions that are irradiated by 500-MeV and 150-keV incident protons (Figs. 4 and 5, respectively). For both of these incident proton energies, Figs. 4a and 5a show that the oxidation of Fe^{2+} ions to Fe^{3+} involves reactions mainly with $HO_2^{\bullet}$, H_2O_2, and the cystamine-radical species $RS^{\bullet}$ and $RSSR^{\bullet+}$. The fastest reaction of Fe^{2+} ions is with the thiyl radicals $RS^{\bullet}$ which is completed within a few microseconds. This is clearly indicated in Fig. 4b and 5b, where we show the time profiles for the extents $\Delta G(Fe^{3+})$ of each of the reactions contributing to the formation of Fe^{3+}, that are calculated from our simulations for both 500-MeV and 150-keV irradiating protons. Interestingly, these thiyl radicals are mainly derived from the RSSR + $H^{\bullet}$ reaction [14], which occurs in a time scale of tenths of a microsecond (see Fig. 6a and b). The $H^{\bullet}$ atoms that did not react with cystamine react with oxygen (with a time scale of the order of one microsecond) to form $HO_2^{\bullet}$, which eventually oxidizes Fe^{2+} ions to Fe^{3+}. The oxidation of Fe^{2+} by $HO_2^{\bullet}$ is slower and requires about 10 ms to complete. Finally, at times longer than ~1 s, there are two additional reactions that contribute to the formation of Fe^{3+} which are almost superimposed; first, the $Fe^{2+} + H_2O_2$ reaction [7] and then the Fe^{2+} + $RSSR^{\bullet+}$ reaction [17]. These two reactions are completed by about 200 s. In fact, the latter two reactions are closely related, as the yield of H_2O_2 contributing to the Fe^{3+} yield in reaction [7] also contributes to the formation of a stoichiometrically-equivalent yield of $^{\bullet}OH$. In our case

(i.e., solutions containing 1 m*M* Fe^{2+} ions and 1 m*M* cystamine), virtually all of the so formed $^{\bullet}OH$ radicals are scavenged by cystamine before they can react with Fe^{2+},[(16)] as can be seen in Figs. 4b and 5b. This explains the sharp decrease in the extent ΔG(RSSR) due to the RSSR + $^{\bullet}OH$ reaction [15] observed in Fig. 6a and b after ~1 s. It also quantitatively explains the corresponding increase in ΔG(RSSR) by reaction [17], since virtually all $RSSR^{\bullet+}$ radical ions generated in the same time interval eventually oxidize Fe^{2+} ions to Fe^{3+} rather than reacting with themselves (Fig. 6a and b).

At low and moderate concentrations, cystamine is less protective at high-LET radiation

Returning to the analysis of Fig. 3, it can be seen that for very low cystamine concentrations, $G(Fe^{3+})$ decreases by a factor of ~1.9 (~7.2 *G*-unit or ~46.5% decrease) when going from low-LET 500-MeV to high-LET 150-keV irradiating protons. This substantial decrease in $G(Fe^{3+})$ values is due essentially to differences in the spatial distributions of deposited energy in the transition from sparse to dense ionizing radiations. Indeed, this behavior is theoretically a consequence of the increased importance of intra-track processes for more densely ionizing radiations at higher LET, which enhance radical-radical combination reactions that produce molecular products. According to eq. (9), the lower the free radical yield that escapes the radiation tracks, the lower the oxidation of ferrous ions, and therefore the Fricke *G*-values. Our results are in full quantitative agreement with the many experimental data reported in the literature on the effect of LET on the chemistry and yields of the Fricke dosimeter[33,41,47,48] (see Fig. 7). produced at a wide variety of times up to ~200 s.[41,48,6025]

[(16)] At the same concentration, the competition between RSSR and Fe^{2+} for the scavenging of $^{\bullet}OH$ is actually quite to the advantage of cystamine, since the rate constant for reaction [15] (1.7×10^{10} M^{-1} s^{-1}) is 50 times larger than that for reaction [3] (3.4×10^{8} M^{-1} s^{-1}).

At low or moderately high cystamine concentrations, Fig. 3 shows that the protective efficacy of this compound decreases with increasing LET of the radiation. The fact that cystamine becomes less effective at high-LET radiation results largely from differences in the relative spatial distributions and reaction kinetics of the transient radiation-induced species within the geometry of the track structure. Two main reasons can be mentioned. On the one hand, the increase of molecular yields with LET at the expense of free radicals – a consequence of the higher radical density for denser ionizing radiations (see above) – makes cystamine less effective, since this compound is most sensitive to the primary radical yields, but rather unreactive toward molecular products. On the other hand, the reduced protective ability of cystamine at high LET is consistent with the fact that the (2D) cylindrical track geometry of the highest LET protons is competitively *less* favorable for the radical scavenging action of the (homogeneously distributed) cystamine molecules than the (3D) spherical spur geometry of the lowest LET incident protons.

The influence of LET decreases at high cystamine concentrations

Interestingly, the overall effect of LET decreases as the cystamine concentration continues to rise to high levels. For example, $G(Fe^{3+})$ for 0.1 *M* cystamine drops by a factor of only 1.3 (~25.6% decrease compared to 46.5% at low concentrations; see above) when going from 500-MeV to 150-keV incident protons. This is clearly shown in Fig. 8 where the ferric ion yields are plotted as a function of LET over the range of ~0.2-75 keV/μm for various concentrations of added cystamine. For cystamine levels above $\sim 10^{-2}$ *M*, it can be seen that $G(Fe^{3+})$ remains relatively constant for low-LET values and then decreases very slowly at higher LET – in contrast to the rapid drop found at low or moderate cystamine levels (see also Fig. 3). The change in the efficacy of cystamine under these conditions is understandable, since at sufficiently high cystamine

concentrations, the cystamine-radical reactions [13]-[15] start competing with the radical-radical combination and recombination reactions in the track regions.[48,82,85] This competition between (intra-track) radical combination/recombination and capture by the cystamine molecules is increasingly in favor of the cystamine-radical reactions as the concentration of cystamine increases further. Consequently, the production of Fe^{3+} is less and less affected by differences in the relative spatial distribution of the radiation-induced radicals within the geometry of the track structure, which in turn explains the reduction in the LET effects at high concentrations of cystamine.

The Fe^{3+} production reaches a lower limit at increasingly higher cystamine concentrations

Finally, another interesting finding is the existence, from a purely mathematical perspective, of a lower limit for the formation of ferric ions with increasing concentration of cystamine. This is clearly shown in Fig. 8 where the $G(Fe^{3+})$-vs.-LET curves tend to be closer and closer together as the cystamine concentration rises from 10^{-3} to 10^{-2} to 0.1 to 1 *M*, the last two curves for 0.1 and 1 *M* being almost superimposed. The reason for this is that at high cystamine concentrations, cystamine rapidly converts[(17)] virtually all of

---

[(17)] From the reciprocal of the scavenging power,[11] defined as the product k[RSSR] (in units of s^{-1}), we can estimate the time scales over which scavenging of e^-_{aq}, $^{\bullet}OH$, and $H^{\bullet}$ by RSSR are occurring. For 1 *M* cystamine, these reactions with cystamine occur at ~24, 59, and 125 ps, respectively. Under these conditions, the competition between RSSR and H^+ for capturing e^-_{aq} tends to favor cystamine, since the $e^-_{aq} + H^+$ reaction [1] is slightly slower, requiring ~110 ps to complete (see above). The $H^{\bullet}$ atoms [generated directly by radiolysis and those formed via reaction [1] by protonation of e^-_{aq}], for their part, mostly react with cystamine because the $H^{\bullet} + O_2$ reaction [2] proceeds much more slowly on a time scale of ~0.2 μs {note that the $H^{\bullet} + Fe^{2+}$ reaction [8] is even slower (~77 μs)}.

the radiolytically generated primary radicals e^-_{aq}, $H^\bullet$, and $^\bullet OH$ into the corresponding thiyl radicals $RS^\bullet$ and the $RSSR^{\bullet+}$ radical ions (reactions [13]-[15]). The fact that $H^\bullet$ and $^\bullet OH$ are quickly scavenged by cystamine not only eliminates the contributions of reactions [3] and [5] to the formation of Fe^{3+} but also of reaction [11], which no longer occurs given the nonoccurrence of reaction [10] and the subsequent absence of production of sulfate radicals $SO_4^{\bullet-}$. In addition, it also significantly reduces the formation of H_2O_2 [since hydrogen peroxide is mainly generated by the reaction of $^\bullet OH$ with itself[10-13]] and thus its contribution to the ferric ion yield in the Fenton reaction [7]. Interestingly, at this limit of elevated cystamine concentrations, both $RS^\bullet$ and $RSSR^{\bullet+}$ formed in reactions [13]-[15] react more rapidly with cystamine (for the former) and with itself (for the latter) than with Fe^{2+},[(18)] leading to the prevailing mechanism:

Finally, the $^\bullet OH$ radicals are almost completely taken up by the disulfide long before they can react with Fe^{2+} ($1/k_3[Fe^{2+}] \sim 3$ μs).

[(18)] Indeed, at 1 *M* cystamine, the reaction [20] of $RS^\bullet$ with RSSR occurs at $1/k_{20}[RSSR] \sim 1$ μs (this time becoming shorter and shorter as the concentration of cystamine continues to increase), which is slightly faster than that with ferrous ions (~4 μs). As for $RSSR^{\bullet+}$, its self-reaction [23] has a rate constant a thousand times greater than that of its reaction [17] with Fe^{2+}. Our simulations show that the contribution of reaction [17] to the production of Fe^{3+} decreases rapidly with increasing cystamine concentrations from 10^{-2} to 0.1 to 1 *M* and reaches a value of less than ~0.23 molecule/100 eV for 1 *M* cystamine (see Fig. 9). The situation at elevated cystamine concentrations is in sharp contrast to that prevailing at low or intermediate concentrations (see above) where reactions [5], [7], [16], and [17] all contribute efficiently to the formation of ferric ions. In order to better visualize the studied system, we have shown in Fig. 10 the evolution over time of the yields of *all* reactive species involved in the radiolysis of the (aerated) Fricke solution

[20] $RS^{\bullet} + RSSR \rightarrow RSSSR + R^{\bullet}$ $k_{20} = 10^6\ M^{-1}\ s^{-1}$ [11,86]

followed by the formation of the peroxyl radical $ROO^{\bullet}$, a strong oxidizing agent,[15,87]

[21] $R^{\bullet} + O_2 \rightarrow ROO^{\bullet}$ $k_{21} = 2 \times 10^9\ M^{-1}\ s^{-1}$

which readily reacts with Fe^{2+} to give Fe^{3+}

[22] $ROO^{\bullet} + Fe^{2+} \xrightarrow{H^+} Fe^{3+} + ROOH$ $k_{22} = 7.9 \times 10^5\ M^{-1}\ s^{-1}$

and

[23] $RSSR^{\bullet+} + RSSR^{\bullet+} \rightarrow RSSR^{2+} + RSSR$ $k_{23} = 2.5 \times 10^9\ M^{-1}\ s^{-1}$ [88-90]

From the above considerations, it readily follows that the lower limit of ferric ion production at high cystamine concentrations comes mainly from reaction [22], which corresponds to the oxidation of Fe^{2+} by the peroxyl radicals $ROO^{\bullet}$ formed in reaction [21]. Figure 9a-c show the time profiles of the extents $\Delta G(Fe^{3+})$ for each of the reactions [5], [7], [16], [17], and [22] that contribute to the formation of Fe^{3+}, as seen in our simulations for low-LET 500-MeV irradiating protons, for the three increasing cystamine concentrations of 0.01, 0.1, and 1 *M*. It can be seen that at 1 *M* cystamine, the contribution of reaction [22] is already quite predominant with a yield of ~3.23 molecules/100 eV, with the contributions of the other reactions [16], [17], [7], and [5] being 0.82, 0.23, 0.21, and 0.01 molecules/100 eV, respectively. Based on calculations performed at 2 and 5 *M* cystamine concentrations, a lower value of $G(Fe^{3+})$ of ~4.6 molecules/100 eV at ~200 s could be estimated at the limit of increasingly higher cystamine concentrations.[(19)] The same limiting $G(Fe^{3+})$ value is only ~3.6

---

containing 1 *M* cystamine, by 500-MeV incident protons at 25 °C and in the interval of $\sim 10^{-12}$ to 200 s.

[(19)] To the extent, of course, that the "direct" effects of radiation on the cystamine molecules are ignored.

molecules/100 eV for high-LET 150-keV incident protons (data not shown here). The difference of ~1 *G*-unit between low- and high-LET radiations is not surprising; it reflects the inability of cystamine, even at the highest concentrations considered in this study, to scavenge the entirety of the early-formed free radicals fast enough (on the picosecond timescale or less) in the columnar regions of the high-LET proton tracks – regions with very high radical concentration – before the intervention of interradical combination or recombination reactions that form the molecular products.

5. SUMMARY AND CONCLUSION

In this work, we investigated the radical scavenging properties of cystamine by examining the behavior of this compound from a purely radiation-chemical perspective with respect to the primary species produced by fast protons under various LET irradiation conditions in the radiolysis of water. The well-known radiolytic oxidation of Fe^{2+} ions to Fe^{3+} in irradiated Fricke dosimeter solutions with cystamine was used as a measure of its radioprotective ability and formed the basis of our method.

This study was done theoretically. Our goal was to better understand the mechanisms of how cystamine, when present during irradiation, actually works at the molecular level as a function of proton energy in the range of 150 keV-500 MeV or equivalently, for LET values between ~72.2 and 0.23 keV/μm, while covering a wide range of cystamine concentrations from 5×10^{-7} to 1 *M*. A complete Monte Carlo track chemistry computer code was used to fully simulate the radiation-induced chemistry of the studied Fricke/cystamine solutions under aerated conditions at 25 °C. Due to the fact that the radiation chemistry of this molecule is reasonably well characterized, we were able to successfully reproduce the experimental yields of Fe^{3+} obtained by various authors for X- and ^{60}Co γ-irradiations over the entire cystamine concentration range studied in the presence of oxygen. Such a quantitative agreement between calculated and

measured $G(Fe^{3+})$ values at low LET provided good confirmation of the validity and consistency of the overall chemical reaction scheme used to describe the cystamine radiation chemistry in aerated Fricke solutions. On this basis, we could then extend our Monte Carlo simulations to elucidate the effects of increasing the LET of the radiation on the mechanism of action of cystamine.

The results obtained in this study clearly demonstrated that the protective effect of cystamine over the Fricke dosimeter solution stems from its radical-capturing ability, which allows this compound to compete with the Fe^{2+} ions for the various primary free radicals of acidic water radiolysis, resulting in greatly reduced ferric ion yields. This sharp decrease in $G(Fe^{3+})$ when cystamine is present during irradiation is a clear signature of the strong antioxidant profile of this compound.

A notable finding from our simulations is that at low or moderately high cystamine concentrations, the protective effect of this compound decreases with increasing LET of the radiation, which generally agrees with the conclusion from earlier work that chemical (i.e., non-biological) radioprotectors are more efficient against low- than high-LET radiation exposure. Although there is still radioprotection against high-LET radiation, the fact that cystamine becomes less active can be explained by differences in the spatial distribution of the reactants within the geometry of the track structure. In fact, as LET increases, the isolated spherical spurs change into dense continuous cylindrical tracks. Under these conditions, the higher local concentration of reactants for denser ionizing radiations promotes interradical combination and recombination reactions in the track stage of radiolysis producing more molecular products such as H_2O_2 or $HO_2^{\bullet}$, which are highly unreactive toward cystamine.

Another important point we made concerns the evolution with LET of the ferric ion production at high cystamine concentrations. Our simulations clearly showed the production of Fe^{3+} at cystamine levels above $\sim 10^{-2}$ *M* was less and less affected by a

change in the LET of the radiation or, in other words, by differences in the geometry of the track structure (spherical spurs *vs.* cylindrical tracks) over the studied range. From a purely mathematical point of view, we also demonstrated the existence of the lower limiting value of $G(Fe^{3+})$ of about 4.6 molecules/100 eV at ~200 s for low-LET 500-MeV irradiating protons at the limit of increasingly large cystamine concentrations. This limit was shown to be mainly due to the oxidation of Fe^{2+} by the peroxyl radicals $ROO^{\bullet}$ formed by addition of oxygen to the organic radicals $R^{\bullet}$ which are produced by reaction of the thiyl radicals $RS^{\bullet}$ with cystamine. This same lower limit was only ~3.6 molecules/100 eV for high-LET 150-keV incident protons. It has been shown that the difference of ~1 *G*-unit between low- and high-LET radiations reflects the inability of cystamine, even at the highest concentrations, to scavenge all of the primary radicals formed early in the columnar regions of the high-LET proton tracks.

The results of this work are obviously of great interest in terms of their predictability. Nevertheless, the good match between calculated and measured yield values at low LET (without any adjustable parameter) supports the computational approach and its usefulness to understand, at the molecular level, indirect radiation damage to complex molecules, such as cystamine – a sulfur-containing molecular system whose radiolysis has never previously been studied by means of Monte-Carlo track chemistry simulations. It also provides good support for the validity and consistency of the kinetic schemes, rate constants, diffusion coefficients and track parameters used in this study to describe the radiolysis of this molecule in aerated Fricke solutions using irradiating protons with different energies in the range of 150 keV-500 MeV. We hope that this basic research will be of interest to clinicians working in the field of proton radiotherapy as well as to scientists involved in the development of risk assessment models for space radiation.

ACKNOWLEDGEMENTS

This work has benefited greatly from many helpful comments and correspondence with Professors P. Wardman and K.-D. Asmus, as well as with our colleagues, the late Professors D. A. Armstrong and C. von Sonntag. The authors also thank Dr. Lisa Whittingstall for her assistance in manuscript editing. Financial support from the Natural Sciences and Engineering Research Council of Canada (Grant No. RGPIN-2015-06100) is gratefully acknowledged.

REFERENCES

1. Hall, E. J.; Giaccia, A. J. Radiobiology for the radiologist. Lippincott Williams & Wilkins, Philadelphia, PA. 2006.
2. Baskar, R.; Lee, K. A.; Yeo, R.; Yeoh, K.-W. *Int. J. Med. Sci.* **2012**, *9*, 193-199,
3. Bump, E. A.; Malaker, K. (*Editors*). Radioprotectors: chemical, biological, and clinical perspectives. CRC Press, Boca Raton, FL. 1998.
4. Kamran, M. Z.; Ranjan, A.; Kaur, N.; Sur, S.; Tandon, V. *Med. Res. Rev*. **2016**, *36*, 461-493.
5. Poggi, M. M.; Coleman, C. N.; Mitchell, J. B. *Curr. Probl. Cancer* **2001**, *25*, 329-412.
6. Wardman, P. *Clin. Oncol.* **2007**, *19*, 397-417.
7. Nukala, U.; Thakkar, S.; Krager, K. J.; Breen, P. J.; Compadre, C. M.; Aykin-Burns, N. *Antioxidants* **2018**, *7*, 33. doi:10.3390/antiox7020033.
8. Conklin, J. J.; Walker, R. I. (*Editors*). Military radiobiology. Academic Press, Orlando, FL. 1987.
9. Azzam, E. I.; Jay-Gerin, J.-P.; Pain, D. *Cancer Lett*. **2012**, *327*, 48-60.
10. Buxton, G. V. *In* Radiation chemistry: principles and applications. *Edited by* Farhataziz and Rodgers, M. A. J. VCH Publishers, New York, NY. 1987. pp. 321-349.
11. Spinks, J. W. T.; Woods, R. J. An introduction to radiation chemistry. 3rd ed. Wiley, New York, NY. 1990.
12. Ferradini C.; Jay-Gerin, J.-P. *Can. J. Chem*. **1999**, *77*, 1542-1575.
13. LaVerne, J. A. *In* Charged particle and photon interactions with matter: chemical, physicochemical, and biological consequences with applications. *Edited by* Mozumder, A. and Hatano, Y. Marcel Dekker, New York, NY. 2004. pp. 403-429.

14. Meesungnoen, J.; Jay-Gerin, J.-P. *In* Charged particle and photon interactions with matter: recent advances, applications, and interfaces. *Edited by* Hatano, Y., Katsumura, Y., and Mozumder, A. Taylor &Francis, Boca Raton, FL. 2011. pp. 355-400.

15. von Sonntag, C. Free-radical-induced DNA damage and its repair: a chemical perspective. Springer-Verlag, Berlin. 2006.

16. ICRU Report No. 16. Linear energy transfer. International Commission on Radiation Units and Measurements, Washington, DC. 1970.

17. Magee, J. L. *Annu. Rev. Nucl. Sci.* **1953**, *3*, 171-192.

18. Freeman, G. R. *In* The study of fast processes and transient species by electron pulse radiolysis. *Edited by* Baxendale, J. H. and Busi, F. D. Reidel Publishing, Dordrecht, Holland. 1982. pp. 19-34.

19. Chatterjee, A.; Holley, W.R. *Adv. Radiat. Biol.* **1993**, *17*, 181-226.

20. Muroya, Y.; Plante, I.; Azzam, E. I.; Meesungnoen, J.; Katsumura, Y.; Jay-Gerin, J.-P. *Radiat. Res.* **2006**, *165*, 485-491.

21. Plante, I.; Filali-Mouhim, A.; Jay-Gerin J.-P. *Radiat. Phys. Chem.* **2005**, *72*, 173-180.

22. O'Neill, P.; Wardman, P. *Int. J. Radiat. Biol.* **2009**, *85*, 9-25.

23. Cadet, J.; Douki, T.; Gasparutto, D.; Ravanat J.-L. *Mutat. Res.* **2003**, *531*, 5-23.

24. Lehnert, S. Biomolecular action of ionizing radiation. Taylor & Francis Group, New York, NY. 2008.

25. Becker, D.; Adhikary, A.; Sevilla, M. D. *In* Charged particle and photon interactions with matter: recent advances, applications, and interfaces. *Edited by* Hatano, Y., Katsumura, Y., and Mozumder, A. Taylor & Francis Group, Boca Raton, FL. 2011. pp. 503-541.

26. Ward, J. F. *In* Radioprotectors and anticarcinogens. *Edited by* Nygaard, O. F. and Simic, M. G. Academic Press, New York, NY. 1983. pp. 73-85.

27. Jayson, G. G.; Owen, T. C.; Wilbraham, A. C. *J. Chem. Soc. (B)* **1967**, 944-949.

28. Bidzilya, V. A.; Golovkova, L. P.; Beregovskaya, N. N.; Basyuk, V. V.; Korol', É. N.; Chuiko, A. A.; Znamenskii, V. V.; Barkaya, V. S. *Pharm. Chem. J.* **1991**, *25*, 782-786.

29. Jayson, G. G.; Wilbraham, A. C. *Chem. Commun. (London).* 1968, 641-642.

30. Lalitha, B.; Mittal, J. P. *Radiat. Eff.* **1971**, *7*, 159-162.

31. Meesat, R.; Jay-Gerin, J.-P.; Khalil, A.; Lepage, M. *J. Phys.: Conf. Ser.* **2009**, *164*, 012006.

32. Meesat, R.; Sanguanmith, S.; Meesungnoen, J.; Lepage, M.; Khalil, A.; Jay-Gerin, J.-P. *Radiat. Res.* **2012**, *177*, 813-826.

33. Fricke, H.; Hart, E. J. *In* Radiation dosimetry. *Edited by* Attix, F. H. and Roesch, W. C. 2nd ed., Vol. II. Academic Press, New York, NY. 1966. pp. 167-239.

34. Watt, D. E. Quantities for dosimetry of ionizing radiations in liquid water. Taylor & Francis, London, UK. 1996.

35. Tommasino, F.; Durante, M. *Cancers* **2015**, *7*, 353-381.

36. Cucinotta, F. A. *PLoS ONE* **2014**, *9*, e96099.

37. Bird, R. P. *Radiat. Res.* **1980**, *82*, 290-296.

38. Sigdestad, C. P.; Grdina, D. J.; Connor, A. M.; Hanson, W. R. *Radiat. Res.* **1986**, *106*, 224-233.

39. Bishayee, A.; Rao, D. V.; Howell, R. W. *Acta Oncol.* **2000**, *39*, 713-720.

40. Dziegielewski, J.; Goetz, W.; Baulch, J. E. *Radiat. Environ. Biophys.* **2010**, *49*, 303-316.

41. Tippayamontri, T.; Sunuchakan, S.; Meesungnoen, J.; Sunaryo, G. R.; Jay-Gerin, J.-P. *Recent Res. Devel. Physical Chem.* **2009**, *10*, 143-211.

42. Das, R. C. *Radiat. Res. Rev*. **1971**, *3*, 121-139.

43. Matthews, R. W. *Int. J. Appl. Radiat. Isot*. **1982**, *33*, 1159-1170.

44. Klassen, N. V.; Shortt, K. R.; Seuntjens, J.; Ross, C. K. *Phys. Med. Biol.* **1999**, *44*, 1609-1624.

45. McEwen, M.; El Gamal, I.; Mainegra-Hing, E.; Cojocaru, C. Determination of the radiation chemical yield (*G*) for the Fricke chemical dosimetry system in photon and electron beams. Report NRC-PIRS-1980. National Research Council Canada, Ottawa, Ontario. 2014.

46. ICRU Report No. 34. The dosimetry of pulsed radiation. International Commission on Radiation Units and Measurements, Bethesda, MD. 1982.

47. Allen, A. O. The radiation chemistry of water and aqueous solutions. D. Van Nostrand Co., Princeton, NJ. 1961.

48. Autsavapromporn, N.; Meesungnoen, J.; Plante. I.; Jay-Gerin, J.-P. *Can. J. Chem*. **2007**, *85*, 214-229.

49. Ferradini, C.; Jay-Gerin, J.-P. *Res. Chem. Intermed.* **2000**, *26*, 549-565.

50. Meesungnoen, J.; Benrahmoune, M.; Filali-Mouhim, A.; Mankhetkorn, S.; Jay-Gerin J.-P. *Radiat. Res.* **2001**, *155*, 269-278.

51. Neta, P.; Huie, R. E.; Ross, A. B. *J. Phys. Chem. Ref. Data* **1988**, *17*, 1027-1284.

52. ICRU Report No. 14. Radiation dosimetry: X rays and gamma rays with maximum photon energies between 0.6 and 50 MeV. International Commission on Radiation Units and Measurements, Washington. 1969.

53. Islam, M. M.; Kanike, V.; Meesungnoen, J.; Lertnaisat, P.; Katsumura, Y.; Jay-Gerin, J.-P. *Chem. Phys. Lett*. **2018**, *693*, 210-215.

54. Tachiya, M. *Radiat. Phys. Chem*. **1983**, *21*, 167-175.

55. Pimblott, S. M.; Pilling, M. J.; Green, N. J. B. *Radiat. Phys. Chem*. **1991**, *37*, 377-388.

56. Pimblott, S. M.; Green, N. J. B. *Res. Chem. Kinet.* **1995**, *3*, 117-174.

57. Frongillo, Y.; Goulet, T.; Fraser, M.-J.; Cobut, V.; Patau, J. P.; Jay-Gerin, J.-P. *Radiat. Phys. Chem.* **1998**, *51*, 245-254.

58. Goulet, T.; Fraser, M.-J.; Frongillo, Y.; Jay-Gerin, J.-P. *Radiat. Phys. Chem.* **1998**, *51*, 85-91.

59. Plante, I. Ph.D. Thesis, Université de Sherbrooke, Sherbrooke, Québec, Canada. 2009.

60. Běgusová, M.; Pimblott, S. M. *Radiat. Prot. Dosim.* **2002**, *99*, 73-76.

61. Elliot, A. J.; Bartels, D. M. The reaction set, rate constants and *g*-values for the simulation of the radiolysis of light water over the range 20° to 350°C based on information available in 2008. Report AECL No. 153-127160-450-001. Chalk River, Ontario: Atomic Energy of Canada Ltd., Chalk River, Ontario. 2009.

62. Jiang, P.-Y.; Katsumura, Y.; Nagaishi, R.; Domae, M.; Ishikawa, K.; Ishigure, K.; Yoshida, Y. *J. Chem. Soc. Faraday Trans.* **1992**, *88*, 1653-1658.

63. Braams, R. *Radiat. Res.* **1966**, *27*, 319-329.

64. Wolff, R. K.; Aldrich, J. E.; Penner, T. L.; Hunt, J. W. *J. Phys. Chem.* **1975**, *79*, 210-219.

65. Buxton, G. V.; Greenstock, C. L.; Helman, W. P.; Ross, A. B. *J. Phys. Chem. Ref. Data* **1988**, *17*, 513-886.

66. Asmus, K.-D. *In* Radiation chemistry: present status and future trends. *Edited by* Jonah, C. D. and Rao, B. S. M. Elsevier, Amsterdam. 2001. pp. 341-393.

67. Schmidt, K. H.; Bartels, D. M. *Chem. Phys.* **1995**, *190*, 145-152.

68. Weston, Jr., R. E.; Schwarz, H. A. Chemical kinetics. Prentice-Hall, Englewood Cliffs, NJ. 1972.

69. Sanguanmith, S.; Muroya, Y.; Tippayamontri, T.; Meesungnoen, J.; Lin, M.; Katsumura, Y.; Jay-Gerin J.-P. *Phys. Chem. Chem. Phys.* **2011**, *13*, 10690-10698.

70. Solomon, T. *J. Chem. Educ.* **2001**, *78*, 1691-1692.

71. Karimi-Maleh, H.; Salimi-Amiri, M.; Karimi, F.; Khalilzadeh, M. A.; Baghayeri, M. *J. Chem.* **2013**, 946230.

72. ICRU Report No. 49. Stopping powers and ranges for protons and alpha particles. International Commission on Radiation Units and Measurements, Bethesda, MD. 1993.

73. Patt, H. M.; Clark, J. W.; Vogel, Jr., H. H. *Proc. Soc. Exp. Biol. Med.* **1953**, *84*, 189-193.

74. Bacq, Z.-M.; Alexander, P. Principes de radiobiologie. Masson, Paris. 1955.

75. Barendsen, G. W.; Walter, H. M. D. *Radiat. Res.* **1964**, *21*, 314-329.

76. Hart, E. J.; Ramler, W. J.; Rocklin, S. R. *Radiat. Res.* **1956**, *4*, 378-393.

77. Barr, N. F.; Schuler, R. H. *J. Phys. Chem.* **1959**, *63*, 808-812.

78. Anderson, A. R.; Hart, E. J. *Radiat. Res.* **1961**, *14*, 689-704.

79. Kochanny, Jr., G. L.; Timnick, A.; Hochanadel, C. J.; Goodman, C. D. *Radiat. Res.* **1963**, *19*, 462-473.

80. Matsui, M.; Seki, H.; Karasawa, T.; Imamura, M. *J. Nucl. Sci. Technol.* **1970**, *7*, 97-104.

81. Sauer, Jr., M. C.; Hart, E. J.; Naleway, C. A.; Jonah, C. D.; Schmidt, K. H. *J. Phys. Chem.* **1978**, *82*, 2246-2248.

82. LaVerne, J. A.; Schuler, R. H. *J. Phys. Chem.* **1987**, *91*, 5770-5776.

83. Elliot, A. J.; Chenier, M. P.; Ouellette, D. C.; Koslowsky, V. T. *J. Phys. Chem.* **1996**, *100*, 9014-9020.

84. Fregene, A. O. *Radiat. Res.* **1967**, *31*, 256-272.

85. Pimblott, S. M.; LaVerne, J. A. *J. Phys. Chem. A* **2002**, *106*, 9420-9427.

86. Bonifačić, M.; Asmus, K.-D. *J. Phys. Chem.* **1984**, *88*, 6286-6290.

87. Neta, P.; Huie, R. E.; Ross, A. B. *J. Phys. Chem. Ref. Data* **1990**, *19*, 413-513.

88. Bonifačić, M.; Schäfer, K.; Möckel, H.; Asmus, K.-D. *J. Phys. Chem*. **1975**, *79*, 1496-1502.

89. Armstrong, D. A. *In* Sulfur-centered reactive intermediates in chemistry and biology. *Edited by* Chatgilialoglu, C. and Asmus, K.-D. Plenum Press, New York, NY. 1990. pp. 121-134.

90. Bonifačić, M.; Asmus, K.-D. *J. Phys. Chem*. **1976**, *80*, 2426-2430.

FIGURE CAPTIONS

Figure 1:

Time evolution of $G(Fe^{3+})$ (in molecule/100 eV) from our Monte Carlo simulations of the radiolysis of Fricke dosimeter solutions (1 m*M* $FeSO_4$ in aerated aqueous 0.4 *M* H_2SO_4) with various concentrations of cystamine, using 150-keV incident protons (LET ~ 72.2 keV/μm) at 25 °C. The different lines correspond to three different cystamine concentrations (indicated to the right of the figure): 10^{-3} *M* (dash-dot line), 10^{-2} *M* (dotted line), and 0.1 *M* (dashed line). For reference, the solid line shows our simulated kinetics of Fe^{3+} ion formation for the Fricke dosimeter without added cystamine under the same irradiation conditions.

Figure 2:

Time evolution of $G(Fe^{3+})$ (in molecule/100 eV) from our Monte Carlo simulations of the radiolysis of Fricke dosimeter solutions (1 m*M* $FeSO_4$ in aerated aqueous 0.4 *M* H_2SO_4) containing various concentrations of cystamine, using 500-MeV incident protons (LET ~ 0.23 keV/μm) at 25 °C. The different lines correspond to four different cystamine concentrations (indicated to the right of the figure): 10^{-4} *M* (dash-dot-dot line), 10^{-3} *M* (dash-dot line), 10^{-2} *M* (dotted line), and 0.1 *M* (dashed line). For reference, the solid line shows our simulated kinetics of Fe^{3+} ion formation for the Fricke dosimeter without added cystamine under the same irradiation conditions.

Figure 3:

Variation of ferric ion yield (in molecule/100 eV) from our Monte Carlo simulations (~200 s after ionization) of the radiolysis of Fricke/cystamine solutions (1 m*M* $FeSO_4$ in aerated aqueous 0.4 *M* H_2SO_4) with cystamine concentration in the range ~5×10^{-7}-0.1 *M*, using 500-MeV (solid line) and 150-keV (dashed line) irradiating

protons (LET ~ 0.23 and 72.2 keV/μm, respectively) at 25 °C. The symbols correspond to experimental Fe^{3+} ion yield data obtained by different authors for 250-kVp X-ray [(●) ref. 29] and ^{60}Co γ-ray [(▲) ref. 30 and (□) ref. 32] irradiations. There is a very good agreement between the results of the simulations using the low-LET 500-MeV incident protons and the experimental yields of Fe^{3+} obtained for X- and γ-irradiations. Unfortunately, in the case of high-LET 150-keV irradiating protons, there are no experimental data available in the literature with which to compare our results.

Figure 4:

Panel a: Time evolution of $G(Fe^{3+})$ (in molecule/100 eV) for 150-keV incident protons (LET ~ 72.2 keV/μm) in the radiolysis of aerated Fricke dosimeter solutions containing 1 m*M* $FeSO_4$ and 1 m*M* cystamine in aqueous 0.4 *M* H_2SO_4 at 25 °C. The concentration of dissolved oxygen used in the calculations is 0.25 m*M*. The solid line shows our simulated kinetics of Fe^{3+} ion formation.

Panel b: Time dependence of the extents $\Delta G(Fe^{3+})$ (in molecule/100 eV) of the different reactions that contribute to the formation of Fe^{3+} ions, calculated from our Monte Carlo simulations in the interval ~10^{-10}-200 s. The oxidation of Fe^{2+} ions to Fe^{3+} involves reactions mainly with $HO_2^{\bullet}$, H_2O_2, and the cystamine-radical species $RS^{\bullet}$ and $RSSR^{\bullet+}$ (see text).

Figure 5:

Panel a: Time evolution of $G(Fe^{3+})$ (in molecule/100 eV) for 500-MeV incident protons (LET ~ 0.23 keV/μm) in the radiolysis of aerated Fricke solutions containing 1 m*M* $FeSO_4$ and 1 m*M* cystamine in aqueous 0.4 *M* H_2SO_4 at 25 °C. The concentration of dissolved oxygen used in the calculations is 0.25 m*M*. The solid line shows our simulated kinetics of Fe^{3+} ion formation.

Panel b: Time dependence of the extents $\Delta G(Fe^{3+})$ (in molecule/100 eV) of the different reactions that contribute to the formation of Fe^{3+} ions, calculated from our Monte-Carlo simulations in the interval ~10^{-10}-200 s. The oxidation of Fe^{2+} ions to Fe^{3+} involves reactions mainly with $HO_2^{\bullet}$, H_2O_2, and the cystamine-radical species $RS^{\bullet}$ and $RSSR^{\bullet+}$ (see text).

Figure 6:

Time dependence of the extents $\Delta G(RSSR)$ (in molecule/100 eV) of the various reactions that contribute to the formation and decay of cystamine (RSSR) (see text), calculated from our Monte-Carlo simulations of the radiolysis of aerated Fricke solutions (1 m*M* $FeSO_4$ and 1 m*M* cystamine in aqueous 0.4 *M* H_2SO_4) by 500-MeV (LET ~ 0.23 keV/μm) (panel a) and 150-keV (LET ~ 72.2 keV/μm) (panel b) incident protons at 25 °C and in the interval ~10^{-10}-200 s.

Figure 7:

Plot of the ferric ion yield $G(Fe^{3+})$ (in molecule/100 eV) from the proton radiolysis of air-saturated Fricke solutions (1 m*M* $FeSO_4$ in aqueous 0.4 *M* H_2SO_4) without cystamine addition, as a function of LET in the range of ~0.2-75 keV/μm at 25 °C. The solid curve shows the values of $G(Fe^{3+})$ obtained from our Monte Carlo simulations (at ~200 s after ionization) using irradiating protons of various initial energies between ~500 MeV and 150 keV. The dashed curve shows results of ref. 48 for oxidation of ferrous sulfate by protons for LET varying from ~0.3 to 15 keV/μm. Experiment: (◁) ref. 76, (▽) ref. 77, (◇) ref. 78, (o) ref. 79, (□) ref. 80, (☆) ref. 81, (Δ) ref. 82, and (▷) ref. 83. For the sake of completeness, experimental $G(Fe^{3+})$ values determined at low LET for a number of X-, γ- and β-rays of a wide range of energy are also shown in the figure: (+), ref. 84 and (×) refs. 44 and 45. Finally, the arrow on the

left of the figure shows the accepted value (15.5 ± 0.2 molecules/100 eV) of the yield of the (aerated) Fricke dosimeter for ^{60}Co γ-rays or fast electrons.

Figure 8:

Effect of LET on the ferric ion yield (in molecule/100 eV) as obtained from our Monte Carlo simulations (at ~200 s following ionization) of the radiolysis of (aerated) Fricke/cystamine solutions (1 m*M* $FeSO_4$ in aerated aqueous 0.4 *M* H_2SO_4) containing various concentrations of cystamine, using irradiating protons in the range of 500 MeV-150 keV, at 25 °C. The concentration of dissolved oxygen used in the calculations is 0.25 m*M*. The different lines correspond to four different cystamine concentrations: 10^{-3} *M* (dashed line), 10^{-2} *M* (short dashed line), 0.1 *M* (dotted line), and 1 *M* (short dotted line). The solid line shows our results for the Fricke dosimeter without added cystamine under the same irradiation conditions.

Figure 9:

Time dependence of the extents $\Delta G(Fe^{3+})$ (in molecule/100 eV) of the various reactions that contribute to the formation of Fe^{3+} ions (see text), calculated from our Monte Carlo simulations of the radiolysis of aerated Fricke solutions (1 m*M* $FeSO_4$ in aqueous 0.4 *M* H_2SO_4) with various concentrations of cystamine: 0.01 *M* (panel a), 0.1 *M* (panel b), and 1 *M* (panel c), using 500-MeV incident protons (LET ~ 0.23 keV/μm) at 25 °C in the interval 10^{-10}-200 s. The concentration of dissolved oxygen used in the calculations is 0.25 m*M*. It can be clearly seen that the formation of ferric ions mainly results from the reactions of Fe^{2+} with $HO_2^{\bullet}$, H_2O_2, and the cystamine-radicals $RS^{\bullet}$ and $RSSR^{\bullet+}$ at 0.01 *M* cystamine. However, with increasing cystamine concentration, the contribution of these different reactions to the formation of Fe^{3+} decreases sharply in favor of the reaction of Fe^{2+} with the peroxyl radical $ROO^{\bullet}$, which largely dominates at 1 *M* cystamine.

Figure 10:

Time evolution of the yields G(X) (in molecule/100 eV) of all reactive species (X) involved in the radiolysis of aerated Fricke dosimeter solutions (1 m*M* $FeSO_4$ in aqueous 0.4 *M* H_2SO_4) with 1 *M* cystamine, as obtained from our Monte Carlo simulations for 500-MeV irradiating protons (LET ~ 0.23 keV/μm) at 25 °C and in the interval ~10^{-12}-200 s. For clarity, $G(RSSR^{\bullet+})$ and $G(HO_2^{\bullet})$ are not shown in the figure as they are very small over the considered time interval. The concentration of dissolved oxygen used in the calculations is 0.25 m*M*.

Figure 1

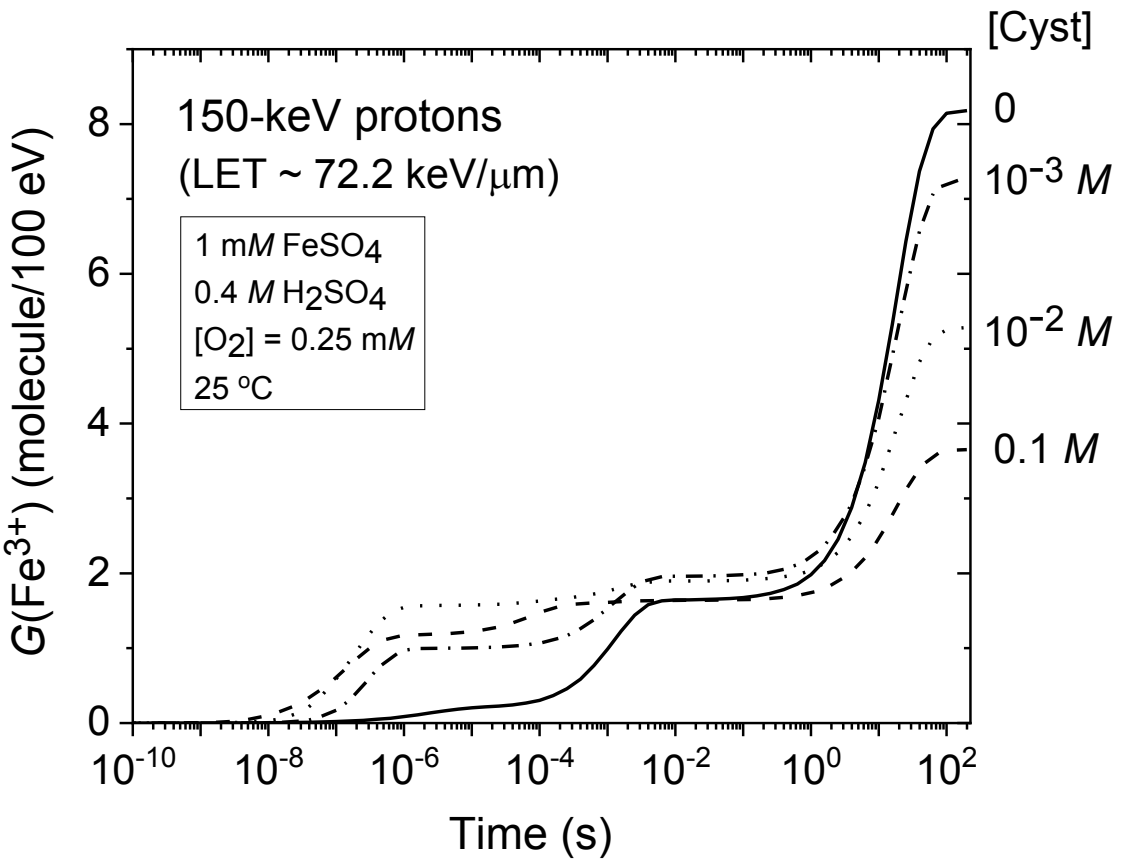
150-keV protons
(LET ~ 72.2 keV/μm)
1 m*M* FeSO4
0.4 *M* H2SO4
[O2] = 0.25 m*M*
25 °C
[Cyst]
0
10-3 *M*
10-2 *M*
0.1 *M*
G(Fe3+) (molecule/100 eV)
Time (s)
0
2
4
6
8
10-10
10-8
10-6
10-4
10-2
100
102

Figure 2

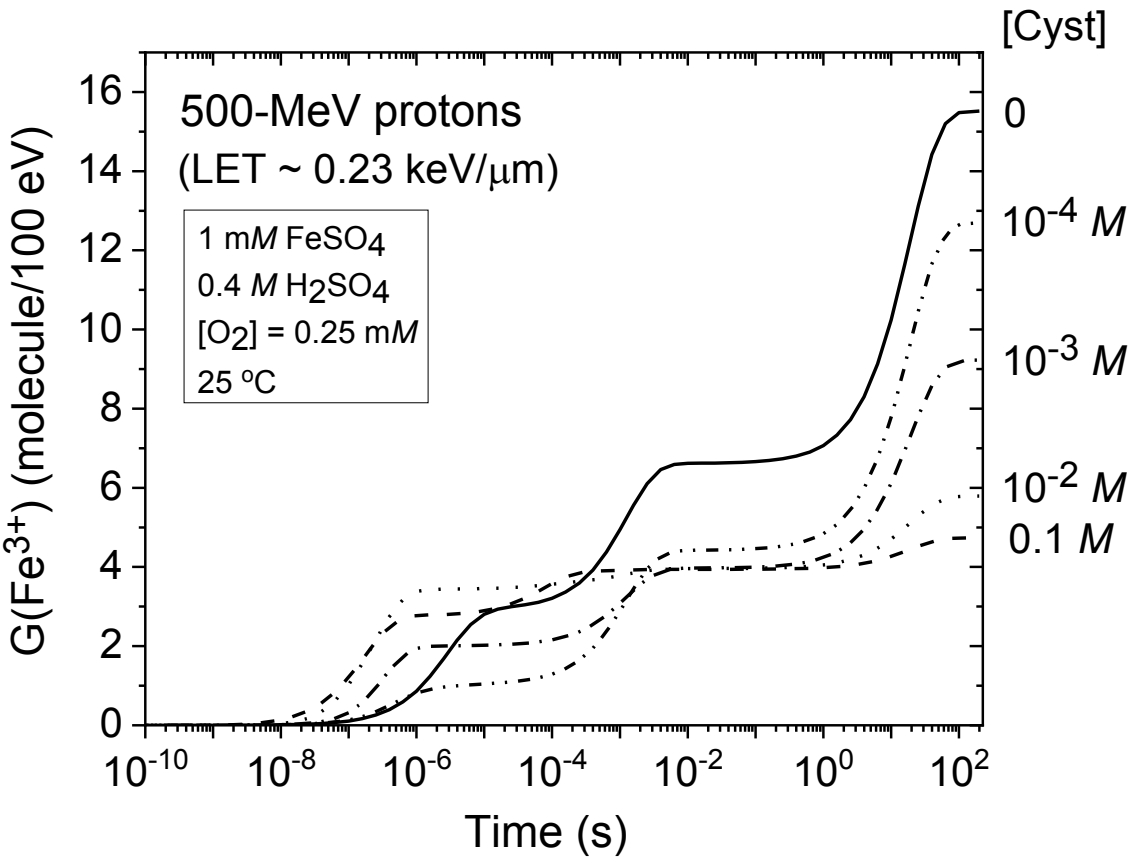
500-MeV protons
(LET ~ 0.23 keV/μm)
1 m*M* FeSO4
0.4 *M* H2SO4
[O2] = 0.25 m*M*
25 °C
G(Fe3+) (molecule/100 eV)
Time (s)
[Cyst]
0
10-4 *M*
10-3 *M*
10-2 *M*
0.1 *M*

Figure 3

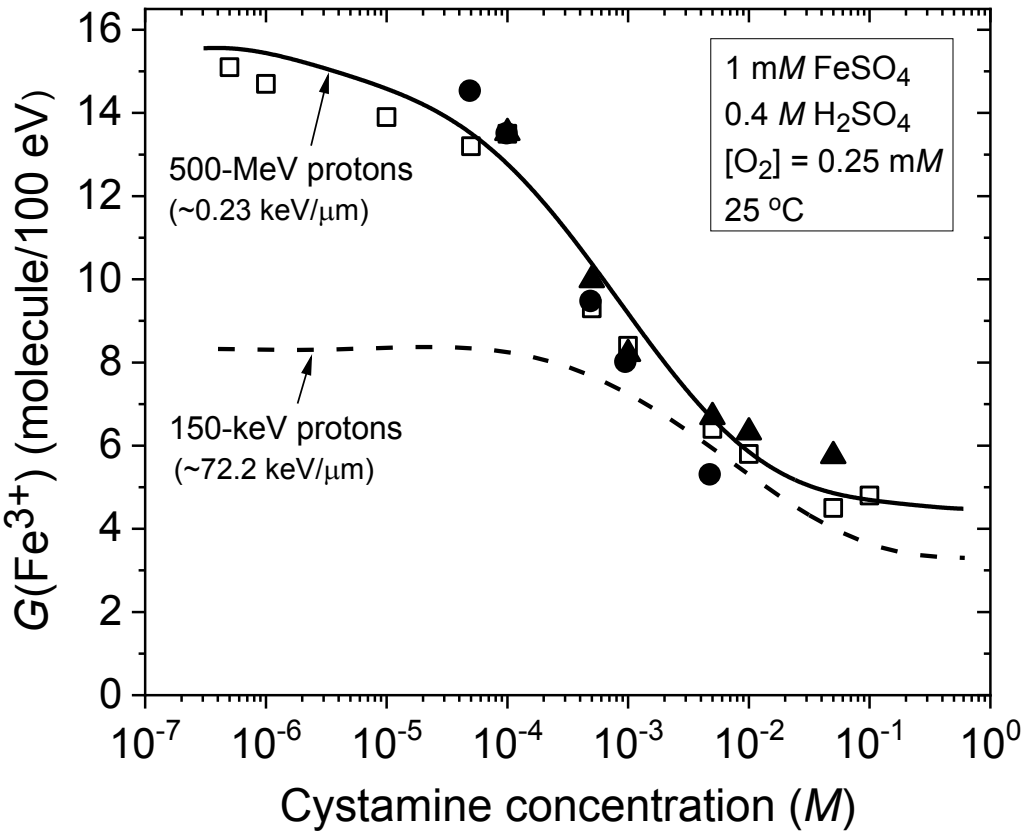
1 m*M* $FeSO_4$
0.4 *M* H_2SO_4
[O_2] = 0.25 m*M*
25 °C
500-MeV protons
(~0.23 keV/μm)
150-keV protons
(~72.2 keV/μm)
$G(Fe^{3+})$ (molecule/100 eV)
Cystamine concentration (*M*)
0
2
4
6
8
10
12
14
16
10^{-7}
10^{-6}
10^{-5}
10^{-4}
10^{-3}
10^{-2}
10^{-1}
10^{0}

Figure 4

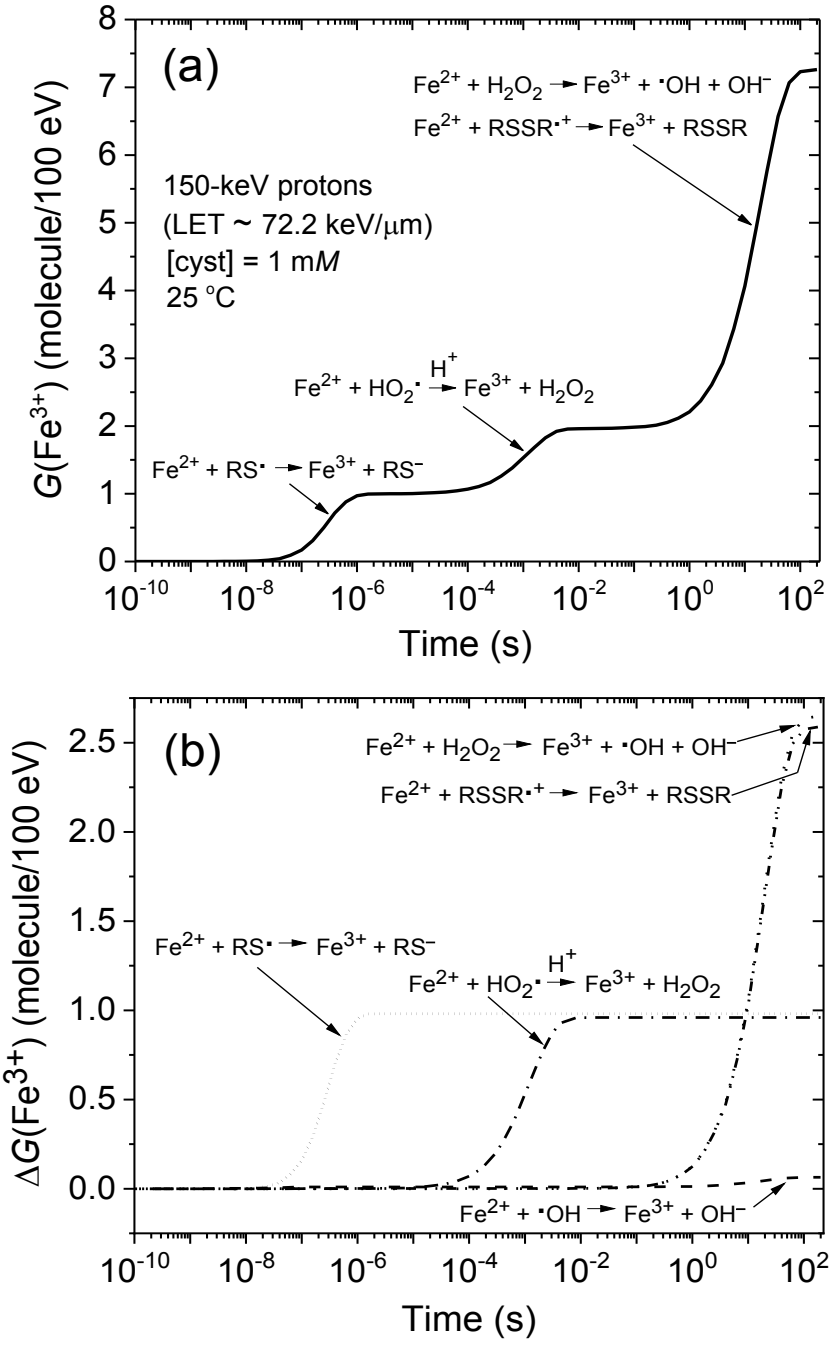
(a)
$Fe^{2+} + H_2O_2 \rightarrow Fe^{3+} + {}^{\bullet}OH + OH^-$
$Fe^{2+} + RSSR^{\bullet+} \rightarrow Fe^{3+} + RSSR$
150-keV protons
(LET ~ 72.2 keV/μm)
[cyst] = 1 m*M*
25 °C
$Fe^{2+} + HO_2^{\bullet} \xrightarrow{H^+} Fe^{3+} + H_2O_2$
$Fe^{2+} + RS^{\bullet} \rightarrow Fe^{3+} + RS^-$
$G(Fe^{3+})$ (molecule/100 eV)
Time (s)
(b)
$Fe^{2+} + H_2O_2 \rightarrow Fe^{3+} + {}^{\bullet}OH + OH^-$
$Fe^{2+} + RSSR^{\bullet+} \rightarrow Fe^{3+} + RSSR$
$Fe^{2+} + RS^{\bullet} \rightarrow Fe^{3+} + RS^-$
$Fe^{2+} + HO_2^{\bullet} \xrightarrow{H^+} Fe^{3+} + H_2O_2$
$Fe^{2+} + {}^{\bullet}OH \rightarrow Fe^{3+} + OH^-$
$\Delta G(Fe^{3+})$ (molecule/100 eV)
Time (s)

Figure 5

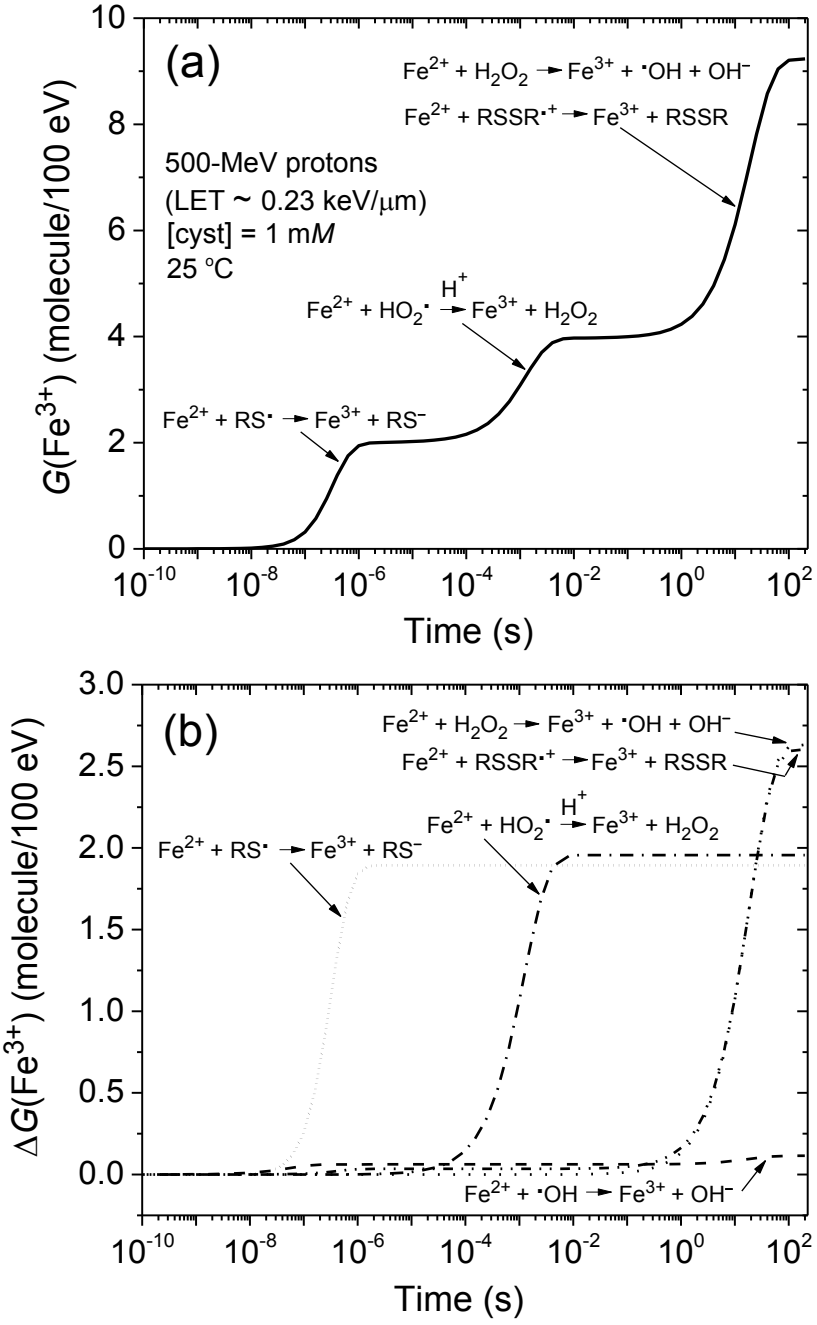
(a)
$Fe^{2+} + H_2O_2 \rightarrow Fe^{3+} + {}^{\bullet}OH + OH^-$
$Fe^{2+} + RSSR^{\bullet+} \rightarrow Fe^{3+} + RSSR$
500-MeV protons
(LET ~ 0.23 keV/μm)
[cyst] = 1 m*M*
25 °C
$Fe^{2+} + HO_2^{\bullet} \xrightarrow{H^+} Fe^{3+} + H_2O_2$
$Fe^{2+} + RS^{\bullet} \rightarrow Fe^{3+} + RS^-$
$G(Fe^{3+})$ (molecule/100 eV)
Time (s)
(b)
$Fe^{2+} + H_2O_2 \rightarrow Fe^{3+} + {}^{\bullet}OH + OH^-$
$Fe^{2+} + RSSR^{\bullet+} \rightarrow Fe^{3+} + RSSR$
$Fe^{2+} + HO_2^{\bullet} \xrightarrow{H^+} Fe^{3+} + H_2O_2$
$Fe^{2+} + RS^{\bullet} \rightarrow Fe^{3+} + RS^-$
$Fe^{2+} + {}^{\bullet}OH \rightarrow Fe^{3+} + OH^-$
$\Delta G(Fe^{3+})$ (molecule/100 eV)
Time (s)

Figure 6

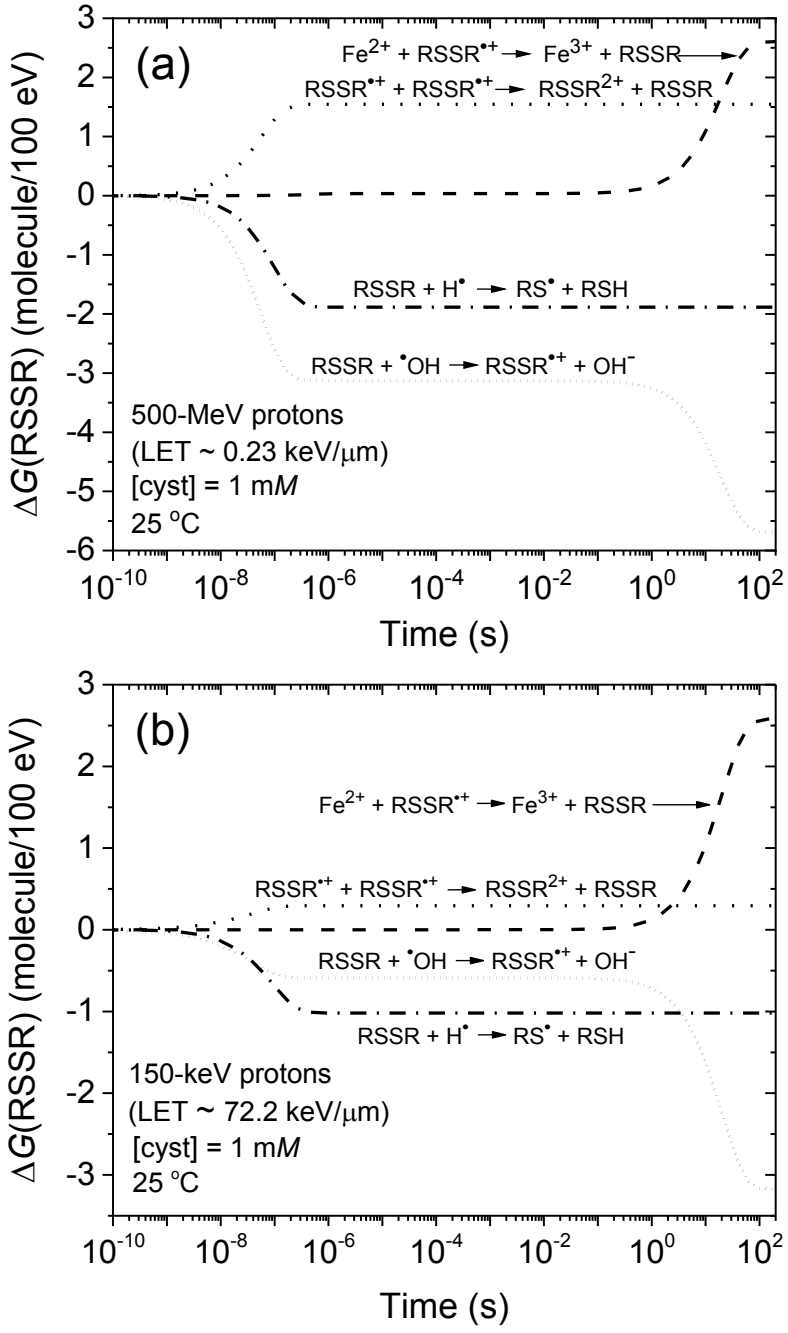
(a)
Fe2+ + RSSR•+ → Fe3+ + RSSR
RSSR•+ + RSSR•+ → RSSR2+ + RSSR
RSSR + H• → RS• + RSH
RSSR + •OH → RSSR•+ + OH−
500-MeV protons
(LET ~ 0.23 keV/μm)
[cyst] = 1 mM
25 °C
ΔG(RSSR) (molecule/100 eV)
Time (s)
(b)
Fe2+ + RSSR•+ → Fe3+ + RSSR
RSSR•+ + RSSR•+ → RSSR2+ + RSSR
RSSR + •OH → RSSR•+ + OH−
RSSR + H• → RS• + RSH
150-keV protons
(LET ~ 72.2 keV/μm)
[cyst] = 1 mM
25 °C
ΔG(RSSR) (molecule/100 eV)
Time (s)

Figure 7

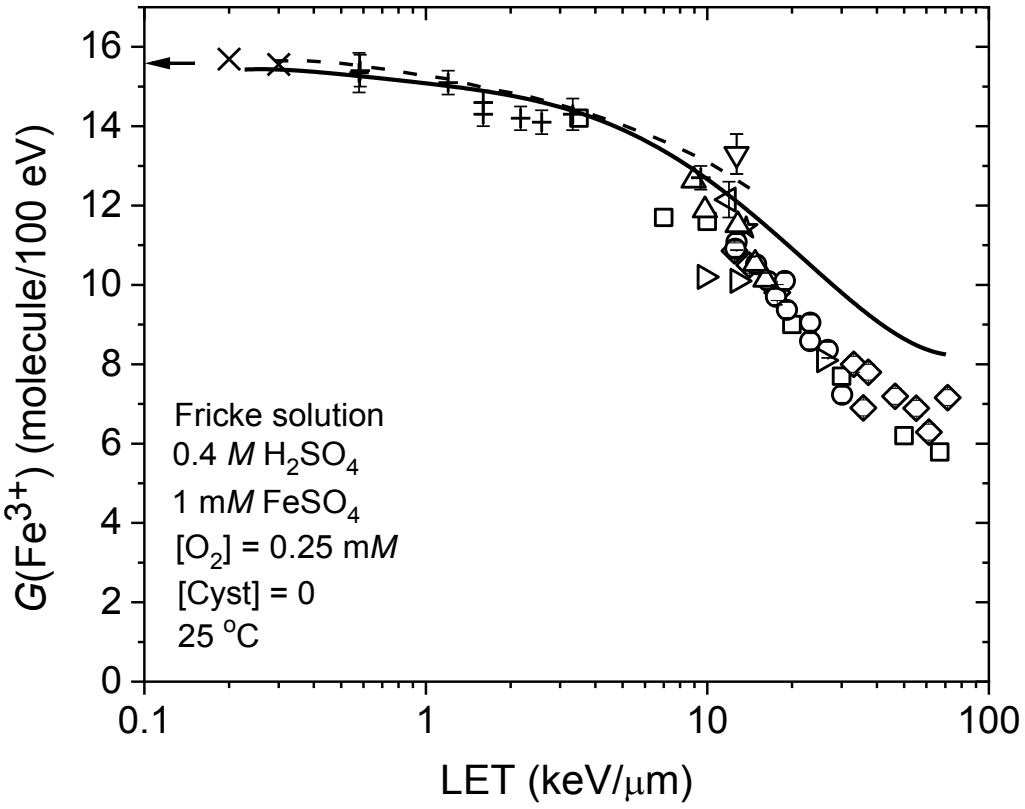
16
14
12
10
8
6
4
2
0
0.1
1
10
100
G(Fe3+) (molecule/100 eV)
LET (keV/μm)
Fricke solution
0.4 M H2SO4
1 mM FeSO4
[O2] = 0.25 mM
[Cyst] = 0
25 °C

Figure 8

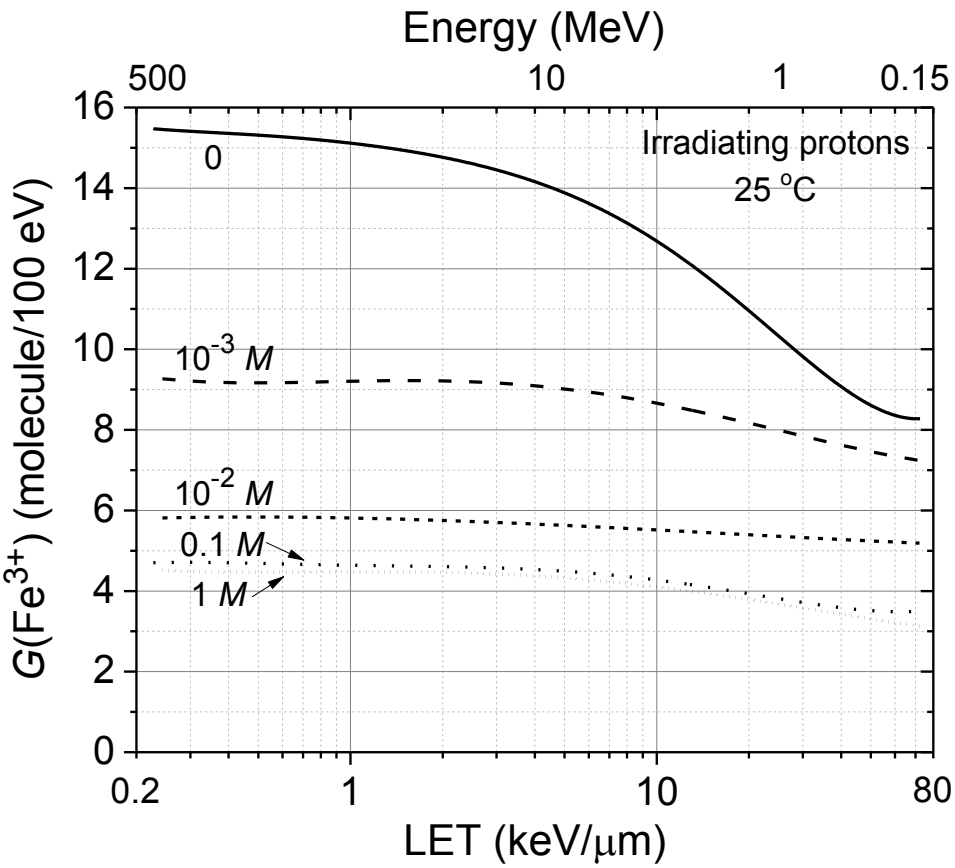
Energy (MeV)
500
10
1
0.15
Irradiating protons
25 °C
0
10-3 M
10-2 M
0.1 M
1 M
G(Fe3+) (molecule/100 eV)
LET (keV/μm)
0.2
1
10
80

Figure 9

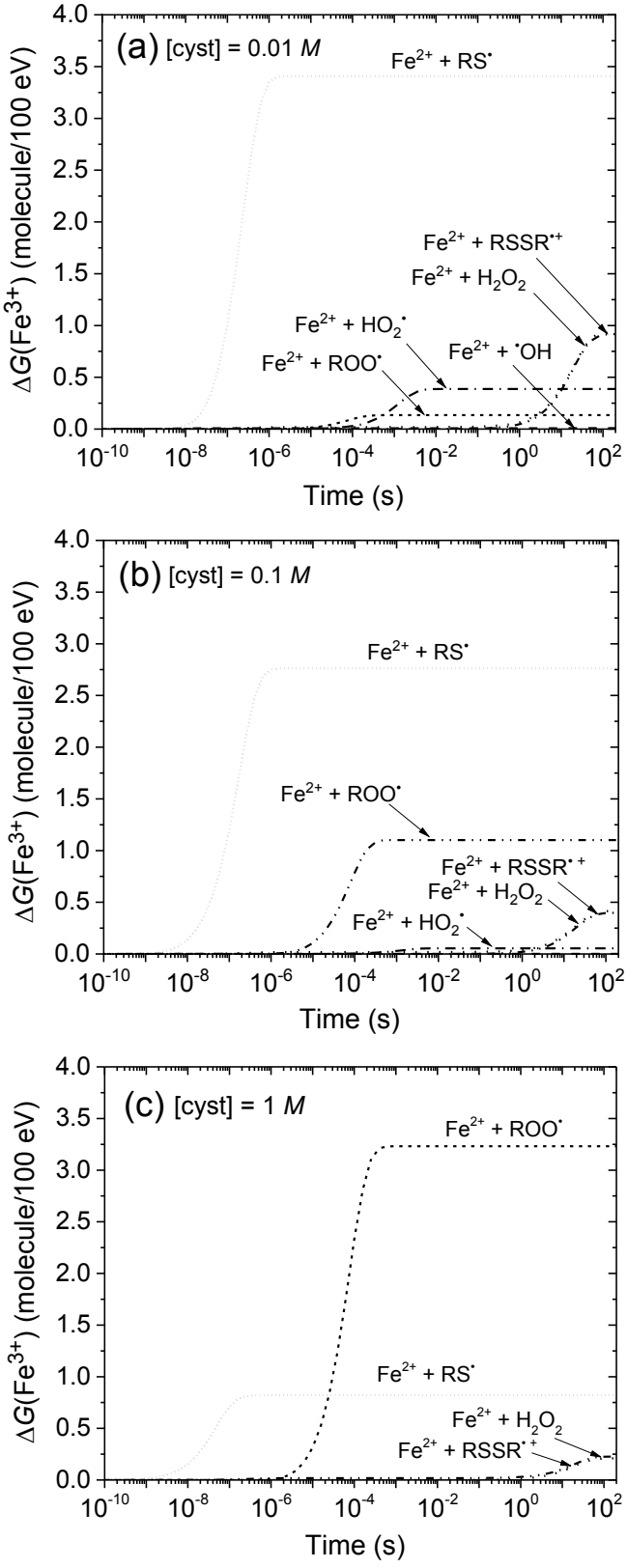
(a) [cyst] = 0.01 M
Fe2+ + RS•
Fe2+ + RSSR•+
Fe2+ + H2O2
Fe2+ + HO2•
Fe2+ + ROO•
Fe2+ + •OH
ΔG(Fe3+) (molecule/100 eV)
Time (s)
(b) [cyst] = 0.1 M
Fe2+ + RS•
Fe2+ + ROO•
Fe2+ + RSSR•+
Fe2+ + H2O2
Fe2+ + HO2•
ΔG(Fe3+) (molecule/100 eV)
Time (s)
(c) [cyst] = 1 M
Fe2+ + ROO•
Fe2+ + RS•
Fe2+ + H2O2
Fe2+ + RSSR•+
ΔG(Fe3+) (molecule/100 eV)
Time (s)

Figure 10

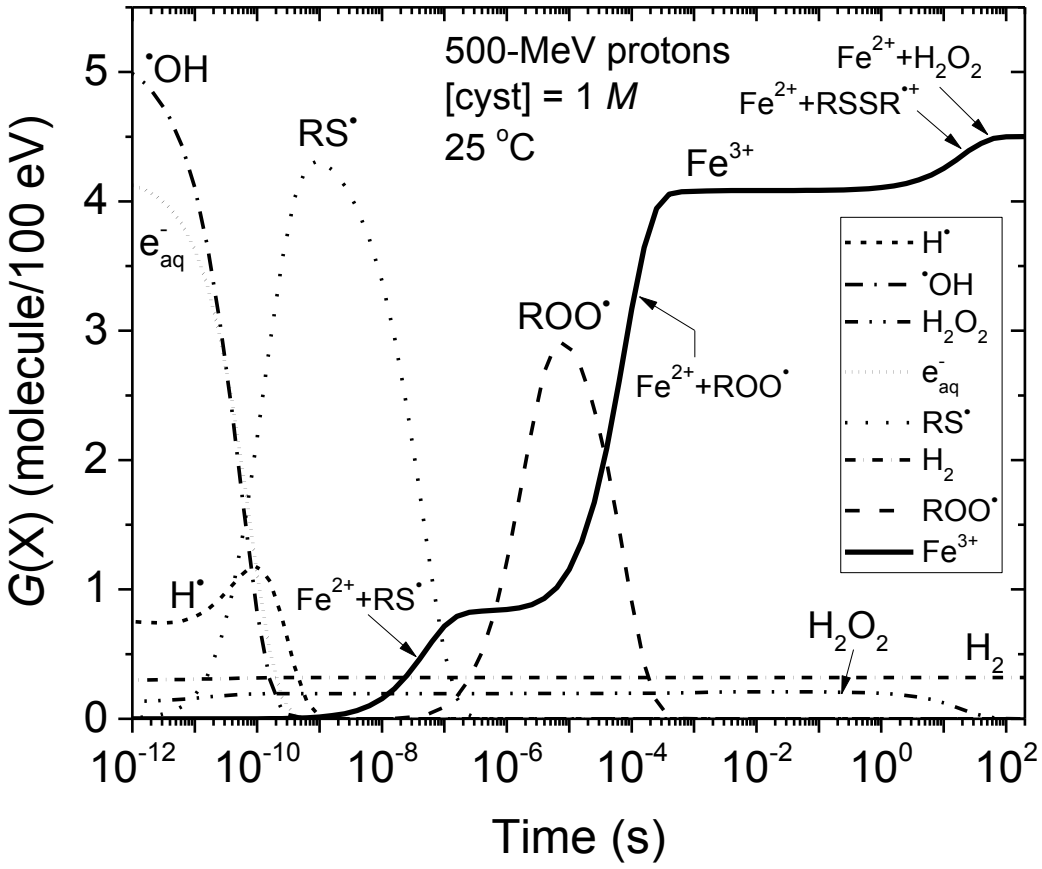
500-MeV protons
[cyst] = 1 M
25 °C
G(X) (molecule/100 eV)
Time (s)
•OH
RS•
e-aq
H•
ROO•
Fe3+
Fe2+ +H2O2
Fe2+ +RSSR•+
Fe2+ +RS•
Fe2+ +ROO•
H2O2
H2
H•
•OH
H2O2
e-aq
RS•
H2
ROO•
Fe3+

7. DISCUSSION

Countless simulations were conducted during this research project to better understand the mechanisms underlying the radioprotective action of cystamine. In this discussion section, we will present a certain number of results that have been achieved, but which were not included in the previous article. In particular, we will present some results on the radioprotective capacity of cystamine when Fricke dosimeter/cystamine solutions are irradiated, not only by fast protons, but also by accelerated helium and carbon ions, i.e., under very high-LET irradiation conditions.

7.1 The effect of LET on the yield of the Fricke dosimeter

It has been known since very early studies with internal and external ^{210}Po α-particle sources that the yield for oxidation of ferrous ions in the Fricke dosimeter is appreciably less for high-LET radiations (such as accelerated ions and neutrons), than for low-LET radiations (e.g., ^{60}Co γ-rays, hard X-rays, fast electrons or high-energy protons) (ALLEN, 1961; FRICKE & HART, 1966; for a recent review, see: TIPPAYAMONTRI et al., 2009).

Figure 7.1 shows the values of $G(Fe^{3+})$ calculated from our Monte Carlo simulations of the radiolysis of aerated solutions of 1 m*M* $FeSO_4$ in 0.4 *M* H_2SO_4 as a function of LET for incident protons, helium and carbon ions of initial energies in the range of 500 MeV-150 keV/nucleon at 25 °C. It is seen that as the LET increases the Fe^{3+} yield diminishes. Our computed values are compared with experimental data of $G(Fe^{3+})$ versus LET obtained over many years by a number of different workers using a variety of radiations of different energies. Despite the relatively large uncertainties of the reported measurements, there is a good agreement between theory and experiment over the whole LET range considered, which in turn gives good support to the validity and consistency of the calculational approach employed in this study to describe the radiolysis of the Fricke dosimeter (see Chapter 4).

This dependence of $G(Fe^{3+})$ on LET is explained by the fact that the production of ferric ions in the Fricke system is *most sensitive* to free-radical yields; indeed, according to equation [20], the lower the yield of radicals that escape the radiation track, the lower the Fricke *G*-values. Since increasing LET has the effect of reducing the free-radical product yields from water, it follows that $G(Fe^{3+})$ also decreases as the LET increases. This behavior directly results from the

increased importance of intra-track processes at higher LET, which enhance radical-radical recombination reactions producing molecular products.

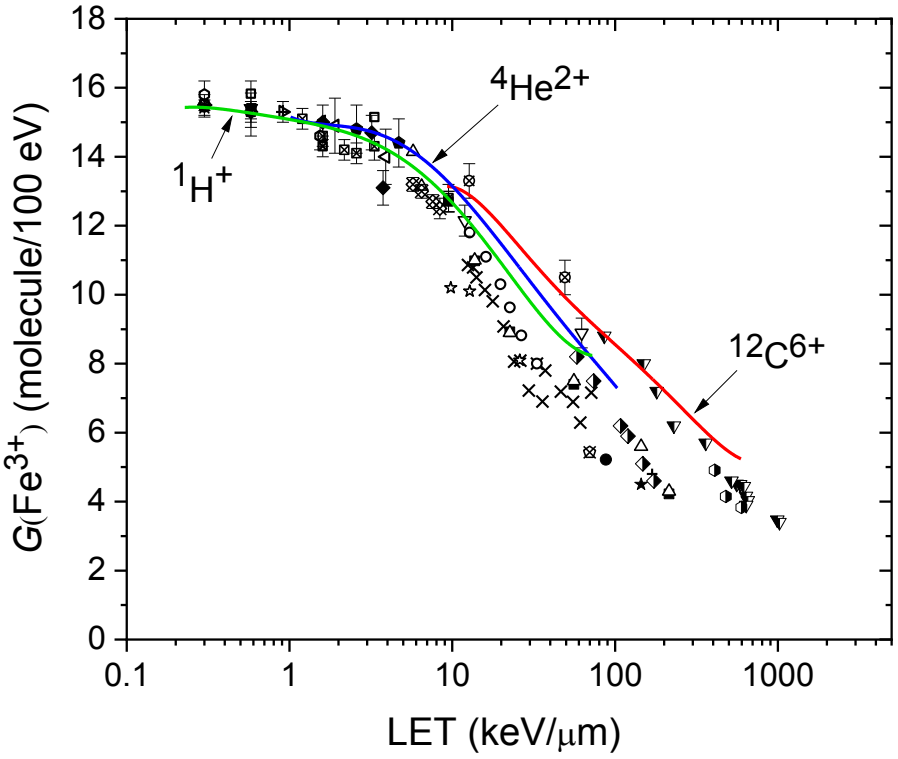

Figure 7.1 – Plot of the ferric ion yield $G(Fe^{3+})$ (in molecule/100 eV) of the radiolysis of aerated Fricke solutions (1 m*M* $FeSO_4$ in aqueous 0.4 *M* H_2SO_4) with no cystamine addition as a function of LET (in keV/μm), at 25 °C. The solid lines show the values of $G(Fe^{3+})$ obtained from our Monte Carlo simulations (at ~200 s after ionization) using incident protons (green), $^4He^{2+}$ (blue) and $^{12}C^{6+}$ (red) ions of various initial energies between ~500 MeV and 150 keV per nucleon. Experiment: (□) HARDWICK (1952*a*, *b*), ALLEN (1954); (▲) HART (1954), McDONELL & HART (1954); (▼) DONALDSON & MILLER (1955); (×) HART et al. (1956); (◆) HAYBITTLE et al. (1956); (○) SCHULER & ALLEN (1956, 1957); (■) SCHULER & BARR (1956), BARR & SCHULER (1959); (◁) BACK & MILLER (1957); (△) LEFORT (1957, 1958); (⬟) GEVANTMAN & PESTANER (1959); (◀) COATSWORTH et al. (1960); (◇) PEISACH & STEYN (1960); (+) ANDERSON & HART (1961); (★) PUCHEAULT (1961); (⬡) SHALEK et al. (1962); (⊠) DAVIES et al. (1963); (⊠) FREGENE (1967); (●) MARIANO & SANTOS (1967); (⊠) ICRU REPORT 17 (1970); (▽) IMAMURA et al. (1970); (◑) MATSUI et al. (1970); (⊠) JULIEN & PUCHEAULT (1972); (⊠) SAUER et al. (1978); (⊞) ICRU REPORT 34 (1982); LAVERNE & SCHULER (1996): data for carbon ions (◗) and for helium ions (•); (◮) ELLIOT et al. (1996).

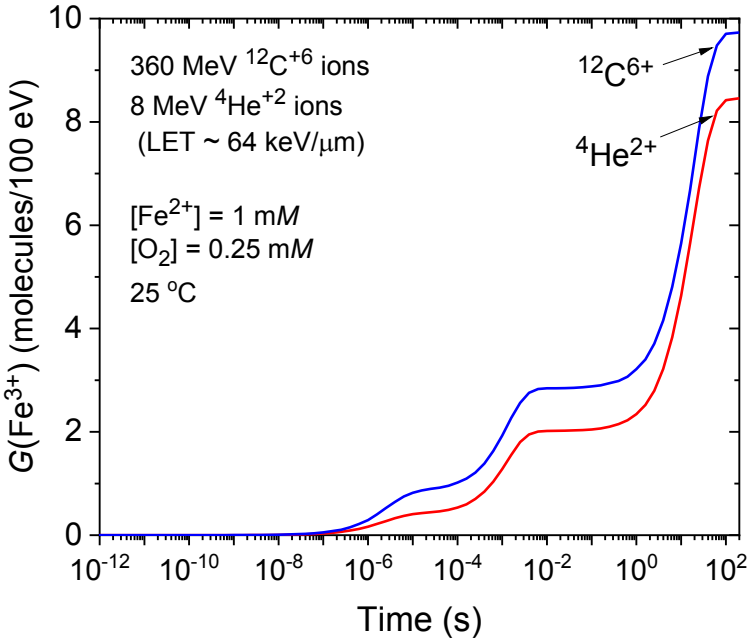

Figure 7.2 – Time evolution of $G(Fe^{3+})$ (in molecule/100 eV) as obtained from our Monte Carlo simulations of the radiolysis of aerated Fricke dosimeter solutions containing 1 m*M* $FeSO_4$ in aqueous 0.4 *M* H_2SO_4 at 25 °C, for incident 8 MeV $^4He^{2+}$ (red solid line) and 360 MeV $^{12}C^{6+}$ (blue solid line) ions, that is, *under the same LET conditions* (~64 keV/μm). The concentration of dissolved oxygen used in the calculations is 0.25 m*M*. As we can see, $G(Fe^{3+})$ is greater for the higher-*Z* ion.

It is also apparent from Fig. 7.1 that LET is not the only parameter that describes the observed yields. Indeed, for the three different types of irradiating ions considered here, at *equal* LET the ferric ion yields are greater for the ion with the higher nuclear charge, that is, in the order $H^+ < He^{2+} < C^{6+}$. Such an irradiating-ion dependence of the yields at a given LET has been frequently noted and has been reviewed briefly in Chapter 3, Sect. 3.1. Recall here that it is explained by subtle differences in the geometry of the ion track structures. These differences originate from the quantum mechanical theory of stopping power ($-dE/dx$) of BETHE (1930), which predicts that, for two incident ions at the same LET, the one with the higher charge will have a higher velocity. As seen before, in terms of track structure, a higher incident ion velocity produces a *larger* radial distribution of energy deposition due to the greater mean energy of ejected secondary electrons (see Fig. 3.5). As a result, the ion with the higher charge is losing its energy in a larger volume around the tracks. In other words, the yields of free radicals that

escape the radiation track are greater for the higher-Z ion, resulting in an increase in Fricke G-values (see equation [20]). Figure 7.2 illustrates this increase in Fe^{3+} formation in the case of the radiolysis of the Fricke dosimeter by two impacting helium and carbon ions, calculated under the same LET conditions.

Despite these difficulties, the LET still remains nowadays the most commonly used single parameter in the radiation chemistry of heavy ions and is usually valid for a given type of particle.

7.2 Influence of added cystamine on the Fricke yield under helium and carbon ion irradiation

In this thesis, our efforts have been primarily oriented to examining the radical scavenging properties of cystamine with respect to the primary species produced by *fast protons under various LET irradiation conditions* in the radiolysis of water. The familiar radiolytic oxidation of ferrous ions in the Fricke dosimeter solution was taken as the basis for our method of protection evaluation. Here, we will present some results on the radioprotective ability of cystamine when Fricke dosimeter/cystamine solutions are irradiated, not by fast protons, but by *accelerated helium and carbon ions*, i.e., under (very) high-LET irradiation conditions. This has an obvious impact on medical physics since the most recent technology for treating cancer involves heavy ion accelerators such as carbon ions. It also has an significant impact in clinical radiotherapy since the interest of "hadrontherapy" (see Chapter 1) is based on the fact that it delivers precision treatment of tumors, exploiting the characteristic shape (the Bragg peak) of the energy deposition in the tissues for charged hadrons (protons, neutrons, and ions). In particular, carbon ions have clear advantages over protons, such as superior biological efficiency and a better depth dose distribution due to a lower lateral diffusion.

Figures 7.3 and 7.4 show, as examples, the kinetics of Fe^{3+} formation as obtained from our simulations of the radiolysis of the Fricke dosimeter under aerated conditions, for irradiating 8 MeV $^{4}He^{2+}$ and 360 MeV $^{12}C^{6+}$ ions, respectively, and in the presence of various concentrations of added cystamine. As we have seen above, the choice of these energies is such that these two ions have the *same* LET (~64 keV/μm), thus offering an optimal comparison as to the effect of the added cystamine concentration.

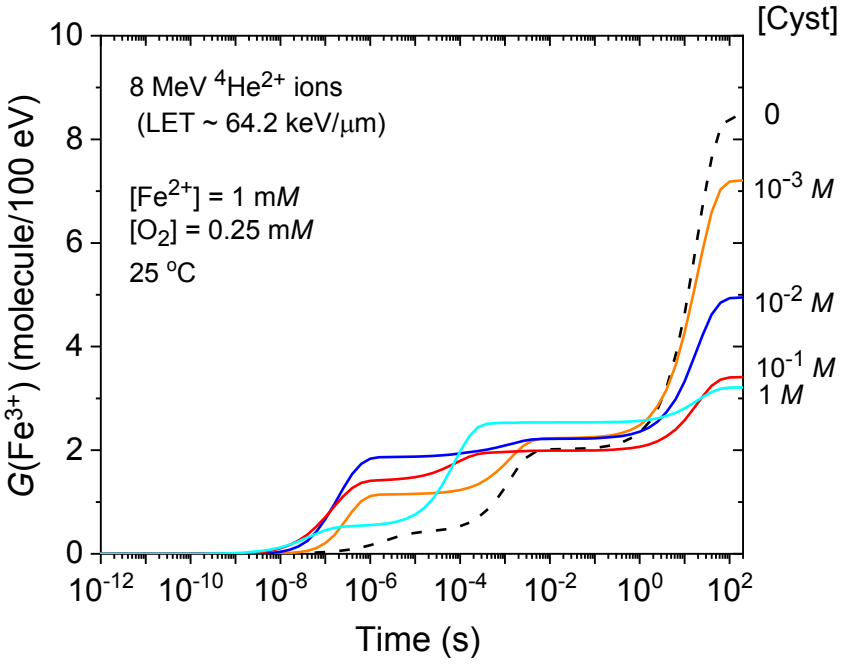

Figure 7.3 – Time evolution of $G(Fe^{3+})$ (in molecule/100 eV) as obtained from our Monte Carlo simulations of the radiolysis of aerated Fricke dosimeter solutions (1 m*M* $FeSO_4$ in aqueous 0.4 *M* H_2SO_4) containing various concentrations of cystamine, using *8 MeV irradiating* $^4He^{2+}$ *ions* (LET ~ 64.2 keV/μm) at 25 °C. The different lines correspond to four different cystamine concentrations, indicated to the right of the figure: 10^{-3} *M* (orange solid line), 10^{-2} *M* (blue solid line), 10^{-1} *M* (red solid line) and 1 *M* (cyan solid line). For reference, the black dashed line shows our simulated kinetics of Fe^{3+} formation for the normal Fricke dosimeter with no added cystamine under the same irradiation conditions. The concentration of dissolved O_2 used in the calculations is 0.25 m*M*.

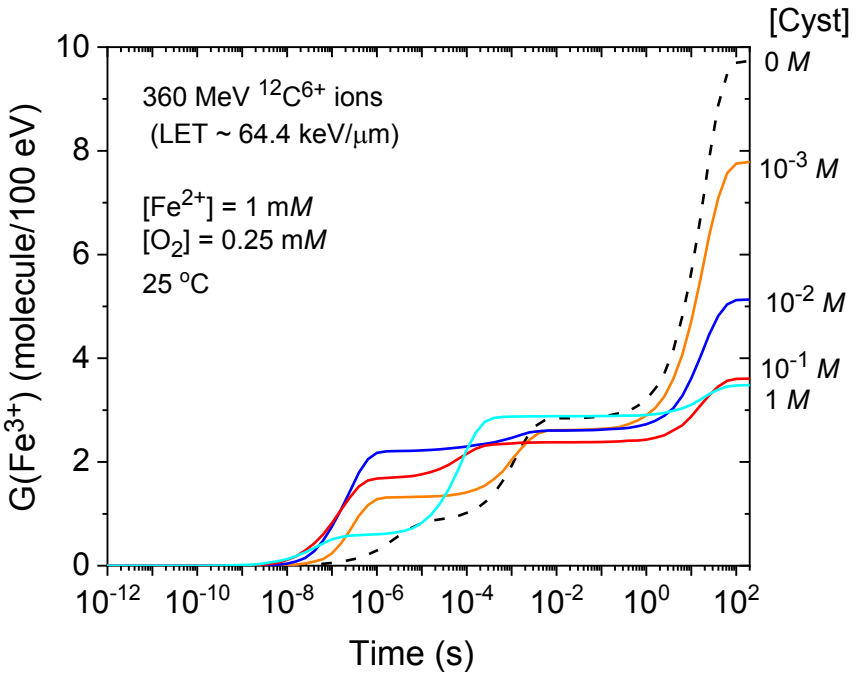

Figure 7.4 – Time evolution of $G(Fe^{3+})$ (in molecule/100 eV) as obtained from our Monte Carlo simulations of the radiolysis of aerated Fricke dosimeter solutions (1 m*M* $FeSO_4$ in aqueous 0.4 *M* H_2SO_4) containing various concentrations of cystamine, using *360 MeV irradiating* $^{12}C^{6+}$ *ions* (LET ~ 64.4 keV/μm), at 25 °C. The different lines correspond to four cystamine concentrations, indicated to the right of the figure: 10^{-3} *M* (orange solid line), 10^{-2} *M* (blue solid line), 10^{-1} *M* (red solid line) and 1 *M* (cyan solid line). For reference, the black dashed line shows our simulated kinetics of Fe^{3+} formation for the Fricke dosimeter with no added cystamine under the same irradiation conditions. The concentration of dissolved O_2 used in the calculations is 0.25 m*M*.

As for fast protons, the results clearly show that, for both $^4He^{2+}$ and $^{12}C^{6+}$ ion irradiations, $G(Fe^{3+})$ decreases sharply at ~200 s with increasing cystamine concentrations. For example, for 8 MeV incident helium ions, $G(Fe^{3+})$ decreases from ~8.45 to about 3.2 molecules/100 eV (~5.25 *G*-unit decrease) when comparing the Fricke solution with no added cystamine to a solution containing 1 *M* of the disulfide (Fig. 7.3). Similarly, for 360 MeV incident carbon ions, that is, at equal LET (~64 keV/μm), this decrease in $G(Fe^{3+})$ amounts to ~6.2 *G* units, $G(Fe^{3+})$ passing from ~9.7 (in the absence of cystamine) to 3.5 (in the presence of 1 *M* added cystamine) molecules/100 eV (Fig. 7.4). This sharp decrease in $G(Fe^{3+})$ demonstrates that the

radioprotective properties of cystamine previously described under fast proton irradiation (see Chapter 6), also hold for heavier, higher-Z charged particle irradiations.

7.3 Influence of LET on the protective effect of cystamine under helium and carbon ion irradiation

In our study in Chapter 6, focused mainly on fast irradiating protons in the LET range of ~0.2-70 keV/µm, we showed that (1) at low and moderate concentrations, cystamine was less protective at high LET, and (2) the overall influence of LET decreased at high cystamine concentrations. We have extended this same study here using helium and carbon ions in the LET ranges from ~1 to 105 and from ~10 to 400 keV/µm, respectively. We present below some results we have obtained, having in perspective a comparative analysis with respect to the two ions considered.

Figure 7.5 shows, for $^4He^{2+}$ ions in the LET range of ~1-105 keV/µm (i.e., in the energy range of ~500-1 MeV/nucleon), the ferric ion yields plotted as a function of LET (or energy, in MeV/nucleon) for various concentrations of added cystamine.

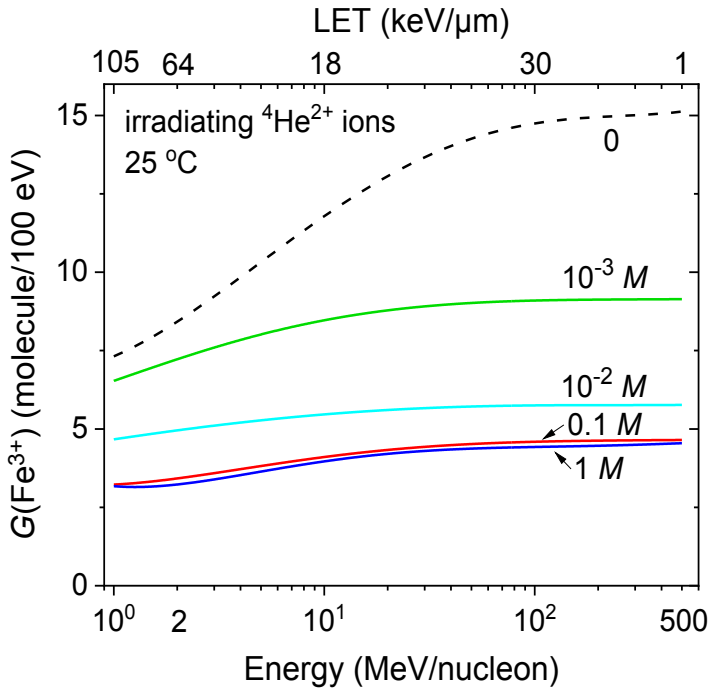

Figure 7.5 – Effect of LET on the ferric ion yield (in molecule/100 eV) as obtained from our Monte Carlo simulations (at ~200 s following ionization) of the radiolysis of Fricke/cystamine solutions (1 mM $FeSO_4$ in aerated aqueous 0.4 M H_2SO_4)

containing various concentrations of cystamine, using irradiating $^{4}He^{2+}$ ions in the LET range of ~1-105 keV/µm (or in the energy range of ~500-1 MeV/nucleon), at 25 °C. The concentration of dissolved O_2 used in the calculations is 0.25 m*M*. The different lines correspond to four different cystamine concentrations: 10^{-3} *M* (green solid line), 10^{-2} *M* (cyan solid line), 0.1 *M* (red solid line), and 1 *M* (blue solid line). For reference, the black dashed line shows our results for the Fricke dosimeter with no added cystamine under the same irradiation conditions.

Similarly, Fig. 7.6 shows, for $^{12}C^{6+}$ ions in the LET range of ~10-400 keV/µm (i.e., in the energy range of ~500-3 MeV per nucleon), the ferric ion yields plotted as a function of LET (or energy, in MeV/nucleon) for various concentrations of added cystamine.

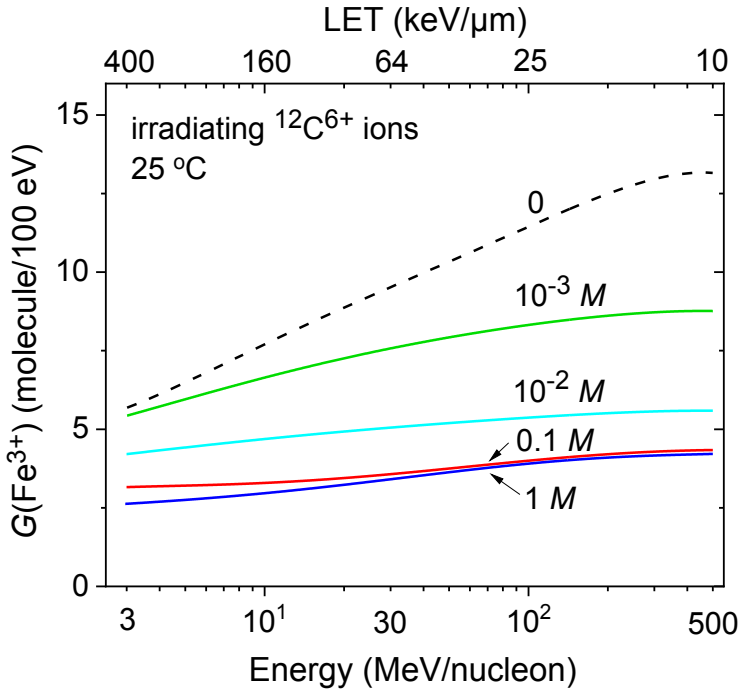

Figure 7.6 – Effect of LET on the ferric ion yield (in molecule/100 eV) as obtained from our Monte Carlo simulations (at ~200 s following ionization) of the radiolysis of Fricke/cystamine solutions (1 m*M* $FeSO_4$ in aerated aqueous 0.4 *M* H_2SO_4) containing various concentrations of cystamine, using irradiating $^{12}C^{6+}$ ions in the LET range of ~10-400 keV/µm (or in the energy range of ~500-3 MeV/nucleon), at 25 °C. The concentration of dissolved O_2 used in the calculations is 0.25 m*M*. The different lines correspond to four different cystamine concentrations: 10^{-3} *M* (green solid line), 10^{-2} *M* (cyan solid line), 0.1 *M* (red solid line), and 1 *M* (blue solid line). For reference, the black dashed line shows our results for the Fricke dosimeter with no added cystamine under the same irradiation conditions.

In a pattern quite similar to the one found for fast irradiating protons (see Fig. 8 of Chapter 6), Figs. 7.5 and 7.6 also show that, at low or moderately high cystamine concentrations, the *protective efficacy of cystamine is less effective at high LET*. This result is further illustrated in Figs. 7.7 and 7.8, where we show the influence of the concentration of added cystamine on the Fricke yield, using irradiating helium and carbon ions of various LET, respectively.

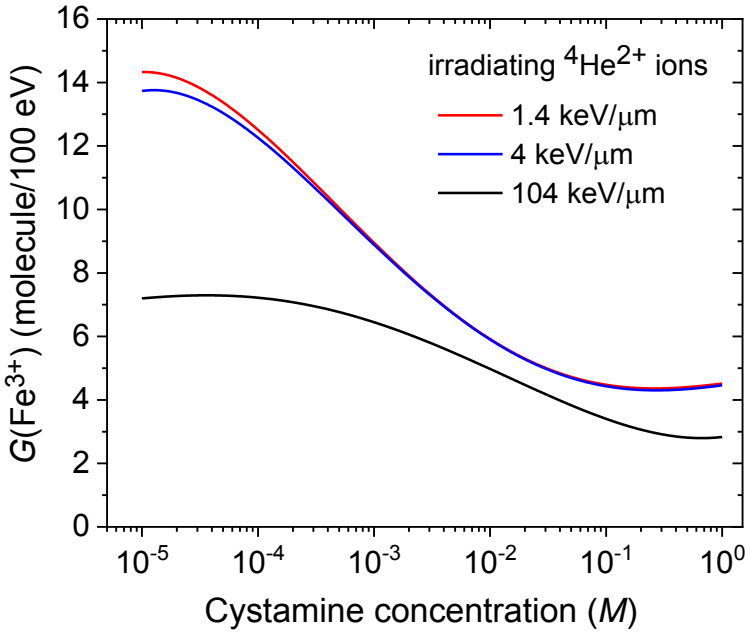

Figure 7.7 – Dependence of ferric ion production from irradiated Fricke/cystamine solutions (1 m*M* $FeSO_4$ in aerated aqueous 0.4 *M* H_2SO_4) upon the concentration of added cystamine in the range of 10^{-5}-1 *M* using irradiating $^4He^{2+}$ ions. The different lines show the Fe^{3+} ion yields (in molecule/100 eV) obtained from our Monte Carlo simulations (at ~200 s following ionization) for three different LET values (in keV/μm): ~1.4 (300 MeV/nucleon, red line), ~4 (70 MeV/nucleon, blue line), and ~104 (1 MeV/nucleon, black line), at 25 °C. The concentration of dissolved O_2 used in the calculations is 0.25 m*M*.

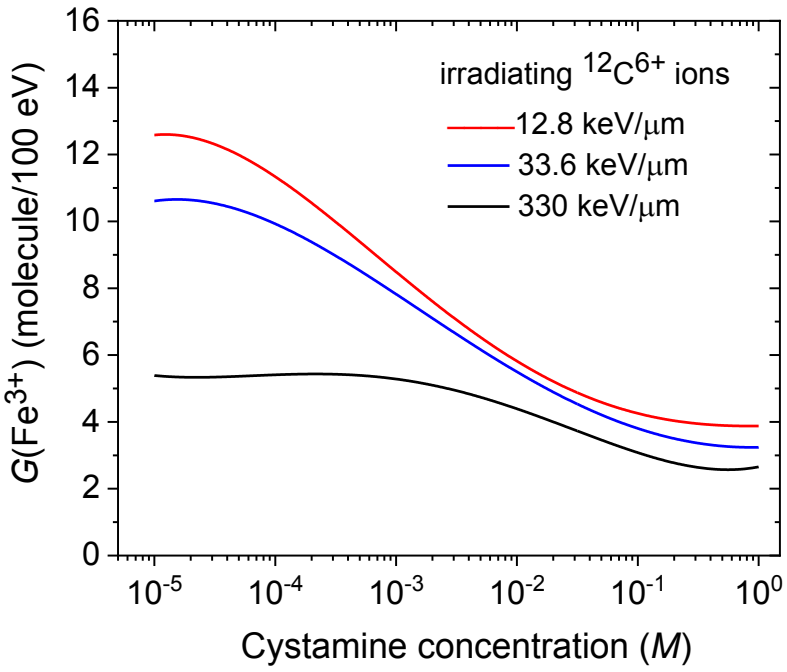

Figure 7.8 – Dependence of ferric ion production from irradiated Fricke/cystamine solutions (1 m*M* $FeSO_4$ in aerated aqueous 0.4 *M* H_2SO_4) upon the concentration of added cystamine in the range of 10^{-5}-1 *M* using irradiating $^{12}C^{6+}$ ions. The different lines show the Fe^{3+} ion yields (in molecule/100 eV) obtained from our Monte Carlo simulations (at ~200 s following ionization) for three different LET values (in keV/μm): ~12.8 (300 MeV/nucleon, red line), ~33.6 (70 MeV/nucleon, blue line), and ~330 (4 MeV/nucleon, black line), at 25 °C. The concentration of dissolved O_2 used in the calculations is 0.25 m*M*.

This decrease in the radioprotective efficacy of cystamine at high LET, observed here for both protons and helium and carbon ions, is fully consistent with previous studies that showed that chemical radioprotectors are more efficient against low- than high-LET radiation exposure. As discussed in Chapter 6, there are essentially two main reasons that explain why cystamine becomes less active when LET increases. These are summarized as follows:

(1) The higher local concentration of reactants for denser ionizing radiations promotes inter-radical combination and recombination reactions in the track stage of radiolysis producing more molecular products such as H_2O_2 or $HO_2^{\bullet}$, which are highly unreactive toward cystamine, and

(2) The (2D) cylindrical track geometry of the highest LET charged particles is competitively *less* favorable for the radical scavenging action of the homogeneously distributed cystamine molecules than the (3D) spherical spur geometry of the lowest LET radiation.

Finally, let us say a few words about the influence of LET on the Fricke yield at high cystamine concentrations. This is illustrated in Figs. 7.5-7.8 for helium and carbon ion irradiations. As for fast protons (see Sect. 4 of Chapter 6), the overall effect of LET decreases as cystamine levels rise above ~10^{-2} *M* whatever the considered irradiating ion, helium or carbon. Indeed, at these high cystamine concentrations, $G(Fe^{3+})$ remains relatively constant, almost not affected by any change in the LET of the radiation. In other words, this means that, under these conditions, the production of Fe^{3+} is less and less affected by differences in the geometry of the track structure (i.e., spherical spurs at low LET vs. cylindrical tracks at high LET) over the considered LET range. Such a result is easily understood and follows from the fact that at sufficiently high cystamine concentrations, the cystamine-radical reactions (see Table 5.2):

$$RSSR + e^-_{aq} \rightarrow RSSR^{\bullet -} \qquad [R1]$$

$$RSSR + H^\bullet \rightarrow RSSRH^\bullet \rightarrow RS^\bullet + RSH \qquad [R2]$$

$$RSSR + {}^\bullet OH \rightarrow RSSR^{\bullet +} + OH^- \qquad [R3]$$

start competing with the radical-radical combination and recombination reactions in the track regions. This competition between intra-track radical combination/recombination and capture by the cystamine molecules is increasingly in favor of the cystamine-radical reactions as the concentration of cystamine increases further, which in turn explains the reduction in the influence of the LET (track structure) on $G(Fe^{3+})$ at high cystamine concentrations.

8. CONCLUSION

In this work, we have investigated quantitatively the chemical action and the radical scavenging properties of cystamine, one of the best-known radioprotectors so far, by studying the behavior of this compound toward the primary species produced in the radiolysis of water, which is the main constituent of living cells and tissues. Unlike previous studies, which considered only sparsely ionizing low-LET γ-irradiation, our aim here was to examine the effects of increasing the LET of the radiation on the radioprotective ability of cystamine. Since relatively little is known about the protection provided by this compound against densely ionizing high-LET radiation, Monte Carlo computer simulations have been a tool of choice to elucidate the underlying molecular mechanisms of its action under high-LET irradiation conditions. The well-known radiolytic oxidation of Fe^{2+} ions to Fe^{3+} in irradiated aqueous ferrous sulfate (Fricke) dosimeter solutions with cystamine was used as a measure of its radioprotective ability and formed the basis for our method.

This study was carried out using different types of radiation, including fast incident protons, helium and carbon ions in the LET range from ~0.2 up to 400 keV/μm. Benefiting from the fact that the radiation chemistry of cystamine is reasonably well characterized, we have been able to successfully simulate the radiation-induced chemistry of the studied Fricke/cystamine solutions while covering a wide range of cystamine concentrations (~5×10^{-7}-1 *M*). In this respect, we should emphasize here that, to our knowledge, this is the first time that the radiolysis of such a sulfur-containing molecular system has been studied by means of Monte Carlo simulation techniques.

Overall, results showed unambiguously that the protecting effect of cystamine toward the Fricke dosimeter solution comes from its radical-capturing ability, which allows this compound to act by competing with the Fe^{2+} ions for the various primary free radicals – e^-_{aq}, $H^\bullet$ atoms, and $^\bullet OH$ radicals – formed early during irradiation of the surrounding water. As a result, the addition of cystamine markedly reduced the yields of Fe^{3+} whatever the ion used. This sharp decrease in $G(Fe^{3+})$ was found to depend greatly upon the energy of the irradiating ion; the higher the LET of the radiation, the lower the radioprotective efficiency of cystamine. Such a decrease in the protection effect of this compound with increasing LET of the radiation agrees very well with the

conclusion from earlier work that chemical (i.e., non-biological) radioprotectors are more efficient against low- than high-LET radiation exposure. Although there is still radioprotection against high-LET radiation, the fact that cystamine becomes less active was readily explained by differences in the spatial distribution of the reactants for denser ionizing radiations within the geometry of the track structure.

For a future work, an extension of this research aims to comprehend the radiation chemistry of Fricke solution in presence of cysteamine. This new compound, commonly expressed as RSH is known due to its great properties as a radioprotector, however, its polarity is a relevant disadvantage within the cell dynamics. One of the hypotheses found says that cystamine is used as a radioprotector due to its remarkable ability to penetrate the cell membrane, but once it is inside de cell, it splits into two molecules of cysteamine, which are the main protagonist of the protection.

The next focus of this project is to understand the chemical mechanism of cysteamine in the Fricke solution in order to simulate its behaviour in comparison with cystamine. Preliminary outcomes have been found along this investigation and will be publish in the near future.

In general, the results of this work are obviously of great interest in terms of their predictability. In this regard, we hope that they will be of interest to clinicians working in the field of “hadrontherapy” (especially, proton and carbon radiotherapy), as well as to scientists involved in the development of risk assessment models for space radiation.

9. ACKNOWLEDGEMENTS

First of all, I would like to thank Dr. Jay-Gerin for his expertise, assistance, guidance and patience throughout the process of writing this thesis. Without his help, this project would not have been possible. Honestly, this experience has changed my life and I have no words to express how grateful I am to him.

As well, I would like to extend my sincere gratitude to my research group members for their support, suggestions and encouragements.

Last but not least, I would like to dedicate this thesis to my mother, who has always been keeping company on long walks.

Once again, I would like to reiterate my gratitude to Dr. Jay-Gerin for trusting in my abilities opening the doors of his laboratory with this amazing opportunity.

10. REFERENCES

ALLEN, A. O. (1948). Radiation chemistry of aqueous solutions. *J. Phys. Colloid Chem.*, *52*(3), 479–490.

ALLEN, A. O. (1954). The yields of free H and OH in the irradiation of water. *Radiat. Res.*, *1*(1), 85–96.

ALLEN, A. O. (1961). *The Radiation Chemistry of Water and Aqueous Solutions*. D. Van Nostrand Co., Princeton, NJ.

AMICHAI, O., & TREININ, A. (1969). Chemical reactivity of O(^3P) atoms in aqueous solution. *Chem. Phys. Lett.*, *3*(8), 611–613.

ANDERSON, A. R., & HART, E. J. (1961). Molecular product and free radical yields in the decomposition of water by protons, deuterons, and helium ions. *Radiat. Res.*, *14*(6), 689–704.

ANDO, K., & KASE, Y. (2009). Biological characteristics of carbon-ion therapy. *Int. J. Radiat. Biol.*, *85*(9), 715–728.

AUTSAVAPROMPORN, N., MEESUNGNOEN, J., PLANTE, I., & JAY-GERIN, J.-P. (2007). Monte Carlo simulation study of the effects of acidity and LET on the primary free-radical and molecular yields of water radiolysis. Application to the Fricke dosimeter. *Can. J. Chem.*, *85*(3), 214–229.

AZZAM, E. I., JAY-GERIN, J.-P., & PAIN, D. (2012). Ionizing radiation-induced metabolic oxidative stress and prolonged cell injury. *Cancer Lett.*, *327*(1-2), 48–60.

BACK, M. H., & MILLER, N. (1957). Use of ferrous sulphate solutions for X-ray dosimetry. *Nature*, *179*(4554), 321–322.

BALLARINI, F., BIAGGI, M., MERZAGORA, M., OTTOLENGHI, A., DINGFELDER, M., FRIEDLAND, W., JACOB, P., & PARETZKE, H. G. (2000). Stochastic aspects and uncertainties in the prechemical and chemical stages of electron tracks in liquid water: A quantitative analysis based on Monte Carlo simulations. *Radiat. Environ. Biophys.*, *39*(3), 179–188.

BARR, N. F., & SCHULER, R. H. (1959). The dependence of radical and molecular yields on linear energy transfer in the radiation decomposition of 0.8 *N* sulfuric acid solutions. *J. Phys. Chem.*, *63*(6), 808–812.

BASKAR, R., LEE, K. A., YEO, R., & YEOH, K.-W. (2012). Cancer and radiation therapy: Current advances and future directions. *Int. J. Med. Sci.*, *9*(3), 193–199.

BĚGUSOVÁ, M., & PIMBLOTT, S. M. (2002). Stochastic simulation of γ radiolysis of acidic ferrous sulfate solution at elevated temperatures. *Radiat. Prot. Dosim.*, *99*(1-4), 73–76.

BECQUEREL, H. (1896). Sur les radiations invisibles émises par les sels d'uranium. *Comptes rendus hebdomadaires des séances de l'Académie des Sciences de Paris*, *122*, 689-694.

BERNAS, A., FERRADINI, C., & JAY-GERIN, J.-P. (1997). On the electronic structure of liquid water: Facts and reflections. *Chem. Phys.*, *222*(2-3), 151–160.

BETHE, H. (1930). Zur Theorie des Durchgangs schneller Korpuskularstrahlen durch Materie. *Ann. Physik*, *397*(3), 325-400.

BIEDENKAPP, D., HARTSHORN, L. G., & BAIR, E. J. (1970). The $O(^1D)$ + H_2O reaction. *Chem. Phys. Lett.*, *5*(6), 379–380.

BITZER, Z. T., GOEL, R., REILLY, S. M., ELIAS, R. J., SILAKOV, A., FOULDS, J., et al. (2018). Effect of flavoring chemicals on free radical formation in electronic cigarette aerosols. *Free Radic. Biol. Med.*, *120*, 72–79.

BLAKELY, E. A., & KRONENBERG, A. (1998). Heavy-ion radiobiology: New approaches to delineate mechanisms underlying enhanced biological effectiveness. *Radiat. Res.*, *150*(5), S126–S145.

BOSCOLO, D., KRÄMER, M., DURANTE, M., FUSS, M. C., & SCIFONI, E. (2018). TRAX-CHEM: A pre-chemical and chemical stage extension of the particle track structure code TRAX in water targets. *Chem. Phys. Lett.*, *698*, 11–18. doi:10.1016/j.cplett.2018.02.051.

BRAHME, A., KÄLLMAN, P., & LIND, B. K. (1989). Optimization of proton and heavy ion therapy using an adaptive inversion algorithm. *Radiother. Oncol.*, *15*(2), 189–197.

BUMP, E. A., & MALAKER, K. (1998). *Radioprotectors: Chemical, Biological, and Clinical Perspectives*. CRC Press, Boca Raton, FL.

BURTON, M. (1969). Radiation chemistry: A god fatherly look at its history and its relation to liquids. *Chem. Eng. News*, *47*(6), 86–96.

BUXTON, G. V. (1987). Radiation chemistry of the liquid state: (1) Water and homogeneous aqueous solutions. In: *Radiation Chemistry: Principles and Applications* (Farhataziz, and Rodgers, M. A. J., Eds.), pp. 321–349. VCH Publishers, New York, NY.

CHATTERJEE, A., & SCHAEFER, H. J. (1976). Microdosimetric structure of heavy ion tracks in tissue. *Radiat. Environ. Biophys.*, *13*(3), 215–227.

CHORZEMPA, M. A. (1971). Ionizing radiation and its chemical effects: A historical study of chemical dosimetry (1902-1962). Ph.D. Thesis, Oregon State University, Corvallis, OR.

CLIFFORD, P., GREEN, N. J. B., OLDFIELD, M. J., PILLING, M. J., & PIMBLOTT, S. M. (1986). Stochastic models of multi-species kinetics in radiation-induced spurs. *J. Chem. Soc., Faraday Trans. 1*, *82*(9), 2673–2689.

COBUT, V. (1993). Simulation Monte Carlo du transport d'électrons non relativistes dans l'eau liquide pure et de l'évolution du milieu irradié: rendements des espèces créées de 10^{-15} à 10^{-7} s. Ph.D. thesis, Université de Sherbrooke, Sherbrooke, Québec, Canada.

COATSWORTH, K., COLLINSON, E., & DAINTON, F. S. (1960). Radical and molecular yields in acidified deuterium oxide. *Trans. Faraday Soc.*, *56*, 1008–1013.

COBUT, V., JAY-GERIN, J.-P., FRONGILLO, Y., & PATAU, J. P. (1996). On the dissociative electron attachment as a potential source of molecular hydrogen in irradiated liquid water. *Radiat. Phys. Chem.*, *47*(2), 247–250.

COBUT, V., FRONGILLO, Y., PATAU, J. P., GOULET, T., FRASER, M.-J., & JAY-GERIN, J.-P. (1998). Monte Carlo simulation of fast electron and proton tracks in liquid water. I. Physical and physicochemical aspects. *Radiat. Phys. Chem.*, *51*(3), 229–243.

CURIE, P., & M^{me} CURIE, S. (1898*a*). Sur une substance nouvelle radio-active, contenue dans la pechblende. *Comptes rendus hebdomadaires des séances de l'Académie des Sciences de Paris*, *127*, 175–178.

CURIE, P., M^{me} CURIE, P., & BÉMONT, G. (1898*b*). Sur une nouvelle substance fortement radio-active, contenue dans la pechblende. *Comptes rendus hebdomadaires des séances de l'Académie des Sciences de Paris*, *127*, 1215–1217.

DAS, R. C. (1971). Radiation chemistry of aqueous aerated ferrous sulphate solution. *Radiat. Res. Rev.*, *3*(2-3), 121–139.

DAVIES, J. V., GREENE, D., KEENE, J. P., LAW, J., & MASSEY, J. B. (1963). A comparison of ionization, calorimetric and ferrous sulphate dosimetry. *Phys. Med. Biol.*, *8*(1), 97–102.

DONALDSON, D. M., & MILLER, N. (1955). Études quantitatives des réactions radiochimiques. III. Oxydation du sulfate ferreux par les particules β. *J. Chim. Phys.*, *52*, 578-584. DOI: 10.1051/jcp/1955520578.

DURANTE, M., & LOEFFLER, J. S. (2010). Charged particles in radiation oncology. *Nat. Rev. Clin. Oncol.*, *7*(1), 37–43.

EBNER, D. K., & KAMADA, T. (2016). The emerging role of carbon-ion radiotherapy. *Front. Oncol.*, *6*, 140.

ELLIOT, A. J., & BARTELS, D. M. (2009). The reaction set, rate constants and g-values for the simulation of the radiolysis of light water over the range 20° to 350 °C based on information available in 2008. Report AECL No. 153-127160-450-001. Atomic Energy of Canada Limited, Chalk River, Ontario, Canada.

ELLIOT, A. J., CHENIER, M. P., OUELLETTE, D. C., & KOSLOWSKY, V. T. (1996). Temperature dependence of *g* values for aqueous solutions irradiated with 23 MeV $^{2}H^{+}$ and 157 MeV $^{7}Li^{3+}$ ion beams. *J. Phys. Chem.*, *100*(21), 9014–9020.

ELLIOT, A. J., McCRACKEN, D. R., BUXTON, G. V., & WOOD, N. D. (1990). Estimation of rate constants for near-diffusion-controlled reactions in water at high temperatures. *J. Chem. Soc., Faraday Trans.*, *86*(9), 1539–1547.

ELSÄSSER, T., WEYRATHER, W. K., FRIEDRICH, T., DURANTE, M., IANCU, G., KRÄMER, M., et al. (2010). Quantification of the relative biological effectiveness for ion beam radiotherapy: Direct experimental comparison of proton and carbon ion beams and a novel approach for treatment planning. *Int. J. Radiation Oncology Biol. Phys.*, *78*(4), 1177–1183.

ENGHARDT, W., DEBUS, J., HABERER, T., HASCH, B. G., HINZ, R., JÄKEL, O., et al. (1999). The application of PET to quality assurance of heavy-ion tumor therapy. *Strahlenther. Onkol.*, *175*(Suppl. 2), 33–36.

FARAGGI, M., & DÉSALOS, J. (1969). Effect of positively charged ions on the "molecular" hydrogen yield in the radiolysis of aqueous solutions. *Int. J. Radiat. Phys. Chem.*, *1*(3), 335–344.

FERRADINI, C. (1979). Actions chimiques des radiations ionisantes. *J. Chim. Phys.*, *76*(7-8), 636–644. doi:10.1051/jcp/1979760636.

FERRADINI, C. (1990). Aspect hétérogène des phénomènes radiolytiques. In: *Actions biologique et chimique des radiations ionisantes* (Tilquin, B., Ed.), Vol. 1, pp. 52–63. Éditions Ciaco, Bruxelles.

FERRADINI, C., & JAY-GERIN, J.-P. (1999). La radiolyse de l'eau et des solutions aqueuses :

historique et actualité. *Can. J. Chem.*, *77*(9), 1542–1575.

FERRADINI, C., & JAY-GERIN, J.-P. (2000). The effect of pH on water radiolysis: A still open question. A minireview. *Res. Chem. Intermed.*, *26*(6), 549–565.

FREGENE, A. O. (1967). Calibration of the ferrous sulfate dosimeter by ionometric and calorimetric methods for radiations of a wide range of energy. *Radiat. Res.*, *31*(2), 256–272.

FRICKE, H., & HART, E. J. (1966). Chemical dosimetry. In: *Radiation Dosimetry* (Attix, F. H., and Roesch, W. C., Eds.), 2nd edn, Vol. II, pp. 167–239. Academic Press, New York, NY.

FRICKE, H., & MORSE, S. (1927). The chemical action of roentgen rays on dilute ferrosulphate solutions as a measure of dose. *Am. J. Roentgenol. Radium Ther.*, *18*, 430–432.

FRICKE, H., & MORSE, S. (1929). The action of X-rays on ferrous sulphate solutions. *Philos. Mag., 7th Ser.*, *7*, 129–141.

FRONGILLO, Y., GOULET, T., FRASER, M.-J., COBUT, V., PATAU, J. P., & JAY-GERIN, J.-P. (1998). Monte Carlo simulation of fast electron and proton tracks in liquid water. II. Nonhomogeneous chemistry. *Radiat. Phys. Chem.*, *51*(3), 245–254.

GEVANTMAN, L. H., & PESTANER, J. F. (1959). Free ion yields in ferrous sulfate solutions irradiated with low-energy X-rays. *J. Chem. Phys.*, *31*(4), 1140.

GLIMELIUS, B., ASK, A., BJELKENGREN, G., BJÖRK-ERIKSSON, T., BLOMQUIST, E., JOHANSSON, B., et al. (2005). Number of patients potentially eligible for proton therapy. *Acta Oncol.*, *44*(8), 836–849.

GOULET, T., & JAY-GERIN, J.-P. (1989). Thermalization of subexcitation electrons in solid water. *Radiat. Res.*, *118*(1), 46–62.

GOULET, T., PATAU, J. P., & JAY-GERIN, J.-P. (1990). Influence of the parent cation on the thermalization of subexcitation electrons in solid water. *J. Phys. Chem.*, *94*(18), 7312–7316.

GOULET, T., JAY-GERIN, J.-P., FRONGILLO, Y., COBUT, V., & FRASER, M.-J. (1996). Rôle des distances de thermalisation des électrons dans la radiolyse de l'eau liquide. *J. Chim. Phys.*, *93*(1), 111–116.

GOULET, T., FRASER, M.-J., FRONGILLO, Y., & JAY-GERIN, J.-P. (1998). On the validity of the independent reaction times approximation for the description of the nonhomogeneous kinetics of liquid water radiolysis. *Radiat. Phys. Chem.*, *51*(1), 85–91.

GRAY, L. H., CONGER, A. D., EBERT, M., HOMSEY, S., & SCOTT, O. C. A. (1953). The concentration of oxygen dissolved in tissues at the time of irradiation as a factor in radiotherapy. *Br. J. Radiol.*, *26*(312), 638–648.

HAGHIGHAT, A. (2015). *Monte Carlo Methods for Particle Transport*. Taylor & Francis Group, Boca Raton, FL.

HALL, E. J., & GIACCIA, A. J. (2006). *Radiobiology for the Radiologist*. 6th edn. Lippincott Williams & Wilkins, Philadelphia, PA.

HALLIWELL, B. (1994). Free radicals, antioxidants, and human disease: Curiosity, cause, or consequence? *The Lancet*, *344*(8924), 721–724.

HALLIWELL, B., & GUTTERIDGE, J. M. C. (2015). *Free Radicals in Biology and Medicine*, 5th edn. Oxford University Press, Oxford, UK.

HAMADA, N., IMAOKA, T., MASUNAGA, S.-I., OGATA, T., OKAYASU, R., TAKAHASHI, A. et al. (2010). Recent advances in the biology of heavy-ion cancer therapy. *J. Radiat. Res.*, *51*(4), 365–383.

HARDWICK, T. J. (1952*a*). The oxidation of ferrous sulphate solutions by γ-rays. The absolute yield. *Can. J. Chem.*, *30*(1), 17–22.

HARDWICK, T. J. (1952*b*). Radiation chemistry investigation of aqueous solutions using P32 and S35 as internal sources. *Can. J. Chem.*, *30*(1), 39–46.

HART, E. J. (1954). Molecular product and free radical yields of ionizing radiations in aqueous solutions. *Radiat. Res.*, *1*(1), 53–61.

HART, E. J., RAMLER, W. J., & ROCKLIN, S. R. (1956). Chemical yields of ionizing particles in aqueous solutions: Effect of energy of protons and deuterons. *Radiat. Res.*, *4*, 378–393.

HAYBITTLE, J. L., SAUNDERS, R. D., & SWALLOW, A. J. (1956). X- and γ irradiation of ferrous sulfate in dilute aqueous solution. *J. Chem. Phys.*, *25*(6), 1213–1217.

HELLER, J. M., Jr., HAMM, R. N., BIRKHOFF, R. D., & PAINTER, L. R. (1974). Collective oscillation in liquid water. *J. Chem. Phys.*, *60*(9), 3483–3486.

HERVÉ DU PENHOAT, M.-A., GOULET, T., FRONGILLO, Y., FRASER, M.-J., BERNAT, P., & JAY-GERIN, J.-P. (2000). Radiolysis of liquid water at temperatures up to 300 °C: A Monte Carlo simulation study. *J. Phys. Chem. A*, *104*(50), 11757–11770.

ICRU REPORT 16 (1970). *Linear Energy Transfer*. International Commission on Radiation Units and Measurements, Washington, D.C.

ICRU REPORT 17 (1970). *Radiation Dosimetry: X rays Generated at Potentials of 5 to 150 kV*. International Commission on Radiation Units and Measurements, Washington, D.C.

ICRU REPORT 34 (1982). *The Dosimetry of Pulsed Radiation*. International Commission on Radiation Units and Measurements, Bethesda, MD.

ICRU REPORT 55 (1996). *Secondary Electron Spectra from Charged Particle Interactions*. International Commission on Radiation Units and Measurements, Bethesda, MD.

IMAMURA, M., MATSUI, M., & KARASAWA, T. (1970). Radiation chemical studies with cyclotron beams. II. The radiolysis of an aqueous ferrous ammonium sulfate solution with carbon- and nitrogen-ion radiations. *Bull. Chem. Soc. Japan*, *43*(9), 2745–2749.

INOKUTI, M. (1971). Inelastic collisions of fast charged particles with atoms and molecules. The Bethe theory revisited. *Rev. Mod. Phys.*, *43*(3), 297–347.

JÄKEL, O., SCHULZ-ERTNER, D., KARGER, C. P., NIKOGHOSYAN, A., & DEBUS, J. (2003). Heavy ion therapy: Status and perspectives. *Technol. Cancer Res. Treat.*, *2*(5), 377–387.

JAYSON, G. G., OWEN, T. C., & WILBRAHAM, A. C. (1967). The radiation chemistry of cystamine sulphate. *J. Chem. Soc.*, 944–949.

JAYSON, G. G., & WILBRAHAM, A. C. (1968). The utilization of the Fricke dosimeter for evaluating the biological radiation-protective potential of water-soluble organic compounds. *Chem. Commun. (London)*, 641–642.

JEMAL, A., BRAY, F., CENTER, M. M., FERLAY, J., WARD, E., & FORMAN, D. (2011). Global cancer statistics. *CA Cancer J. Clin.*, *61*(2), 69–90.

JIANG, P.-Y., KATSUMURA, Y., NAGAISHI, R., DOMAE, M., ISHIKAWA, K., ISHIGURE, K., & YOSHIDA, Y. (1992). Pulse radiolysis study of concentrated sulfuric acid solutions. Formation mechanism, yield and reactivity of sulphate radicals. *J. Chem. Soc. Faraday Trans.*, *88*(12), 1653–1658.

JULIEN, R., & PUCHEAULT, J. (1972). Radiolyses de solutions aqueuses par des rayonnements à ionisations denses. III. Oxydation de Fe^{II} et réduction de Ce^{IV} dans les solutions sulfuriques irradiées par des protons de faible énergie. *J. Chim. Phys.*, *69*(10), 1561–1568.

KAMADA, T., TSUJII, H., BLAKELY, E. A., DEBUS, J., DE NEVE, W., DURANTE, M., et al. (2015). Carbon ion radiotherapy in Japan: An assessment of 20 years of clinical

experience. *Lancet Oncol.*, *16*(2), e93–e100.

KANIKE, V., MEESUNGNOEN, J., & JAY-GERIN, J.-P. (2015). Transient acid pH effect in tracks in the radiolysis of water: Does this effect contribute to biological damage caused by ionizing radiation? *Austin J. Nucl. Med. Radiother.*, *2*(1), 1011.

KAPLAN, I. G., & MITEREV, A. M. (1987). Interaction of charged particles with molecular medium and track effects in radiation chemistry. In: *Advances in Chemical Physics* (Prigogine, I., and Rice, S. A., Eds.), Vol. 68, pp. 255–386. Wiley, New York, NY.

KARAMITROS, M., MANTERO, A., INCERTI, S., FRIEDLAND, W., BALDACCHINO, G., BARBERET, P., et al. (2011). Modeling radiation chemistry in the Geant4 toolkit. *Prog. Nucl. Sci. Technol.*, *2*, 503–508.

KATZ, R. (1970). RBE, LET and z/β^{α}. *Health Phys.*, *18*(2), 175.

KIMMEL, G. A., ORLANDO, T. M., VÉZINA, C., & SANCHE, L. (1994). Low-energy electron-stimulated production of molecular hydrogen from amorphous water ice. *J. Chem. Phys.*, *101*(4), 3282–3286.

KLASSEN, N. V., SHORTT, K. R., SEUNTJENS, J., & ROSS, C. K. (1999). Fricke dosimetry: The difference between $G(Fe^{3+})$ for ^{60}Co γ-rays and high-energy x-rays. *Phys. Med. Biol.*, *44*(7), 1609–1624.

KOMATSU, S., FUKUMOTO, T., DEMIZU, Y., MIYAWAKI, D., TERASHIMA, K., SASAKI, R., et al. (2011). Clinical results and risk factors of proton and carbon ion therapy for hepatocellular carcinoma. *Cancer*, *117*(21), 4890–4904.

KRÄMER, M., JÄKEL, O., HABERER, T., KRAFT, G., SCHARDT, D., & WEBER, U. (2000). Treatment planning for heavy-ion radiotherapy: Physical beam model and dose optimization. *Phys. Med. Biol.*, *45*(11), 3299–3317.

KREIPL, M. S., FRIEDLAND, W., & PARETZKE, H. G. (2009). Time- and space-resolved Monte Carlo study of water radiolysis for photon, electron and ion irradiation. *Radiat. Environ. Biophys.*, *48*(1), 11–20.

KUPPERMANN, A. (1959). Theoretical foundations of radiation chemistry. *J. Chem. Educ.*, *36*(6), 279–285.

LALITHA, B., & MITTAL, J. P. (1971). Electron transfer reaction in the radiation chemistry of some biologically important disulphide compounds. *Radiat. Eff.*, *7*(3-4), 159–162.

LAVERNE, J. A. (2000). Track effects of heavy ions in liquid water. *Radiat. Res.*, *153*(5), 487–496.

LAVERNE, J. A. (2004). Radiation chemical effects of heavy ions. In: *Charged Particle and Photon Interactions with Matter: Chemical, Physicochemical, and Biological Consequences with Applications* (Mozumder, A., and Hatano, Y., Eds.), pp. 403–429. Marcel Dekker, New York, NY.

LAVERNE, J. A., & MOZUMDER, A. (1993). Concerning plasmon excitation in liquid water. *Radiat. Res.*, *133*(3), 282–288.

LAVERNE, J. A., & PIMBLOTT, S. M. (1995). Electron energy-loss distributions in solid, dry DNA. *Radiat. Res.*, *141*(2), 208–215.

LAVERNE, J. A., & SCHULER, R. H. (1987). Track effects in radiation chemistry: Production of $HO_2^{\bullet}$ in the radiolysis of water by high-LET ^{58}Ni ions. *J. Phys. Chem.*, *91*(26), 6560–6563.

LAVERNE, J. A., & SCHULER, R. H. (1996). Radiolysis of the Fricke dosimeter with ^{58}Ni and ^{238}U ions: Response for particles of high linear energy transfer. *J. Phys. Chem.*, *100*(39), 16034–16040.

LEFORT, M. (1957). Phénomènes de réductions provoqués par les rayonnements nucléaires sur les solutions aqueuses de composés minéraux. *J. Chim. Phys.*, *54* (xx), 782–788.

LEFORT, M. (1958). Radiation chemistry. *Annu. Rev. Phys. Chem.*, *9*, 123-156.

LEVIN, W. P., KOOY, H., LOEFFLER, J. S., & DELANEY, T. F. (2005). Proton beam therapy. *Br. J. Cancer*, *93*(8), 849–854.

LI, J., NIE, Z., ZHENG, Y. Y., DONG, S., & LOH, Z.-H. (2013). Elementary electron and ion dynamics in ionized liquid water. *J. Phys. Chem. Lett.*, *4*(21), 3698–3703.

LIU, S., SEMENCIW, R., PROBERT, A., & MAO, Y. (2001). Cervical cancer in Canada: Changing patterns in incidence and mortality. *Int. J. Gynecol. Cancer*, *11*(1), 24–31.

LOMAX, A. J., BOEHRINGER, T., CORAY, A., EGGER, E., GOITEIN, G., GROSSMANN, M., et al. (2001). Intensity modulated proton therapy: A clinical example. *Med. Phys.*, *28*(3), 317–324.

MAGEE, J. L. (1953). Radiation chemistry. *Annu. Rev. Nucl. Sci.*, *3*, 171–192.

MAGEE, J. L., & CHATTERJEE, A. (1980). Radiation chemistry of heavy-particle tracks. 1. General considerations. *J. Phys. Chem.*, *84*(26), 3529–3536.

MAGEE, J. L., & CHATTERJEE, A. (1987). Track reactions of radiation chemistry. In: *Kinetics of Nonhomogeneous Processes* (Freeman, G. R., Ed.), pp. 171–214. Wiley, New York, NY.

MARIANO, M. H., & SANTOS, M. L. (1967). Radiolysis of dilute aerated sulfuric acid solutions with 5.3-MeV alpha particles. *Radiat. Res.*, *32*(4), 905–914.

MARRETT, L. D., DE, P., AIRIA, P., DRYER, D., & STEERING COMMITTEE OF CANADIAN CANCER STATISTICS 2008. (2008). Cancer in Canada in 2008. *Can. Med. Assoc. J.*, *179*(11), 1163–1170.

MARSALEK, O., ELLES, C. G., PIENIAZEK, P. A., PLUHAŘOVÁ, E., VANDEVONDELE, J., BRADFORTH, S. E., & JUNGWIRTH, P. (2011). Chasing charge localization and chemical reactivity following photoionization in liquid water. *J. Chem. Phys.*, *135*, 224510.

MATSUI, M., SEKI, H., KARASAWA, T., & IMAMURA, M. (1970). Radiation chemical studies with cyclotron beams, (I) Fricke solution. *J. Nucl. Sci. Technol.*, *7*(2), 97–104.

MATTHEWS, R. W. (1982). Aqueous chemical dosimetry. *Int. J. Appl. Radiat. Isot.*, *33*(11), 1159–1170.

McDONELL, W. R., & HART, E. J. (1954). Oxidation of aqueous ferrous sulfate solutions by charged particle radiations. *J. Am. Chem. Soc.*, *76*(8), 2121–2124.

McEWEN, M., EL GAMAL, I., MAINEGRA-HING, E., & COJOCARU, C. (2014). Determination of the radiation chemical yield (G) for the Fricke chemical dosimetry system in photon and electron beams. Report NRC-PIRS-1980. National Research Council Canada, Ottawa, Ontario, Canada.

MEDICAL EXCELLENCE JAPAN. (2018). Guide for heavy ion radiotherapy. Available online at http://www.hirt-japan.info/en/medical/.

MEESAT, R., JAY-GERIN, J.-P., KHALIL, A., & LEPAGE, M. (2009). Evaluation of the radiation-sensitizer/protector and/or antioxidant efficiencies using Fricke and polyacrylamide gel dosimeters. *J. Phys.: Conf. Ser.*, *164*, 012006.

MEESAT, R., SANGUANMITH, S., MEESUNGNOEN, J., LEPAGE, M., KHALIL, A., & JAY-GERIN, J.-P. (2012). Utilization of the ferrous sulfate (Fricke) dosimeter for evaluating the radioprotective potential of cystamine: Experiment and Monte Carlo simulation. *Radiat. Res.*, *177*(6), 813–826.

MEESUNGNOEN, J., BENRAHMOUNE, M., FILALI-MOUHIM, A., MANKHETKORN, S.,

& JAY-GERIN, J.-P. (2001). Monte Carlo calculation of the primary radical and molecular yields of liquid water radiolysis in the linear energy transfer range 0.3-6.5 keV/μm: Application to ^{137}Cs gamma rays. *Radiat. Res.*, *155*(2), 269–278.

MEESUNGNOEN, J., JAY-GERIN, J-P., FILALI-MOUHIM, A., & MANKHETKORN, S. (2002*a*). Low-energy electron penetration range in liquid water. *Radiat. Res.*, *158*(5), 657–660.

MEESUNGNOEN, J., JAY-GERIN, J.-P., FILALI-MOUHIM, A., & MANKHETKORN, S. (2002*b*). On the temperature dependence of the primary yield and the product $G\varepsilon_{max}$ of hydrated electrons in the low-LET radiolysis of liquid water. *Can. J. Chem.*, *80*(7), 767-773.

MEESUNGNOEN, J., & JAY-GERIN, J.-P. (2005). High-LET radiolysis of liquid water with $^{1}H^{+}$, $^{4}He^{2+}$, $^{12}C^{6+}$, and $^{20}Ne^{9+}$ ions: Effects of multiple ionization. *J. Phys. Chem. A*, *109*(29), 6406–6419.

MEESUNGNOEN, J., & JAY-GERIN, J.-P. (2011). Radiation chemistry of liquid water with heavy ions: Monte Carlo simulation studies. In: *Charged Particle and Photon Interactions with Matter. Recent Advances, Applications, and Interfaces* (Hatano, Y., Katsumura, Y., and Mozumder, A., Eds.), pp. 355–400. Taylor & Francis Group, Boca Raton, FL.

MEESUNGNOEN, J., SANGUANMITH, S., & JAY-GERIN, J.-P. (2015). Yields of H_2 and hydrated electrons in low-LET radiolysis of water determined by Monte Carlo track chemistry simulations using phenol/N_2O aqueous solutions up to 350 °C. *RSC Adv.*, *5*(94), 76813–76824.

MILLER, A. B., HOOGSTRATEN, B., STAQUET, M., & WINKLER, A. (1981). Reporting results of cancer treatment. *Cancer*, *47*(1), 207–214.

MIN, C.-H., KIM, C. H., YOUN, M.-Y., & KIM, J.-W. (2006). Prompt gamma measurements for locating the dose falloff region in the proton therapy. *Appl. Phys. Lett.*, *89*(18), 183517.

MIRSALEH KOHAN, L., SANGUANMITH, S., MEESUNGNOEN, J., CAUSEY, P., STUART, C.R., & JAY-GERIN, J.-P. (2013). Self-radiolysis of tritiated water. 1. A comparison of the effects of ^{60}Co γ-rays and tritium β-particles on water and aqueous solutions at room temperature. *RSC Adv.*, *3*(42), 19282–19299.

MOZUMDER, A. (1999). *Fundamentals of Radiation Chemistry*. Academic Press, San Diego, CA.

MOZUMDER, A., & MAGEE, J. L. (1966*a*). Model of tracks of ionizing radiations for radical reaction mechanisms. *Radiat. Res.*, *28*(2), 203–214.

MOZUMDER, A., & MAGEE, J. L. (1966*b*). Theory of radiation chemistry. VII. Structure and reactions in low LET tracks. *J. Chem. Phys.*, *45*(9), 3332–3341.

MOZUMDER, A., CHATTERJEE, A., & MAGEE, J. L. (1968). Theory of radiation chemistry. IX. Model and structure of heavy particle tracks in water. In: *Advances in Chemistry Series* (Gould, R. F., Ed.), Vol. 81, pp. 27–48. American Chemical Society, Washington, DC.

MOZUMDER, A., & MAGEE, J. L. (1975). The early events of radiation chemistry. *Int. J. Radiat. Phys. Chem.*, *7*(2-3), 83-93.

MUNZENRIDER, J. E., & LIEBSCH, N. J. (1999). Proton therapy for tumors of the skull base. *Strahlenther. Onkol.*, *175*(Suppl. 2), 57–63.

MUROYA, Y., MEESUNGNOEN, J., JAY-GERIN, J.-P., FILALI-MOUHIM, A., GOULET, T., KATSUMURA, Y., & MANKHETKORN, S. (2002). Radiolysis of liquid water: An attempt to reconcile Monte Carlo calculations with new experimental hydrated electron yield data at early times. *Can. J. Chem.*, *80*(10), 1367–1374. doi:10.1139/v02-173.

MUROYA, Y., PLANTE, I., AZZAM, E. I., MEESUNGNOEN, J., KATSUMURA, Y., & JAY-GERIN, J.-P. (2006). High-LET ion radiolysis of water: Visualization of the formation and evolution of ion tracks and relevance to the radiation-induced bystander effect. *Radiat. Res.*, *165*(4), 485–491.

NAIR, C. K. K., PARIDA, D. K., & NOMURA, T. (2001). Radioprotectors in radiotherapy. *J. Radiat. Res.*, *42*(1), 21–37.

NETA, P., HUIE, R. E., & ROSS, A. B. (1988). Rate constants for reactions of inorganic radicals in aqueous solution. *J. Phys. Chem. Ref. Data*, *17*(3), 1027–1284.

NIKJOO, H., UEHARA, S., & EMFIETZOGLOU, D. (2012). *Interaction of Radiation with Matter*. Taylor & Francis Group, Boca Raton, FL.

NIKOGHOSYAN, A., SCHULZ-ERTNER, D., DIDINGER, B., JÄKEL, O., ZUNA, I., HÖSS, A., et al. (2004). Evaluation of therapeutic potential of heavy ion therapy for patients with locally advanced prostate cancer. *Int. J. Radiat. Oncol. Biol. Phys.*, *58*(1), 89–97.

NIKOGOSYAN, D. N., ORAEVSKY, A. A., & RUPASOV, V. I. (1983). Two-photon ionization and dissociation of liquid water by powerful laser UV radiation. *Chem. Phys.*, *77*(1), 131–143.

NODA, K., FURUKAWA, T., IWATA, Y., KANAI, T., KANAZAWA, M., KANEMATSU, N., et al. (2006). Design of carbon therapy facility based on 10 years experience at HIMAC. *Nucl. Instrum. Methods Phys. Res. A*, *562*(2), 1038–1041.

NODA, K., FURUKAWA, T., FUJISAWA, T., IWATA, Y., KANAI, T., KANAZAWA, M., et al. (2007). New accelerator facility for carbon-ion cancer-therapy. *J. Radiat. Res.*, *48*(Suppl. A), A43–A54.

OGURA, H., & HAMILL, W. H. (1973). Positive hole migration in pulse-irradiated water and heavy water. *J. Phys. Chem.*, *77*(25), 2952–2954.

OLSEN, D. R., BRULAND, Ø. S., FRYKHOLM, G., & NORDERHAUG, I. N. (2007). Proton therapy – A systematic review of clinical effectiveness. *Radiother. Oncol.*, *83*(2), 123–132.

PAGANETTI, H. (2012). Range uncertainties in proton therapy and the role of Monte Carlo simulations. *Phys. Med. Biol.*, *57*(11), R99–R117.

PAGANETTI, H., NIEMIERKO, A., ANCUKIEWICZ, M., GERWECK, L. E., GOITEIN, M., LOEFFLER, J. S., & SUIT, H. D. (2002). Relative biological effectiveness (RBE) values for proton beam therapy. *Int. J. Radiation Oncology Biol. Phys.*, *53*(2), 407–421.

PALCIC, B., & SKARSGARD, L. D. (1984). Reduced oxygen enhancement ratio at low doses of ionizing radiation. *Radiat. Res.*, *100*(2), 328–339.

PARETZKE, H. G. (1987). Radiation track structure theory. In: *Kinetics of Nonhomogeneous Processes* (Freeman, G. R., Ed.), pp. 89–170. Wiley, New York, NY.

PARODI, K., MAIRANI, A., BRONS, S., HASCH, B. G., SOMMERER, F., NAUMANN, J., et al. (2012). Monte Carlo simulations to support start-up and treatment planning of scanned proton and carbon ion therapy at a synchrotron-based facility. *Phys. Med. Biol.*, *57*(12), 3759–3784.

PARTICLE THERAPY CO-OPERATIVE GROUP. (2018). Particle therapy facilities in operation (last update: August 2018). Available online at https://www.ptcog.ch/index.php/facilities-in-operation.

PASTINA, B., LAVERNE, J. A., & PIMBLOTT, S. M. (1999). Dependence of molecular hydrogen formation in water on scavengers of the precursor to the hydrated electron. *J. Phys. Chem. A*, *103*(29), 5841–5846.

PASTINA, B., & LAVERNE, J. A. (2001). Effect of molecular hydrogen on hydrogen peroxide in water radiolysis. *J. Phys. Chem. A*, *105*(40), 9316–9322.

PEDRONI, E., BACHER, R., BLATTMANN, H., BÖHRINGER, T., CORAY, A., LOMAX, A., et al. (1995). The 200-MeV proton therapy project at the Paul Scherrer Institute: Conceptual design and practical realization. *Med. Phys.*, *22*(1), 37–53.

PEISACH, M., & STEYN, J. (1960). Radiolytic oxidation of ferrous solutions with standardized internal sources of phosphorus-32. *Nature*, *187*(4731), 58–59.

PIMBLOTT, S. M., & GREEN, N. J. B. (1995). Recent advances in the kinetics of radiolytic processes. In: *Research in Chemical Kinetics* (Compton, R. G., and Hancock, G., Eds.), Vol. 4, pp. 117–174. Elsevier, Amsterdam.

PIMBLOTT, S. M., & LAVERNE, J. A. (2002). Effects of track structure on the ion radiolysis of the Fricke dosimeter. *J. Phys. Chem. A*, *106*(41), 9420–9427.

PIMBLOTT, S. M., & MOZUMDER, A. (2004). Modeling of physicochemical and chemical processes in the interactions of fast charged particles with matter. In: *Charged Particle and Photon Interactions with Matter: Chemical, Physicochemical, and Biological Consequences with Applications* (Mozumder, A., and Hatano, Y., Eds.), pp. 75–103. Marcel Dekker, New York, NY.

PIMBLOTT, S. M., PILLING, M. J., & GREEN, N. J. B. (1991). Stochastic models of spur kinetics in water. *Radiat. Phys. Chem.*, *37*(3), 377–388.

PLANTE, I., FILALI-MOUHIM, A., & JAY-GERIN, J.-P. (2005). SimulRad: A Java interface for a Monte Carlo simulation code to visualize in 3D the early stages of water radiolysis. *Radiat. Phys. Chem.*, *72*(2-3), 173–180.

PLANTE, I., 2009. Développement de codes de simulation Monte-Carlo de la radiolyse de l'eau et de solutions aqueuses par des électrons, ions lourds, photons et neutrons. Applications à divers sujets d'intérêt expérimental. Ph.D. thesis, Université de Sherbrooke, Sherbrooke, Québec, Canada.

PLATZMAN, R. L. (1955). Subexcitation electrons. *Radiat. Res.*, *2*(1), 1–7.

PLATZMAN, R. L. (1958). The physical and chemical basis of mechanisms in radiation biology. In: *Radiation Biology and Medicine. Selected Reviews in the Life Sciences* (Claus, W. D., Ed.), pp. 15–72. Addison-Wesley, Reading, MA.

PLATZMAN, R. L. (1962*a*). Superexcited states of molecules. *Radiat. Res.*, *17*(3), 419–425.

PLATZMAN, R. L. (1962*b*). Dissociative attachment of subexcitation electrons in liquid water, and the origin of radiolytic "molecular" hydrogen. In: *Abstracts of Papers, Second*

International Congress of Radiation Research, Harrogate, England, August 5-11, 1962. p. 128.

PREMARATNE, S., AMARATUNGA, D. T., MENSAH, F. E., & McNAMARA, J. J. (2018). Significance of oxygen free radicals in the pathophysiology of hemorrhagic shock - A protocol. *Int. J. Surg. Protocols*, *9*, 15–19.

PUCHEAULT, J. (1961). Actions des rayons alpha sur les solutions aqueuses. In: *Actions chimiques et biologiques des radiations* (Haïssinsky, M., Ed.), Vol. 5, pp. 31–84. Masson, Paris.

REINA, M., & MARTÍNEZ, A. (2017). Free radicals interacting with Cu, Ag and Au clusters. *Comp. Theor. Chem.*, *1120*, 24–33.

RÖNTGEN, W. C. (1895). Über eine neue Art von Strahlen. *Sitzungsberichte der Physikalisch-Medizinischen Gesellschaft zu Würzburg*, No. 9, pp. 132–141.

ROWNTREE, P., PARENTEAU, L., & SANCHE, L. (1991). Electron stimulated desorption via dissociative attachment in amorphous H_2O. *J. Chem. Phys.*, *94*(12), 8570–8576.

RUDD, M. E. (1990). Cross sections for production of secondary electrons by charged particles. *Radiat. Prot. Dosim.*, *31*(1/4), 17-22.

SAMUEL, A. H., & MAGEE, J. L. (1953). Theory of radiation chemistry. II. Track effects in radiolysis of water. *J. Chem. Phys.*, *21*(6), 1080–1087.

SANGUANMITH, S., MUROYA, Y., MEESUNGNOEN, J., LIN, M., KATSUMURA, Y., MIRSALEH KOHAN, L., et al. (2011). Low-linear energy transfer radiolysis of liquid water at elevated temperatures up to 350 °C: Monte Carlo simulations. *Chem. Phys. Lett.*, *508*(4-6), 224–230.

SANGUANMITH, S., MEESUNGNOEN, J., MUROYA, Y., LIN, M., KATSUMURA, Y., & JAY-GERIN, J.-P. (2012). On the spur lifetime and its temperature dependence in the low linear energy transfer radiolysis of water. *Phys. Chem. Chem. Phys.*, *14*(48), 16731–16736.

SAUER, M. C., Jr., SCHMIDT, K. H., HART, E. J., NALEWAY, C. A., & JONAH, C. D. (1977). LET dependence of transient yields in the pulse radiolysis of aqueous systems with deuterons and α particles. *Radiat. Res.*, *70*(1), 91–106.

SAUER, M. C., Jr., HART, E. J., NALEWAY, C. A., JONAH, C. D., & SCHMIDT, K. H. (1978). Pulse radiolysis with $^{2}H^{+}$ and $^{4}He^{2+}$. Fast and slow formation of Fe^{3+} in acidic Fe^{2+} solutions. *J. Phys. Chem.*, *82*(20), 2246–2248.

SCHARDT, D., ELSÄSSER, T., & SCHULZ-ERTNER, D. (2010). Heavy-ion tumor therapy: Physical and radiobiological benefits. *Rev. Mod. Phys.*, *82*(1), 383–425.

SCHMIDT, K. H., & BARTELS, D. M. (1995). Lack of ionic strength effect in the recombination of hydrated electrons: $(e^-)_{aq} + (e^-)_{aq} \rightarrow 2(OH^-) + H_2$. *Chem. Phys.*, *190*(1), 145–152.

SCHOLZ, M., KELLERER, A. M., KRAFT-WEYRATHER, W., & KRAFT, G. (1997). Computation of cell survival in heavy ion beams for therapy. The model and its approximation. *Radiat. Environ. Biophys.*, *36*(1), 59–66.

SCHULER, R. H., & ALLEN, A. O. (1956). Yield of the ferrous sulfate radiation dosimeter: an improved cathode-ray determination. *J. Chem. Phys.*, *24*(1), 56–59.

SCHULER, R. H., & ALLEN, A. O. (1957). Radiation chemistry studies with cyclotron beams of variable energy: Yields in aerated ferrous sulfate solution. *J. Am. Chem. Soc.*, *79*(7), 1565–1572.

SCHULER, R. H., & BARR, N. F. (1956). Oxidation of ferrous sulfate by ionizing radiations from (n, α) reactions of boron and lithium. *J. Am. Chem. Soc.*, *78*(22), 5756–5762.

SCHULZ-ERTNER, D., & TSUJII, H. (2007). Particle radiation therapy using proton and heavier ion beams. *J. Clin. Oncol.*, *25*(8), 953–964.

SHALEK, R. J., SINCLAIR, W. K., & CALKINS, J. C. (1962). The relative biological effectiveness of 22-Mevp X-rays, cobalt-60 gamma rays, and 200-Kvcp X-rays. II. The use of the ferrous sulfate dosimeter for X-ray and gamma-ray beams. *Radiat. Res.*, *16*(3), 344–351.

SLATER, J. D., ROSSI, C. J., YONEMOTO, L. T., BUSH, D. A., JABOLA, B. R., LEVY, R. P., et al. (2004). Proton therapy for prostate cancer: The initial Loma Linda University experience. *Int. J. Radiation Oncology Biol. Phys.*, *59*(2), 348–352.

SOLOMON, T. (2001). The definition and unit of ionic strength. *J. Chem. Educ.*, 78(12), 1691–1692.

SPINKS, J. W. T., & WOODS, R. J. (1990). *An Introduction to Radiation Chemistry*, 3rd edn. Wiley, New York, NY.

STERNICZUK, M., & BARTELS, D. M. (2016). Source of molecular hydrogen in high-temperature water radiolysis. *J. Phys. Chem. A*, *120*(2), 200–209.

STORER, J. B., HARRIS, P. S., FURCHNER, J. E., & LANGHAM, W. H. (1957). The relative

biological effectiveness of various ionizing radiations in mammalian systems. *Radiat. Res.*, *6*(2), 188–288.

SUIT, H. D. (2003). Protons to replace photons in external beam radiation therapy? *Clin. Oncol.*, *15*(1), S29–S31.

SUZUKI, M., KASE, Y., YAMAGUCHI, H., KANAI, T., & ANDO, K. (2000). Relative biological effectiveness for cell-killing effect on various human cell lines irradiated with heavy-ion medical accelerator in Chiba (HIMAC) carbon-ion beams. *Int. J. Radiation Oncology Biol. Phys.*, *48*(1), 241–250.

SWIATLA-WOJCIK, D., & BUXTON, G. V. (1995). Modeling of radiation spur processes in water at temperatures up to 300 °C. *J. Phys. Chem.*, *99*(29), 11464–11471.

TAUBE, H. (1957). Photochemical reactions of ozone in solution. *Trans. Faraday Soc.*, *53*, 656–665. doi: 10.1039/TF9575300656.

TIPPAYAMONTRI, T., SANGUANMITH, S., MEESUNGNOEN, J., SUNARYO, G., & JAY-GERIN, J.-P. (2009). Fast neutron radiolysis of the ferrous sulfate (Fricke) dosimeter: Monte Carlo simulations. *Recent Res. Devel. Physical Chem.*, *10*, 143–211.

TOBUREN, L. H. (2004). Ionization and secondary electron production by fast charged particles. In: *Charged Particle and Photon Interactions with Matter: Chemical, Physicochemical, and Biological Consequences with Applications* (Mozumder, A., and Hatano, Y., Eds.), pp. 31–74. Marcel Dekker, New York, NY.

TORRE, L. A., BRAY, F., SIEGEL, R. L., FERLAY, J., LORTET-TIEULENT, J., & JEMAL, A. (2015). Global cancer statistics, 2012. *CA Cancer J. Clin.*, *65*(2), 87–108.

TURNER, J. E., DOWNING, D. J., & BOGARD, J. S. (2012). *Statistical Methods in Radiation Physics*. Wiley-VCH Verlag GmbH & Co. KGaA. Weinheim, Germany.

UEHARA, S., & NIKJOO, H. (2006). Monte Carlo simulation of water radiolysis for low-energy charged particles. *J. Radiat. Res.*, *47*(1), 69–81.

VALKO, M., LEIBFRITZ, D., MONCOL, J., CRONIN, M. T. D., MAZUR, M., & TELSER, J. (2007). Free radicals and antioxidants in normal physiological functions and human disease. *Int. J. Biochem. Cell Biol.*, *39*(1), 44–84.

VON SONNTAG, C. (2006). *Free-Radical-Induced DNA Damage and its Repair: A Chemical Perspective*. Springer-Verlag, Berlin.

WALIGÓRSKI, M. P. R., HAMM, R. N., & KATZ, R. (1986). The radial distribution of dose

around the path of a heavy ion in liquid water. *Nucl. Tracks Radiat. Measur.*, *11*(6), 309–319.

WARD, J. F. (1971). Deoxynucleotides – Models for studying mechanisms of strand breakage in DNA – I. Protection by sulphydryl compounds. *Int. J. Radiat. Phys. Chem.*, *3*(3), 239–249.

WARD, J. F. (1983). Chemical aspects of DNA radioprotection. In: *Radioprotectors and Anticarcinogens* (Nygaard, D. F., and Simic, M. G., Eds.), pp. 73–85. Academic Press, New York.

WARDMAN, P. (2007). Chemical radiosensitizers for use in radiotherapy. *Clin. Oncol.*, *19*(6), 397–417.

WARDMAN, P. (2009). The importance of radiation chemistry to radiation and free radical biology (The 2008 Silvanus Thompson Memorial Lecture). *Br. J. Radiol.*, *82*(974), 89–104.

WENZL, T., & WILKENS, J. J. (2011). Modelling of the oxygen enhancement ratio for ion beam radiation therapy. *Phys. Med. Biol.*, *56*(11), 3251–3268.

WESTON, R. E., Jr., & SCHWARZ, H. A. (1972). *Chemical Kinetics*. Prentice-Hall, Englewood Cliffs.

WILSON, C. D., DUKES, C. A., & BARAGIOLA, R. A. (2001). Search for the plasmon in condensed water. *Phys. Rev. B*, *63*(12), 121101.

YAMASHITA, S., KATSUMURA, Y., LIN, M., MUROYA, Y., MAEYAMA, T., & MURAKAMI, T. (2008). Water radiolysis with heavy ions of energies up to 28 GeV. 2. Extension of primary yield measurements to very high LET values. *Radiat. Phys. Chem.*, *77*(10-12), 1224–1229.

ZIEGLER, J. F., BIERDACK, J. P., & ZIEGLER, M. D. (2015). *SRIM – The Stopping and Range of Ions in Matter*. SRIM Co., Chester, MD.